UNIVERSITY OF OKLAHOMA

GRADUATE COLLEGE

# MIXED AXION-NEUTRALINO DARK MATTER IN THE SUPERSYMMETRIC DFSZ MODEL

A DISSERTATION

SUBMITTED TO THE GRADUATE FACULTY

in partial fulfillment of the requirements for the

Degree of

DOCTOR OF PHILOSOPHY

By

HASAN BARIS SERCE

Norman, Oklahoma

2016

MIXED AXION-NEUTRALINO DARK MATTER
IN THE SUPERSYMMETRIC DFSZ MODEL

A DISSERTATION APPROVED FOR THE
HOMER L. DODGE DEPARTMENT OF PHYSICS AND ASTRONOMY

BY

Dr. Howard Baer, Chair

Dr. Ronald Kantowski

Dr. Chung Kao

Dr. Ralf Schmidt

Dr. Patrick Skubic

# Table of Contents

# Abstract

The lack of evidence for weak scale supersymmetry (SUSY) from LHC Run-I at $\sqrt{s} = 8$ TeV and Run-II with $\sqrt{s} = 13$ TeV results have caused a paradigm shift in expected phenomenology of SUSY models. The spectrum of sparticle (SUSY particle) masses has been pushed to a higher, multi-TeV energy scale. The spectrum was predicted to lie not too far beyond the weak scale typified by $Z$ and $W$ masses based on *naturalness* in pre-LHC years. In such models, the neutralino (the lightest SUSY particle) can account for the measured dark matter (DM) relic density. At the higher mass scale, correct relic density can only be obtained by enhanced annihilations or more naturally, by a low $\mu$ term.

Although it has not been discovered at the colliders yet, SUSY still remains the most attractive solution for the big hierarchy problem. In this thesis, I investigate SUSY models with mixed axion-neutralino dark matter with two MSSM scenarios: CMSSM (with a standard neutralino overabundance) and NUHM2 (with a standard neutralino underabundance). The NUHM2 model with a low $\mu$ gives a natural SUSY spectrum defined by the $\Delta_{\rm EW}$ measure. Phenomenological implications of the two component dark matter scenarios are studied in detail.

# I. Introduction

## I.1. Standard Model

### I.1.1. Particle Content and Symmetry Groups

The Standard Model (SM) of particle physics - a theory concerning the electromagnetic (EM), weak and strong nuclear interactions - describes all the basic constituents of matter that have been discovered so far. Matter particles include 3 generations of spin 1/2 quarks and leptons, while the strong nuclear force is mediated by 8 color gluons, the weak force by $W^{\pm}$, $Z$ bosons and EM by the photon. Discovery of the Higgs boson [1, 2], which has a mass $m_h = 125.09 \pm 0.21$ (stat.) $\pm 0.11$ (syst.) GeV based on precision measurements [3], confirms the particle content of the Standard Model. The elementary particles of the SM are listed in Table 1.

| | Fermions | | | Bosons |
|---|---|---|---|---|
| | $1^{st}$ generation | $2^{nd}$ generation | $3^{rd}$ generation | Higgs |
| Quarks | Up | Charm | Top | Gluon |
| | Down | Strange | Bottom | Photon |
| Leptons | Electron Neutrino | Muon Neutrino | Tau Neutrino | Z |
| | Electron | Muon | Tau | W |

Table 1: Particles in Standard Model

The SM is a renormalizable quantum field theory that describes the known microscopic interactions, combining the electroweak theory with quantum chromodynamics (QCD). The combination of strong, weak and electroweak interactions is described by a $SU(3)_C \times SU(2)_L \times U(1)_Y$ gauge theory involving quarks and leptons. This is a combination of the Glashow-Weinberg-Salam model of electroweak interactions with QCD. In this model, the $SU(3)_C \times SU(2)_L \times U(1)_Y$ group is spontaneously broken into $SU(3)_C \times U(1)_Q$ at the weak scale. As a

result of the weak isospin and hypercharge symmetries being spontaneously broken, gauge bosons obtain mass and the symmetry is confined to electromagnetism and color symmetry: $SU(3)_C \times U(1)_Q$. The theory does not truly unify weak and electromagnetic interactions as $SU(2)_L \times U(1)_Y$ gauge couplings describe two interactions with two coupling constants.

The representations in the SM for the first fermion generation can be written as:

| | |
|---|---|
| Left-handed Quarks: | $\begin{pmatrix} u_L^r & u_L^g & u_L^b \\ d_L^r & d_L^g & d_L^b \end{pmatrix}$ |
| Left-handed Leptons: | $\begin{pmatrix} \nu_L^e \\ e_L^- \end{pmatrix}$ |
| Right-handed neutrino: | $\nu_R^e$ |
| Right-handed electron: | $e_R^-$ |
| Right-handed up quarks: | $\begin{pmatrix} u_R^r & u_R^g & u_R^b \end{pmatrix}$ |
| Right-handed down quarks: | $\begin{pmatrix} d_R^r & d_R^g & d_R^b \end{pmatrix}$ |

where r, g, b stands for the 3 color charges of $SU(3)_C$ gauge group: red, green and blue respectively. Note that right-handed neutrino is shown for completeness (16 fields in total). Since $SU(2)_L$ gauge symmetry (weak interaction) can only be applied to left handed fermions, they are represented in doublets.

### I.1.2. Electroweak Symmetry Breaking

The electroweak interaction is spontaneously broken into the $SU(3)_C \times U(1)_Q$ subgroup by the Brout-Englert-Higgs mechanism [4] when the Higgs boson develops a vacuum expectation value ($vev$). In this mechanism, the Higgs Lagrangian

is given by:

$$\mathcal{L}_{Higgs} = (D^{\mu}\phi)^{\dagger} D_{\mu}\phi - V(|\phi|^2) \tag{1}$$

where $\phi$ is a $SU(2)_L$ doublet of spin-0 field and $V(|\phi|^2)$ is the famous Mexican hat-type Higgs potential:

$$V(|\phi|^2) = -\mu'^{\,2}\phi^{\dagger}\phi + \lambda(\phi^{\dagger}\phi)^2. \tag{2}$$

The origin of the Higgs potential represents an unstable equilibrium for $\mu'^{\,2} > 0$, hence a non-zero *vev* develops at:

$$\langle\phi\rangle = \sqrt{\frac{\mu'^{\,2}}{\lambda}} = v \ . \tag{3}$$

We can define the real part of $\phi$ in unitary gauge as:

$$\phi = \begin{pmatrix} 0 \\ \frac{v+h}{\sqrt{2}} \end{pmatrix}. \tag{4}$$

Here $h$ is the Higgs field with 0 vacuum value. Plugging $\phi$ in $\mathcal{L}_{Higgs}$ gives expressions for the $W$ and $Z$ boson masses, then one can calculate $v \simeq 246$ GeV. For a real scalar field, the mass term in the Lagrangian appears in the form:

$$\mathcal{L} \ni \frac{1}{2}m^2\phi^2 \tag{5}$$

hence $m_h = \sqrt{2\lambda v^2} = \sqrt{2\mu'^{\,2}}$. Using the experimental result $m_h \simeq$125 GeV, we find $\lambda \simeq 0.129$.

The discovery of the Higgs boson is a triumph of contemporary physics in that it provides the first hard evidence for the existence of fundamental scalar fields. In the SM, the Higgs boson is responsible for giving mass to gauge bosons and

| **Interaction:** | **Mediator (Boson):** | **Relative Strength:** | **Symmetry Group:** |
|---|---|---|---|
| Electromagnetic | Photon | 1 | $U(1)_Q$ |
| Strong | Gluon | 1000 | $SU(3)_C$ |
| Weak | W | $10^{-11}$ | $SU(2)_Y$ |
| | Z | | |

Table 2: Interactions in Standard Model

also fermions by Yukawa terms generating Dirac mass for fermions.

### I.1.3. Forces in Standard Model

The Standard Model can successfully explain three of the four interactions in nature by three associated forces: *electromagnetic, strong,* and *weak* forces. Their relative strength, force carriers and symmetry groups are listed in Table 2. The fourth interaction is gravity, which interacts via *gravitational* force and is mediated by the theoretical particle called *graviton*. While gravitational force is the most familiar force in our daily life, its relative strength is extremely small and it is not a part of the SM.

All particles except neutrinos, which are not charged under $U(1)_Q$ symmetry (no electric charge), feel electromagnetic interaction with the exchange of *photons*. Likewise, quarks are charged under $SU(3)_C$ color symmetry so they interact with the strong interaction via the exchange of *gluons*. Every left-handed particle in SM can be represented in a $SU(2)_L$ doublet and interact via weak interaction; right-handed particles do not interact with the $W$ boson, but they have $U(1)_Y$ generators so they are represented by singlets.

### I.1.4. Physics Beyond the Standard Model

The SM successfully describes a vast assortment of phenomena observed in experimental particle physics but cannot be a complete theory since it is insufficient

to explain the following:

- ◆ Neutrino Mass : The SM assumes massless neutrinos. However, it has been observed that neutrinos change their flavor while they propagate through space. Neutrino oscillation is a proof of massive neutrinos. To set the scale, the *Planck* Collaboration reported that the sum of neutrino masses is constrained to $\sum m_\nu < 0.23$ eV [5]. This problem is easily remedied via the introduction of gauge singlet right-hand neutrinos $v_R^i$ to the SM.

- ◆ Dark Matter and Dark Energy : Only 4.6% of the Universe is comprised of atoms; 24% of the Universe is dark matter and the remaining 71.4% is dark energy [6]. There is no candidate for dark matter in the SM.

- ◆ Matter-Antimatter Asymmetry : The SM does not introduce an explanation for the origin of the matter-antimatter asymmetry which is quantified by the measurement of the baryon to photon ratio $\simeq (6.2 \pm 0.5) \times 10^{-10}$ [7].

- ◆ Gravitational Force

Apart from experimental results and observations, the SM is also challenged by theoretical problems:

- Gauge Coupling Unification : The Standard Model describes the strong, weak and electromagnetic interactions with three different coupling constants for the gauge groups $SU(3)_C$, $SU(2)_Y$, $U(1)_Q$. Symmetries are expected to be restored at high energy scales and the number of coupling constants reduce into only one coupling constant associated with grand unified gauge group, which is the original motivation for grand unified theories (GUT), see Fig. 1.

- Big Hierarchy Problem : Scalar fields in the SM, eg. the Higgs boson, receive large quantum corrections unless protected by an additional symme-

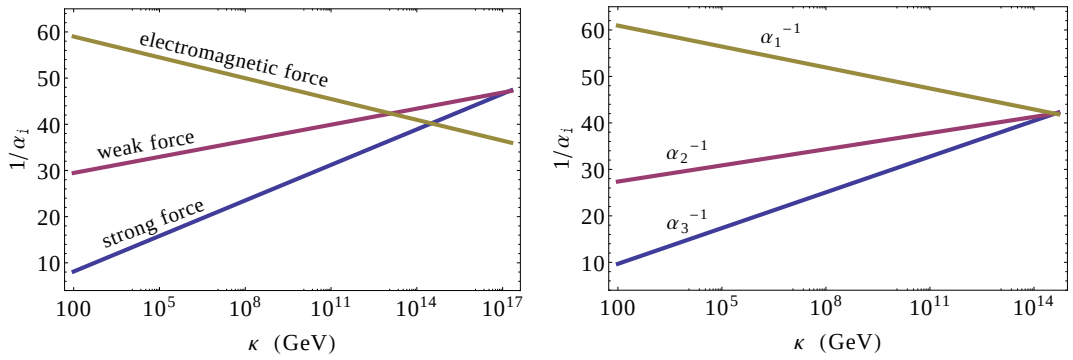


(a) (b)

Figure 1: Evolution of gauge couplings (a) SM gauge couplings from weak scale to GUT scale. In frame (b) gauge coupling unification in SU(5) is shown as an example for unification in GUTs.

try. With no theory beyond SM, the quadratic divergences that the Higgs boson receives should be cancelled with enormous levels of fine-tuning.

- Strong CP Problem : The experimental bound for the $\theta$ parameter associated with the QCD Lagrangian is very small: $\theta \ll 10^{-10}$. The question of why it is so small is known as the strong CP problem [8]. If the SM ought not to be a fine-tuned theory, the CP-violating term must be forbidden by an additional symmetry.

- Electroweak Symmetry Breaking (EWSB) : Although the SM accomodates electroweak symmetry breaking by spontaneous breaking of the symmetry, it does not explain it.

## I.2. Supersymmetry

### I.2.1. Motivation

Supersymmetry (SUSY) is a symmetry between bosons and fermions. For each boson (fermion), there exists a partner fermion (boson). SUSY, if it exists, must

be a broken symmetry since no supersymmetric particles have been observed at the weak scale. SUSY elegantly solves the Big Hierarchy problem by cancelling quadratic divergences and providing the symmetry to protect the Higgs mass from receiving large corrections. In the SM, the one-loop corrected physical Higgs boson mass can be written as:

$$m_h{}^2 \simeq m_{h0}{}^2 + \frac{c}{16\pi^2}\Lambda^2 \tag{6}$$

where $m_{h0}$ is the bare Higgs mass and the second term denotes the quadratically divergent correction. The cut-off $\Lambda$ is interpreted as the scale where the SM ceases to be valid. In SUSY every SM boson (fermion) has a fermionic (bosonic) supersymmetric partner, so not only one-loop but all quadratically divergent terms are cancelled out at all orders.

Moreover, SUSY models can explain:

- Neutrino Mass: Neutrinos can gain mass by seesaw mechanism [9] (There do also exist solutions using the seesaw mechanism without supersymmetry.).
- Dark Matter : The lightest supersymmetric particle (LSP) is stable in R-parity conserving models. The neutralino LSP is a popular candidate of DM in SUSY models.
- Matter-Antimatter Asymmetry: Lepton asymmetry can be generated via several supersymmetric baryogenesis mechanisms.
- Gravity : In local SUSY or supergravity models, the spin-2 graviton along with its supersymmetric partner spin-3/2 gravitino are the gravitational force carriers.

- Electroweak Symmetry Breaking : EWSB occurs when the soft SUSY breaking mass $m^2_{H_u}$ is driven to negative values via renormalization group equation (RGE) running.

- Gauge Coupling Unification : The measured gauge couplings at scale $Q = m_Z$, when extrapolated to $M_{GUT}$ are found to unify in SUSY.

The simplest supersymmetric model is called "Minimal Supersymmetric Standard Model" (MSSM) [19] which is the direct supersymmetric extension of the standard model. The MSSM requires two Higgs doublets for consistent implementation.

### I.2.2. MSSM

The MSSM is the simplest extension of the SM, introducing the minimum number of extra particle states and interactions. In such an extension, all particles in the SM must have a superpartner whose spin differs by 1/2. The gauge symmetry of MSSM is chosen to be the same as that of the SM; $SU(3)_C \times SU(2)_L \times U(1)_Y$. Spin-0 partners of fermions are called *sfermions*. By the same analogy, leptons are called *sleptons* and quarks are called *squarks*. In SUSY, a Higgs doublet can couple only to either up-type or down-type quarks and leptons so MSSM requires the introduction of two Higgs doublets with opposite hypercharges. Two Higgs doublets are also needed because the fermionic superpartner of the Higgs boson, *higgsino*, would cause gauge anomaly without its counterpart. The solution requires two Higgs doublets with hypercharge $Y = \pm 1/2$ so that the total contribution to the anomaly traces from the fermionic members of the Higgs supermultiplets are cancelled out [10]. The two doublets are classified as giving mass to up-type quarks ($H_u$) or down-type quarks ($H_d$). The part of the

superpotential that contain Yukawa interactions can be written as:

$$W_{\text{Yukawa}} = \sum_{i,j=1,3} \left[ (\mathbf{f}_u)_{ij} \epsilon_{ab} \hat{Q}_i^a \hat{H}_u^b \hat{U}_j^c + (\mathbf{f}_d)_{ij} \hat{Q}_i^a \hat{H}_{da} \hat{D}_j^c + (\mathbf{f}_e)_{ij} \hat{L}_i^a \hat{H}_{da} \hat{E}_j^c + \mu \hat{H}_u \hat{H}_d \right] \tag{7}$$

where $\mu$ is the higgsino mass parameter that gives mass to SM gauge bosons and the Higgs boson and the higgsinos. The rest of the matter content is represented by: $\hat{Q}_i$ left-handed squark doublets, $\hat{U}_i^c$ left-handed up squark singlets, $\hat{D}_i^c$ left-handed down squark singlets, $\hat{L}_i$ left-handed slepton doublets and $\hat{E}_i^c$ left handed slepton singlets.

When $m_{H_u}^2$ is driven to negative values by the large top Yukawa coupling of $Z$ via RGE running, electroweak symmetry is broken and five physical Higgs states form: the light Higgs $h$ (SM higgs), the heavy scalar Higgs $H^0$, two charged Higgs $H^\pm$ and one pseudo-scalar Higgs $A$. The MSSM has 124 free parameters (only 19 in SM). One of the main virtues of the MSSM is the gauge coupling unification at GUT scale.

It is common to assume unified parameters at GUT scale:

$$\begin{aligned} g_C = g_L = g_Y &\equiv g_{GUT} \\ m_{Q_i}^2 = m_{U_i}^2 = m_{D_i}^2 = m_{L_i}^2 = m_{E_i}^2 = m_{H_u}^2 = m_{H_d}^2 &\equiv m_0^2 \\ M_1 = M_2 = M_3 &\equiv m_{1/2} \\ A_t = A_b = A_\tau &\equiv A_0 \end{aligned} \tag{8}$$

where $M_1$, $M_2$ and $M_3$ are gaugino mass parameters (bino, wino and gluino respectively), $A_{t,b,\tau}$ are trilinear $A$ terms coupled to Yukawa couplings. One more parameter should be defined in order to simplify MSSM parameter space:

$$\tan\beta = \frac{v_u}{v_d} \tag{9}$$

where $v_u$ and $v_d$ are the *vev*s of the neutral higgs scalars $h_u$ and $h_d$ after EWSB. With such definitions, it is enough to specify just five parameters $m_0$, $m_{1/2}$, $A_0$, sign($\mu$), tan$\beta$ to determine the weak scale spectra of the model. This is called the minimal supergravity (mSUGRA) or the Constrained MSSM (CMSSM) model.

## I.3. Dark Matter in Supersymmetry

### I.3.1. A Brief Introduction to the Early Universe

Derivations in this section are extracted from *The Early Universe* by Kolb & Turner [12]. The expanding Universe can be described by the Einstein equations in general relativity. WMAP9 [6] results show that the Universe is homogenous and isotropic which can be described by the Friedmann-Robertson-Walker (FRW) metric:

$$ds^2 = dt^2 - R^2(t)[\frac{dr^2}{1-kr^2} + r^2 d\theta^2 + r^2 \sin^2\theta d\phi^2] \tag{10}$$

where $R^2(t)$ is the scale factor, $(t, r, \theta, \phi)$ are comoving coordinates and k defines the curvature as:

$$\begin{aligned} k = -1 &\longrightarrow \text{open Universe} \\ k = 0 &\longrightarrow \text{flat Universe} \\ k = 1 &\longrightarrow \text{closed Universe.} \end{aligned} \tag{11}$$

Using the FRW metric, the Einstein equations lead to the Friedmann equation:

$$H^2 + \frac{k}{R^2} = \frac{8\pi G}{3}\rho \tag{12}$$

Here $H$ is the Hubble parameter defined as $H = \dot{R}/R$ and $\rho$ is the energy density. The Friedmann equation can be combined with the continuity equation:

$$\dot{\rho} + 3H(\rho + p) = 0 \tag{13}$$

where $p$ is the pressure of the comoving volume, to give the evolution of $\rho$ for the three scenarios of the Universe:

$$\begin{aligned} \text{Radiation dominated} &\longrightarrow \rho \propto R^{-4} \\ \text{Matter dominated} &\longrightarrow \rho \propto R^{-3} \\ \text{Vacuum dominated} &\longrightarrow \rho \propto \text{constant} \end{aligned} \tag{14}$$

The early Universe was dominated by extremely hot and dense gas of relativistic particles followed by a fast expansion (inflation). During inflation, the Universe became flat and dominated by the potential energy of the *inflaton*, a scalar field which drives inflation. At the end of inflation, the Universe is matter dominated by the inflaton scalar field and then the inflaton decays into relativistic particles. During the decay of the inflaton, the Universe is reheated to a temperature $T_R$ (reheat temperature):

$$T_R \simeq \left(\frac{90}{4\pi^2 g_*}\right)^{1/4} \sqrt{\Gamma_\phi \; M_{Pl}} \tag{15}$$

where $g_*$ denotes the effective number of relativistic particle species in equilibrium:

$$g_* = \sum_{i=bosons} \left(\frac{T_i}{T}\right)^4 + \frac{7}{8} \sum_{j=fermions} \left(\frac{T_j}{T}\right)^4. \tag{16}$$

Using the above equations, energy density, entropy density and number density can be computed as:

$$\begin{aligned} \rho_R &= \frac{\pi^2}{30} g_* T^4 \\ s &= \frac{2\pi^2}{45} g_{*S} T^3 \\ n_R &= \frac{\zeta(3)}{\pi^2} g_{*S} T^3 \end{aligned} \tag{17}$$

where $g_{*S}$ denotes the effective degrees of freedom of entropy:

$$g_{*S} = \sum_{i=bosons} g_i \left(\frac{T_i}{T}\right)^3 + \frac{7}{8} \sum_{j=fermions} g_j \left(\frac{T_j}{T}\right)^3 \tag{18}$$

The present cold dark matter (CDM) density can be computed by solving coupled Boltzmann equations starting from the reheat temperature ($T = T_R$) at the end of inflation until today. The Boltzmann equation for a weakly interacting massive particle (WIMP), $X$, is given by:

$$\dot{n_X} + 3Hn_X = -\langle \sigma_{ann} v \rangle (n_X^2 - n_{eq}^2). \tag{19}$$

In the general picture, most of the constituents of the Universe are in thermal equilibrium at $T = T_R$. As the Universe cools down, departures from thermal equilibrium begin. The WIMPs ($X$) decouple from the thermal bath when the temperature drops to $T \lesssim m_X$. The number density starts to decrease exponentially until the scattering term becomes comparable to the Hubble term: $\langle \sigma_{ann} v \rangle n_X \simeq H(T_{Fr})$ since WIMPs stop annihilating (freeze-out) and the relic density after freeze-out remains almost constant. The temperature at which the relic density stabilizes is called the freeze-out temperature, $T_{Fr}$. The evolution of the thermal DM abundance as the temperature drops is illustrated in Fig. 2 for the neutralino LSP: higgsino- and bino-like WIMPs. As the thermally av-

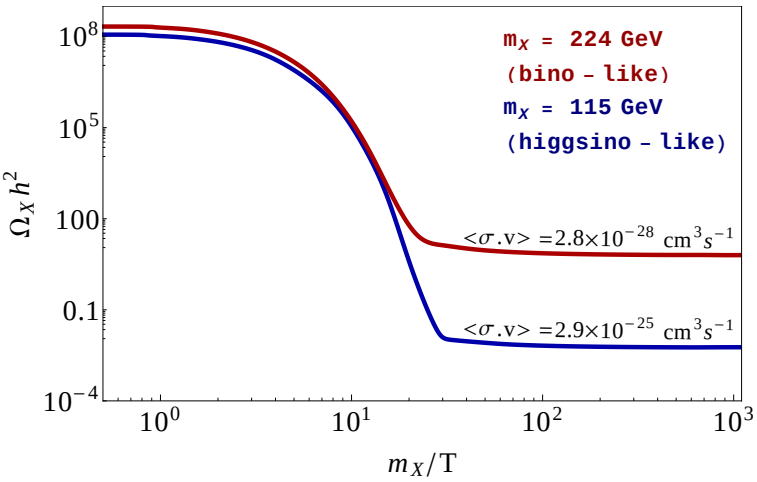


Figure 2: Evolution of thermal DM abundance as a function of $m_X/T$.

eraged cross section $\langle\sigma_{ann}v\rangle$ increases, the final dark matter density decreases since more annihilation takes place. In Fig. 2, $\langle\sigma_{ann}v\rangle$ values are given at $v_X \simeq 0$ when Universe cooled down. The WIMP is a good dark matter candidate (see Ref. [13] for a recent review) that can satisfy the measured relic density.

### I.3.2. Neutralino LSP

In the MSSM, the neutralino mass matrix is given by [14]:

$$M_{Neutral} = \begin{bmatrix} 0 & \mu & -\frac{gv_u}{\sqrt{2}} & \frac{g'v_u}{\sqrt{2}} \\ \mu & 0 & -\frac{gv_d}{\sqrt{2}} & -\frac{g'v_d}{\sqrt{2}} \\ -\frac{gv_u}{\sqrt{2}} & \frac{gv_d}{\sqrt{2}} & M_2 & 0 \\ \frac{g'v_u}{\sqrt{2}} & -\frac{g'v_d}{\sqrt{2}} & 0 & M_1 \end{bmatrix} \tag{20}$$

which is real and Hermitian and so can be diagonalized by an orthogonal transformation. As stated before, $M_1$ and $M_2$ are the bino and wino mass parameters respectively and $\mu$ is the supersymmetric higgsino mass. The mass of the lightest neutralino is the smallest eigenvalue of the matrix. The neutralino mass eigenstate can be expressed in the linear combination of basis states, an admixture of

bino/wino/higgsino states :

$$X = \alpha\tilde{B} + \beta\tilde{W} + \gamma\tilde{H}_d + \delta\tilde{H}_u \tag{21}$$

with $|\alpha|^2 + |\beta|^2 + |\gamma|^2 + |\delta|^2 = 1$. Naively, the type of the lightest neutralino is determined by the hierarchy between $M_1$, $M_2$ and $\mu$. The neutralino LSP can be bino-like, higgsino-like or wino-like:

$$\begin{aligned} |M_{1,2}| \gg |\mu| \quad &: \text{two lighter neutralinos are higgsino-like} \\ |M_2|, |\mu| \gg |M_1| \; &: \text{neutralino is bino-like} \\ |M_1|, |\mu| \gg |M_2| \; &: \text{neutralino is wino-like .} \end{aligned} \tag{22}$$

The neutralino LSP is stable due to $R$-parity conservation (required to stabilize the proton) and the conserved quantum number is given by:

$$P_R = (-1)^{3(B-L)+2s} \tag{23}$$

where $B$ and $L$ are the *Baryon* and *Lepton* numbers respectively and $s$ is the spin of the particle. SM particles are $R$-even whereas SUSY particles are $R$-odd particles. The MSSM Lagrangian does not contain the interactions:

$$W_{\text{MSSM}} \not\ni \hat{L}\hat{H}_u, \hat{L}\hat{L}\hat{E}, \hat{L}\hat{Q}\hat{D}, \hat{U}\hat{D}\hat{D} \tag{24}$$

hence R-parity is conserved. The first three terms in Eq. (24) contain interactions that violate lepton number and the interaction in the last term violates baryon number. Although it is sufficient to impose baryon and lepton number conservation to avoid proton decay, R-parity conservation is required for a stable LSP.

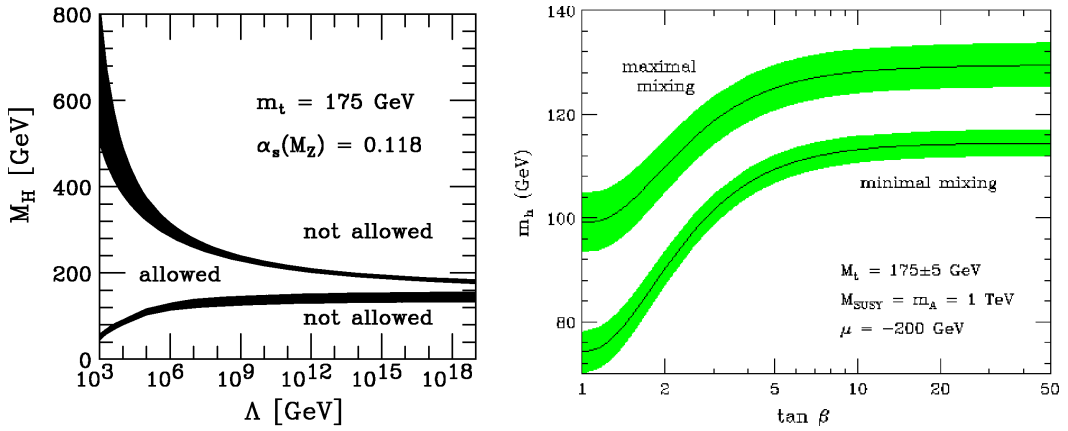


(a) (b)

Figure 3: (a) $m_h$ lower and upper bounds with uncertainties in SM, taken from Ref. [16]. (b) $m_h$ with maximal and minimal top-squark mixings in MSSM, taken from Ref. [17]

R-parity conservation arises naturally in $SO(10)$ SUSY GUT models [15] which allow only matter-matter-higgs couplings by the gauge symmetry of the model whereas R-parity violating couplings are either matter-higgs or matter-matter-matter.

### I.3.3. LHC vs CMSSM: Implications of 125 GeV Higgs Boson

In the SM, the upper bound for the Higgs boson is predicted to be 800 GeV [16]. In the MSSM, $m_h$ is calculated at the 1-loop level as [17]:

$$m_h^2 \simeq M_Z^2 \cos^2 2\beta + \frac{3g^2}{8\pi^2}\frac{m_t^4}{m_W^2}\left[\ln\frac{m_{\tilde{t}}^2}{m_t^2} + \frac{X_t^2}{m_{\tilde{t}}^2}\left(1 - \frac{X_t^2}{12m_{\tilde{t}}^2}\right)\right] \tag{25}$$

where $X_t = A_t - \mu/\tan\beta$. In the case $\mu \ll A_t$, $X_t$ becomes similar to the top-squark coupling; $X_t \simeq A_t$. Eq. (25) puts an upper limit $m_h \lesssim 135$ GeV for $m_{SUSY} \lesssim 2$ TeV. These conditions are shown in Fig. 3. The lower limit for $m_h$ was reported as $m_h \gtrsim 114.4$ GeV by the LEP-II working group in 2003 [18]. The discovery of the Higgs boson at Linear Hadron Collider (LHC) in 2012 with

$m_h \simeq$125 GeV squarely fits in the region predicted by supersymmetry.

However, in the CMSSM it is considered to be too heavy in the context of *naturalness* which favors $m_h \simeq 115$ GeV [20] using the fine-tuning measure $\Delta_{\mathrm{EENZ/BG}}$ [21] so-called Barbieri-Giudice measure, $\Delta_{\mathrm{BG}}$ with 4 free parameters. The Barbieri-Giudice measure tells how sensitive $m_Z^2$ is with respect to fundamental parameters of the models, $c_i$:

$$\Delta_{\mathrm{BG}} \equiv \max\left[c_i\right] \quad \text{where} \quad c_i = \left|\frac{\partial \ln m_Z^2}{\partial \ln p_i}\right| = \left|\frac{p_i}{m_Z^2}\frac{\partial m_Z^2}{\partial p_i}\right| \tag{26}$$

It has been argued that $\Delta_{\mathrm{BG}}$, applied to effective theories with multiple independent soft terms, overestimates electroweak fine-tuning in supersymmetric theories by claiming fine-tuning of dependent quantities one against another [22].

Another fine-tuning measure was proposed by Baer et al. [23]: $\Delta_{\mathrm{EW}}$ which compares the largest contribution on the right-hand side of Eq. (27) to the value of $m_Z^2/2$.

$$\frac{m_Z^2}{2} = \frac{(m_{H_d}^2 + \Sigma_d^d) - (m_{H_u}^2 + \Sigma_u^u)\tan^2\beta}{(\tan^2\beta - 1)} - \mu^2 \tag{27}$$

Eq. (27) is the well-known condition from minimization of the Higgs potential for electroweak symmetry breaking to occur. Electroweak fine-tuning is defined as:

$$\Delta_{\mathrm{EW}} \equiv max_i\left(|C_i|\right)/(m_Z^2/2) \tag{28}$$

where $C_{H_u} = -m_{H_u}^2\tan^2\beta/(\tan^2\beta - 1)$, $C_{H_d} = m_{H_d}^2/(\tan^2\beta - 1)$ and $C_\mu = -\mu^2$, along with definitions for the radiative corrections $C_{\Sigma_u^u(k)}$ and $C_{\Sigma_d^d(k)}$ [23]. Low $\Delta_{\mathrm{EW}}$ assures that there are no large cancellations on the right-hand side of Eq. (27). It is shown that when applied properly by combining dependent soft terms, $\Delta_{\mathrm{BG}} \simeq \Delta_{\mathrm{EW}}$, so $\Delta_{\mathrm{EW}}$ is used as the naturalness measure for the rest of the thesis.

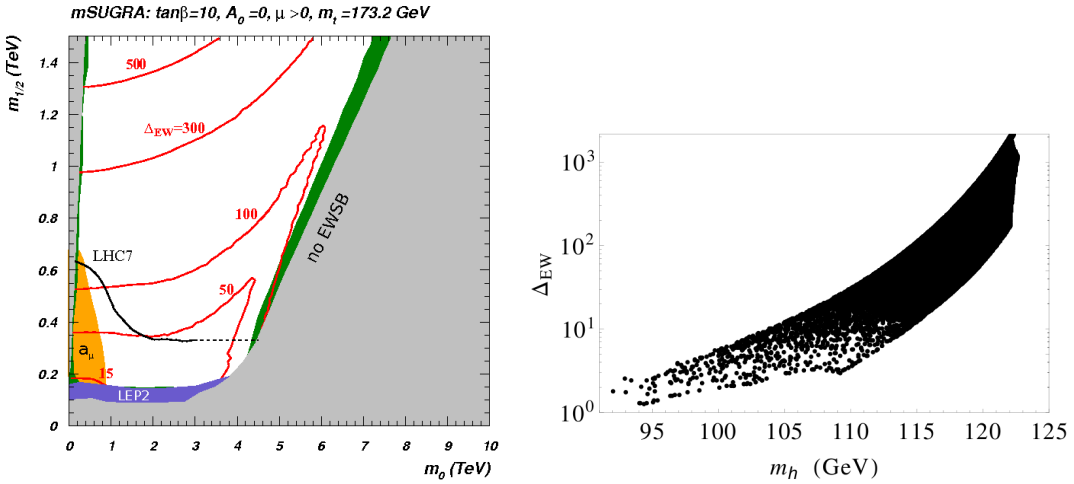


(a) (b)

Figure 4: CMSSM with $A_0$=0, $\tan\beta$=10 (a) $\Delta_{\rm EW}$ contours on $m_{1/2}$ vs. $m_0$ plane, taken from Ref. [24]. The green shaded area shows the region where $\Omega_{\widetilde{Z}_1}h^2 \leq 0.12$. (b) $\Delta_{\rm EW}$ vs. Higgs mass from a scan over $m_0 < 8$ TeV, $m_{1/2} < 3$ TeV.

The CMSSM after the Higgs boson discovery has been studied in detail in Refs. [24, 25]. It is shown that CMSSM parameter space with $A_0$=0 is ruled-out, Higgs mass cannot reach up to 125 GeV unless $A_0 \gtrsim 2m_0$ or $A_0 \lesssim -1.4m_0$ (these limits are for $\tan\beta$=10). In the left panel of Fig. 4, $m_h < 123$ GeV in the whole parameter space and the right panel shows how $\Delta_{\rm EW}$ increases with increasing $m_h$. In the CMSSM, the measured value of the Higgs mass can easily be found with large $A_0$ such as $A_0$= -2$m_0$ as shown in Fig. 5, which gives large mixing in the top squark sector [26].

For $m_h$ = 125 GeV, $\Delta_{\rm EW}$ >1000 which makes it quite unnatural. In Fig. 5(b) the low $m_{1/2}$ and low $m_0$ portions of the plane marked LHCb are excluded due to the large $B_s \to \mu^+\mu^-$ branching fraction. A complete scan over CMSSM parameter space shows lower values of $\Delta_{\rm EW}$ ($\Delta_{\rm EW}$ <100) can be achieved at $m_0$ ≃8 TeV and $A_0/m_0$ ≃0.6 [24]. In this case, the points that satisfy Higgs mass and LHC constraints with low $\Delta_{\rm EW}$ predict DM relic density $\Omega_{\widetilde{Z}_1}h^2 \sim O(10)$ which is two orders of magnitude higher than the measured value.

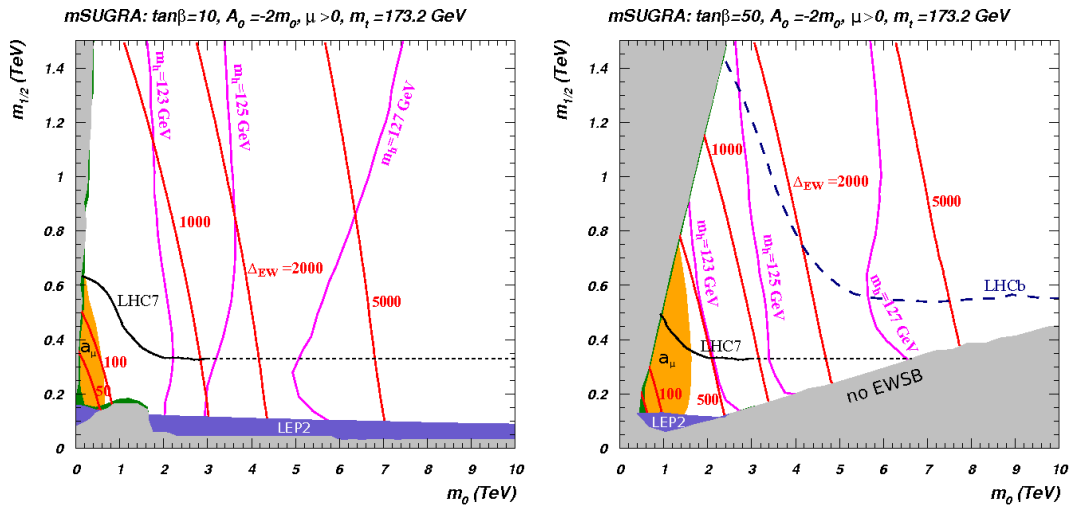


(a) (b)

Figure 5: CMSSM with $A_0 = -2m_0$, taken from Ref. [24]. (a) $m_{1/2}$ vs. $m_0$ plane with $\tan\beta = 10$. (b) $m_{1/2}$ vs. $m_0$ plane with $\tan\beta$=55. The green shaded area shows the region where $\Omega_{\tilde{Z}_1}h^2 \leq 0.12$.

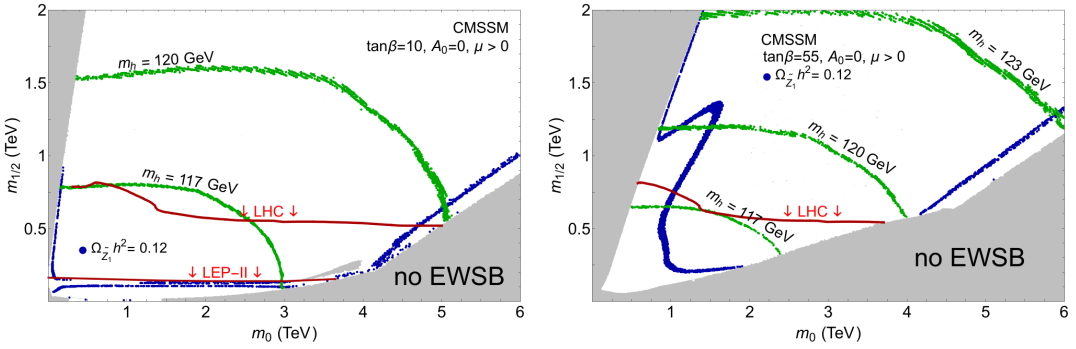


(a) (b)

Figure 6: CMSSM with $A_0$=0 with LEP-II ($m_{W_1^{+/-}}$ >103.5 GeV) and LHC bounds (excluded region on $m_0$ vs $m_{1/2}$ plane). (a) $m_{1/2}$ vs. $m_0$ plane with $\tan\beta$=10. (b) $m_{1/2}$ vs. $m_0$ plane with $\tan\beta$=55. Blue dots form strips where $\Omega_{\tilde{Z}_1}h^2$= 0.12.

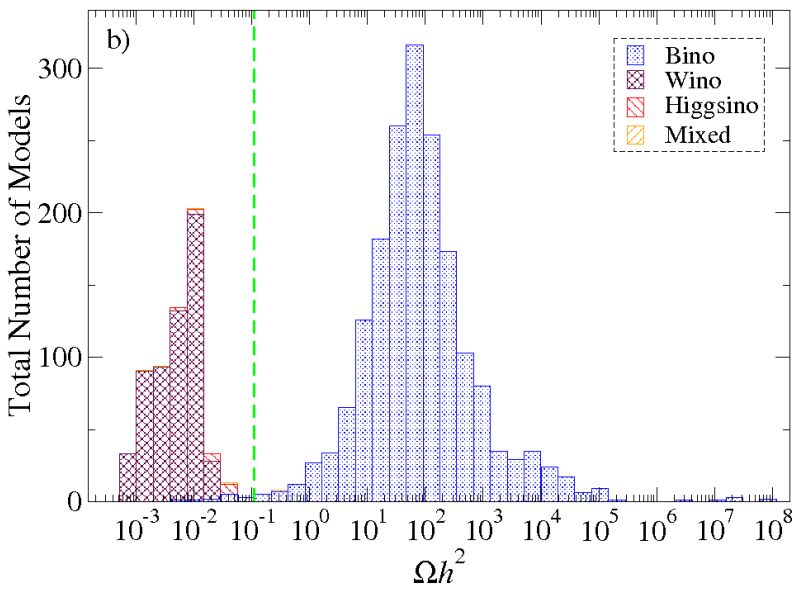


Figure 7: Projection of the number of models with $m_{\widetilde{Z}_1}$ <500 GeV generated by a linear scan over SUGRA-19 parameters, taken from Ref. [27]

It can be concluded that LEP-II and LHC searches disfavor the CMSSM model. The CMSSM [19] was a very succesful model since it was proposed over 20 years ago. In Fig. 6, the preferred parameter region is shown for $\tan\beta$=10 and 55. The model could naturally explain the DM relic density before imposing LEP-II [18] (chargino mass, $m_{W_1^{+/-}} > 103.5$ GeV), LHC [28] and Higgs mass constraints. In frames 6(a) and (b), $m_h < 121$ GeV and $m_h < 123$ GeV respectively throughout the whole parameter space. The $h/Z$ resonance in Fig. 6(a) region is completely ruled out by the chargino mass constraint from LEP-II, and in Fig. 6(b) the bulk of the strip (blue dots) that satisfy measured relic density due to $A, H$ resonance is in the region where $m_h$ <121 GeV.

Indeed, a scan over the 19-parameter SUGRA model shows that $\Omega_{\widetilde{Z}_1}h^2$=0.12 value lies in the least probable region [27]. In Fig. 7, the number of models (with bino/wino/higgsino LSP) generated by a linear scan are projected. The majority

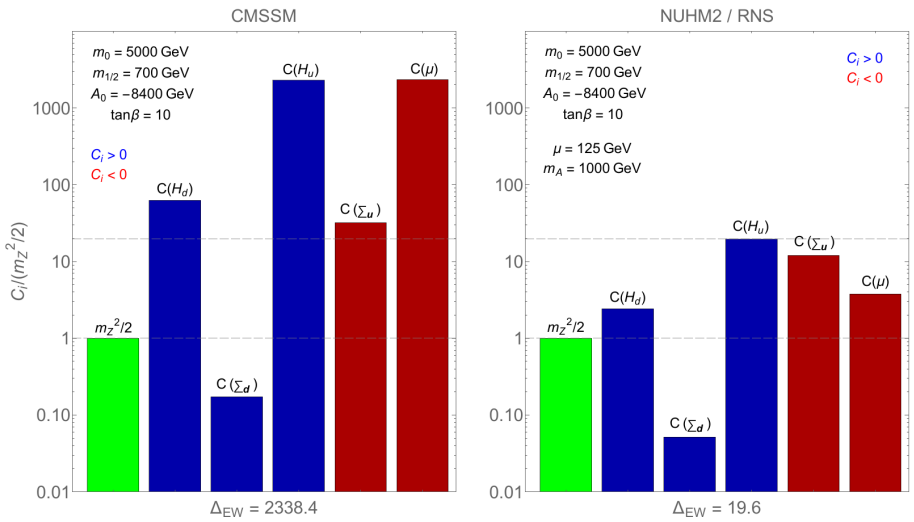


Figure 8: Plot of contributions to $m_Z^2/2$ from a CMSSM and an RNS (NUHM2) model with the same $m_0$, $m_{1/2}$, $A_0$ and $\tan\beta$ values. RNS model has two extra parameters: $\mu = 125$ GeV and $m_A = 1000$ GeV. Red bars denote negative contributions while blue bars denote positive contributions on the right hand side of Eq. (27).

of models contain *over*-produced neutralino LSP; on the other hand, if wino or higgsino is the LSP, the neutralino is *under*-produced and such models form a considerable fraction. In Ref. [27], models that are considered require LEP-II constraints on chargino mass and on Higgs mass $m_h$ >111 GeV which includes 3 GeV theoretical uncertainty of computation.

### I.3.4. NUHM2 Model

The discovery of the Higgs boson at $m_h \simeq$125 GeV disfavor the CMSSM due to the fact that it cannot naturally explain dark matter relic density and has a large $\Delta_{\rm EW}$ value in most of the parameter space, as noted in the previous section. An alternative to CMSSM is the Non-Universal Higgs Mass (NUHM) models [29] where additional free parameters are introduced to CMSSM. With the additional parameters, GUT scale Higgs masses ($m_{H_u}$ and $m_{H_d}$) are not equal to $m_0$.

NUHM2 has $m_{H_u}^2 \neq m_{H_d}^2 \neq {m_0}^2$ at GUT scale. In this model, electroweak

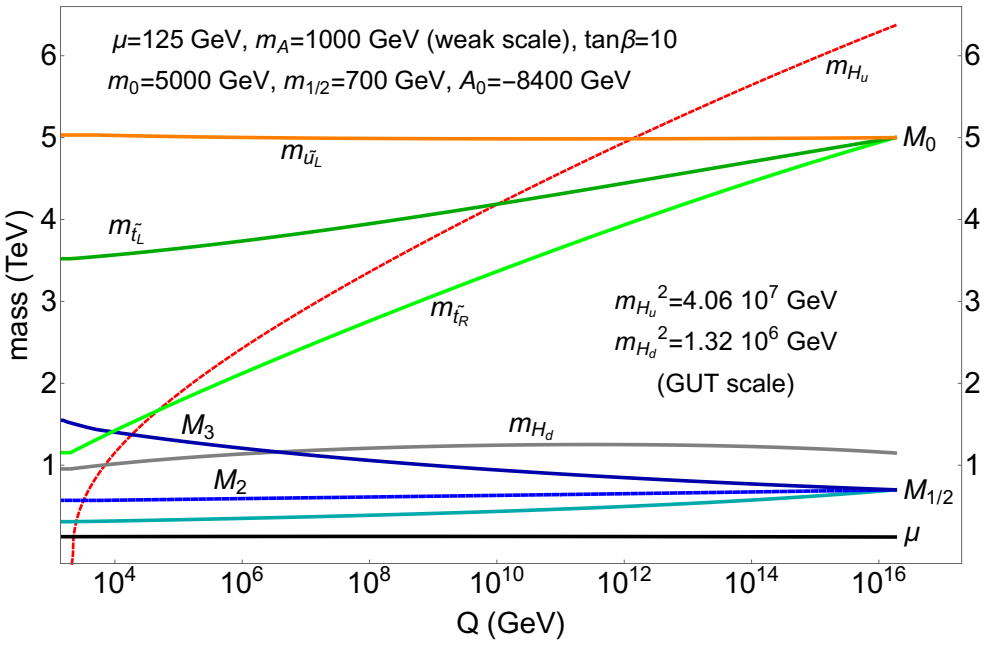


Figure 9: Evolution of soft symmetry-breaking parameters from GUT to weak scale for the RNS benchmark point in Ref. [33].

symmetry is also broken *radiatively* when $m_{H_u}^2$ is driven to negative values due to radiative corrections. Models with radiatively-driven naturalness (RNS) [23], with modest fine-tunings only at the 10% level, occur in NUHM2 models. RNS models are characterized by the presence of light higgsinos with mass $\mu \sim 100-300$ GeV. Fig. 8 shows the comparison of $C_i$ values in Eq. (28) between a CMSSM and an RNS benchmark point with same $m_0$, $m_{1/2}$, $A_0$ and $\tan\beta$ values. For CMSSM, the value of $\mu^2$ is fine-tuned so that a large, unnatural cancellation occurs between $\mu^2$ and $m_{H_u}^2$ to gain a $Z$ mass right at 91.2 GeV in Eq. (27). As a consequence; $\Delta_{\rm EW}$ in CMSSM $\gg \Delta_{\rm EW}$ in RNS.

In Fig. 9, the running of the masses from GUT to weak scale for an RNS benchmark point (BP) can be seen explicitly. The benchmark point is chosen so that $\mu$=125 GeV and $m_A$=1000 GeV at the weak scale. $m_{H_u}^2$ crosses zero at a scale $m_{\rm SUSY} \sim \sqrt{m_{\tilde{t_L}} \times m_{\tilde{t_R}}}$ and EW symmetry is *barely* broken. This phenomenon is known as *criticality* [30] and considered as natural in minimal

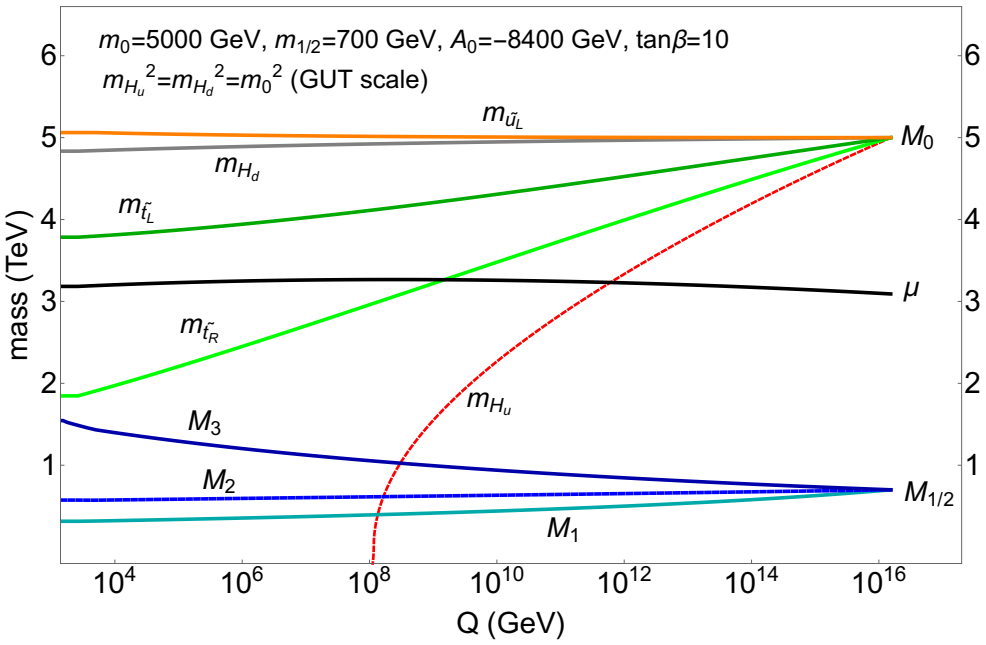


Figure 10: Evolution of soft symmetry-breaking parameters from GUT to weak scale for a generic CMSSM benchmark point.

supergravity [31]. In supersymmetric models with barely broken EW symmetry leading to $m^2_{H_u}(weak) \sim -m^2_Z$, the string landscape statistically favors higher values of soft terms while also the soft terms are anthropically drawn so that $m_{weak} \sim 100 - 200$ GeV [32]. The combined pull on soft terms points to the region where $m_h \simeq 125$ GeV.

In CMSSM where $m^2_{H_u}$=$m^2_{H_d}$=$m_0{}^2$ at GUT scale, the picture is quite different. $m^2_{H_u}$ is driven to negative at a much higher energy scale (see Fig. 10) and the $\mu$ term is at several TeV for the points that satisfy Higgs mass. Neutralino dark matter is mostly bino and overproduced. These models cannot satisfy $\Omega^{std}_{\tilde{Z}_1}h^2 = 0.12$ unless there is an additional moduli field that dilutes the cold dark matter density [34] or the LSP decays via R-parity violating interactions. In RNS models, the higgsino is underproduced. However, this is not a problem but an advantage once the axion is introduced as the second dark matter component. The axion comes along with a solution to the strong CP problem and the SUSY

$\mu$ problem (DFSZ axion). Mixed axion-neutralino dark matter is explored in detail in Ch.III.

## I.4. Peccei-Quinn Symmetry

### I.4.1. Strong CP Problem and PQ Solution

In the QCD sector of the SM, a $U(2)_L \times U(2)_R$ chiral symmetry of the light quark sector can be recast as $U(2)_V \times U(2)_A$ (Vector $\times$ Axial). The vector symmetry gives familiar nuclear isospin and baryon number conservation while rank 4 $U(2)_A$ is spontaneously broken and should give rise to *four* (not *three*) Goldstone bosons (or four pions). This is known as the $U(1)_A$ problem [35].'t Hooft resolved the problem via discovery of the QCD $\theta$ vacuum which does not respect $U(1)_A$ symmetry [36]. As a consequence, the QCD Lagrangian contains a CP-violating term:

$$\mathcal{L} \ni \bar{\theta}\frac{g_s^2}{32\pi}G_{A\mu\nu}\tilde{G}_A^{\mu\nu} \tag{29}$$

where $\bar{\theta} \equiv \theta + arg\ det(M)$ and $M$ is the quark mass matrix. Measurements of the neutron electric dipole moment (EDM) imply that $\bar{\theta} \ll 10^{-10}$ leading to a huge fine-tuning in $\bar{\theta}$; this is known as the strong CP problem. The strong CP problem is solved by introducing Peccei-Quinn (PQ) symmetry [37] and the concomitant axion field $a$ [38]. Peccei and Quinn showed that the $G\tilde{G}$ term dynamically settles to zero when $U(1)_{\rm PQ}$ is broken. Weinberg and Wilczek pointed out that there must be an associated Nambu-Goldstone boson for the broken symmetry: the axion, $a$. The effective axion-gluon-gluon interaction is given by:

$$\mathcal{L}_{eff} \ni \bar{\theta}\frac{g_s^2}{32\pi}G_{A\mu\nu}\tilde{G}_A^{\mu\nu} + C_a\frac{a}{f_a}\frac{g_s^2}{32\pi}G_{A\mu\nu}\tilde{G}_A^{\mu\nu} \tag{30}$$

where $C_a$ is a model dependent constant and $f_a$ is the axion decay constant. Color anomaly factors have been absorbed in $C_a/f_a$ for now. The effective potential is minimized by:

$$\langle a \rangle = -\bar{\theta}\frac{f_a}{C_a} \implies \bar{\theta} = -\frac{\langle a \rangle C_a}{f_a} \tag{31}$$

So when the axion acquires its vacuum expectation value, $G\tilde{G}$ term vanishes to all orders. The $U(1)_{\rm PQ}$ breaking mechanism is studied in detail in Sect.III.1.3. Two well-known examples of PQ models are the DFSZ (Dine-Fischler-Srednicki-Zhitnitsky) [39] and the KSVZ (Kim-Shifman-Vainshtein-Zakharov) [40] axion models. In the Peccei-Quinn augmented MSSM (PQMSSM), the axion superfield is defined as [42]:

$$A = \frac{1}{\sqrt{2}}(s + ia) + \sqrt{2}\theta\tilde{a} + \theta^2 F_a \tag{32}$$

where $a$ is the axion field, $\tilde{a}$ is spin-$\frac{1}{2}$ fermionic partner of axion called *axino* and $s$ is the spin-0 *saxion* field. In gravity mediation, $m_{\tilde{a}}$ and $m_s$ are both expected to be of order of $m_{3/2}$. WIMPs are produced thermally and also produced via production and subsequent decay of both axinos and saxions. For the purpose of this study, supersymmetric versions of the two models (SUSY DFSZ and SUSY KSVZ) are briefly described in the next two sections.

### I.4.2. SUSY DFSZ Model

The DFSZ model is an extension of the SM with two Higgs doublets augmented with a SM *singlet field* where Higgs fields carry PQ charges. In the SUSY DFSZ model, Higgs doublet *superfields* carry PQ charges (so the SUSY $\mu$ term is in fact forbidden) [41]:

$$W_{\rm DFSZ} \ni \lambda\frac{S^2}{M_{Pl}}H_u H_d \tag{33}$$

where $S$ is a *singlet superfield* charged under PQ symmetry. Under PQ symmetry breaking, $S$ receives a *vev*, $\langle S \rangle \sim v_{\rm PQ}$ so that an effective $\mu$ term is generated with:

$$\mu \sim \lambda \, v_{\rm PQ}^2 / M_{Pl} \tag{34}$$

where $v_{\rm PQ}$ is the PQ symmetry-breaking scale with $v_{\rm PQ} \sim 10^{10-12}$ GeV. The axion supermultiplet couples to Higgs fields with an interaction:

$$\mathcal{L}_{\rm DFSZ} = \int d^2\theta (1 + B\theta^2) \mu e^{c_H A / v_{\rm PQ}} H_u H_d, \tag{35}$$

where $c_H$ is the PQ charge of the Higgs bilinear operator and $c_H$=2 since $H_u$ and $H_d$ both carry a PQ charge +1 and $(1 + B\theta^2)$ is a SUSY-breaking spurion field [44]. The spurion parametrizes the effect of SUSY-breaking and the $\theta$ are anti-commuting superspace coordinates. In the SUSY DFSZ model, axino (or saxion) thermal production rate is proportional to [43]:

$$\langle \sigma_{(I+J \to \tilde{a}(s)+\cdots)} v \rangle \propto \left( \frac{\mu}{f_a} \right)^2 \frac{M^2}{T^4} K_2 \left( M/T \right) \tag{36}$$

where $K_2$ is the modified Bessel function of the second kind and $M$ is the threshold energy for the process (either Higgsino or axino/saxion mass). The production is maximal at $T \simeq M/3$ so the axino-saxion yield is *independent* of $T_R$ ($T_R \gg M$). Couplings in the SUSY DFSZ model can be extracted by integrating out Eq. (35).

Possible saxion decay channels in this model with approximate decay widths are (domain wall number, $N_{\rm DW} = 1$ for simplicity) [44]:

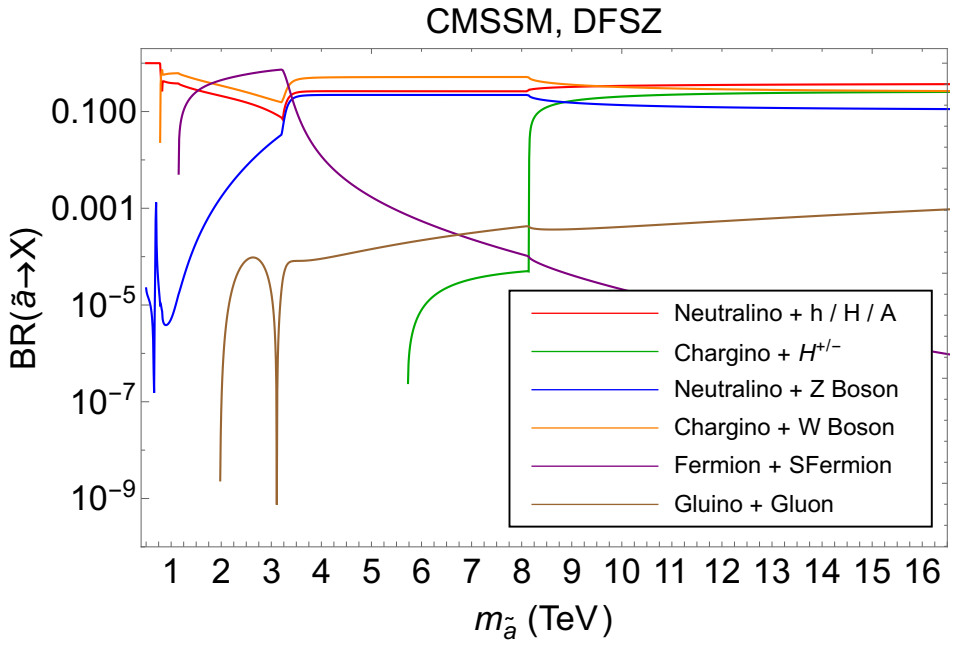


(a)

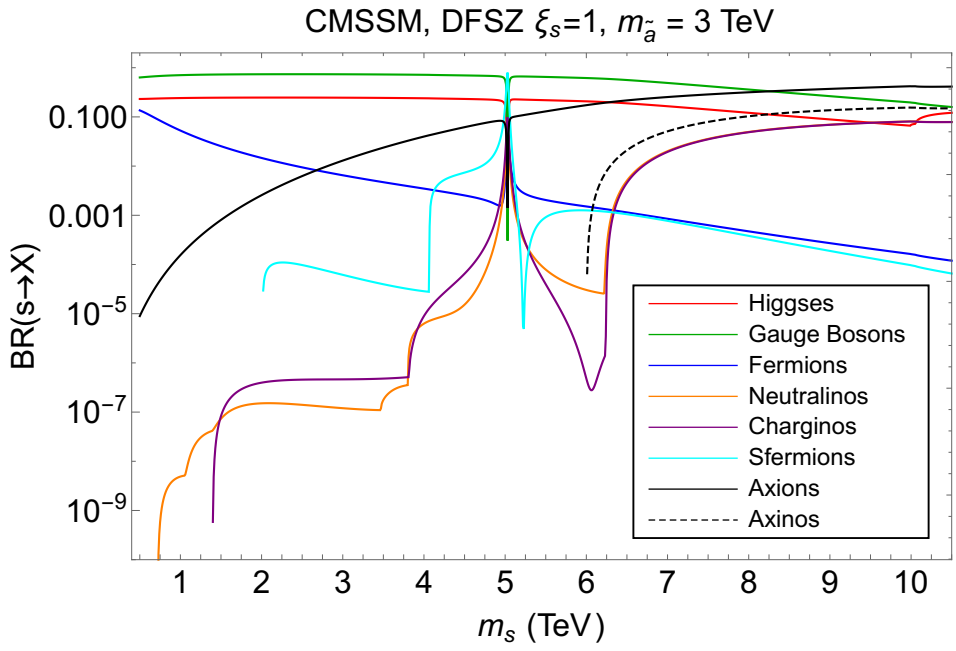


(b)

Figure 11: (a) Axino and (b) Saxion branching fractions in SUSY DFSZ model for the CMSSM benchmark point (with parameters listed in Appendix A.2.)

- $s \to hh$ / $HH$ / $hH$ / $AA$ / $H^+H^-$ (Higgs pairs):

$$\begin{aligned}
\Gamma(s \to hh) &\approx \frac{c_H^2}{8\pi}\frac{\mu^4}{f_a^2}\left(1 - \frac{m_A^2\cos^2\beta}{\mu^2}\right)^2 \frac{1}{m_s}, \\
\Gamma(s \to HH) &\approx \frac{c_H^2}{8\pi}\frac{\mu^4}{f_a^2}\left(1 + \frac{m_A^2\cos^2\beta}{\mu^2}\right)^2 \frac{1}{m_s}, \\
\Gamma(s \to hH) &\approx \frac{c_H^2}{16\pi}\left(\frac{m_A^2\cos\beta}{f_a}\right)^2 \frac{1}{m_s}, \\
\Gamma(s \to H^+H^-) &\simeq 2 \times \Gamma(s \to AA) \\
&\approx \frac{c_H^2}{4\pi}\frac{\mu^4}{f_a^2}\left(1 + \frac{m_A^2\cos^2\beta}{\mu^2}\right)^2 \frac{1}{m_s}.
\end{aligned}$$

- $s \to ZZ$ / $W^+W^-$ / $ZA$ / $W^+H^-$/ $W^-H^+$

  (gauge bosons / $Z$ + pseudo scalar Higgs/ $W$ + charged Higgs):

$$\begin{aligned}
\Gamma(s \to W^+W^-) &\simeq 2 \times \Gamma(s \to ZZ) \\
&= \frac{c_H^2}{4\pi}\frac{\mu^4}{f_a^2}\left(1 - \frac{m_A^2\cos^2\beta}{\mu^2}\right)^2 \frac{1}{m_s}, \\
\Gamma(s \to W^+H^-) &= \Gamma(s \to W^-H^+) \simeq \Gamma(s \to ZA) \approx \frac{c_H^2}{8\pi}\frac{m_A^4\cos^2\beta}{f_a^2}\frac{1}{m_s}.
\end{aligned}$$

- $s \to f\bar{f}$ (quark + antiquark):

$$\Gamma(s \to f\bar{f}) \approx \frac{N_c}{2\pi}\frac{c_H^2 m_f^2}{f_a^2}\frac{\mu^4}{m_s^3}\left(1 - \frac{m_A^2\cos^2\beta}{2\mu^2}\right)^2.$$

- $s \to \widetilde{Z}_i\widetilde{Z}_j$ / $\widetilde{W}_i\widetilde{W}_j$ (neutralino or chargino pairs):

$$\begin{aligned}
\Gamma(s \to \widetilde{Z}_i\widetilde{Z}_j) &\approx \frac{c_H^2}{32\pi}\left(\frac{\mu}{f_a}\right)^2 m_s, \\
\Gamma(s \to \widetilde{W}_i\widetilde{W}_j) &\approx \frac{c_H^2}{32\pi}\left(\frac{\mu}{f_a}\right)^2 m_s.
\end{aligned}$$

- $s \to \tilde{f}\tilde{f}$ (squarks):

$$\Gamma(s \to \tilde{f}\tilde{f}) \approx \frac{N_c}{\pi}\frac{c_H^2\mu^4}{f_a^2}\frac{m_f^4}{m_s^5}\left(1 - \frac{m_A^2\cos^2\beta}{2\mu^2}\right)^2.$$

- $s \to aa$ / $\tilde{a}\tilde{a}$ (axions / axinos):

$$\begin{aligned}\Gamma(s \to aa) &= \frac{\xi^2 m_s^3}{32\pi f_a^2}, \\ \Gamma(s \to \tilde{a}\tilde{a}) &= \frac{\xi^2}{4\pi}\frac{m_{\tilde{a}}^2 m_s}{f_a^2}\left(1 - 4\frac{m_{\tilde{a}}^2}{m_s^2}\right)^{3/2}.\end{aligned}$$

- $s \to \tilde{g}\tilde{g}/gg$ (gluinos / gluons) [45, 46]:

$$\begin{aligned}\Gamma(s \to \tilde{g}\tilde{g}) &= \frac{\alpha_s^2 m_s m_{\tilde{g}}^2}{4\pi^3 f_a^2}\left(1 - \frac{4m_{\tilde{g}}^2}{m_s^2}\right)^{3/2}, \\ \Gamma(s \to gg) &= \frac{\alpha_s^2 m_s^3}{16\pi^3 f_a^2}.\end{aligned}$$

Similarly, axino-higgsino mixing from the superpotential (Eq. (35)) result in axino trilinear couplings. Axino decay channels and decay widths are given by [44]:

- $\tilde{a} \to \widetilde{Z}_i h$ / $\widetilde{Z}_i H$ / $\widetilde{Z}_i A$ (neutralino + Higgs) in the heavy axino limit $m_{\tilde{a}} \gg \mu$:

$$\Gamma(\tilde{a} \to \widetilde{Z}_i\phi) \approx \frac{3c_H^2}{16\pi}\left(\frac{\mu}{f_a}\right)^2 m_{\tilde{a}},$$

  where $\phi = h,\ H$ and $A$.

- $\tilde{a} \to \widetilde{W}_i^{\pm}H^{\mp}$ (chargino + Higgs):

$$\Gamma(\tilde{a} \to \widetilde{W}_i^{\pm}H^{\mp}) \approx \frac{c_H^2}{8\pi}\left(\frac{\mu}{f_a}\right)^2 m_{\tilde{a}}$$

  (in the heavy axino limit).

- $\tilde{a} \to \widetilde{Z}_i Z$ / $\widetilde{W}_i^{\pm} W^{\mp}$ (neutralino + $Z$ boson / chargino + $W$ boson):

$$\begin{aligned} \Gamma(\tilde{a} \to \widetilde{Z}_i Z\ ) &\approx \frac{c_H^2}{16\pi}\left(\frac{\mu}{f_a}\right)^2 m_{\tilde{a}}, \\ \Gamma(\tilde{a} \to \widetilde{W}_i^{\pm} W^{\mp}) &\approx \frac{c_H^2}{8\pi}\left(\frac{\mu}{f_a}\right)^2 m_{\tilde{a}}. \end{aligned}$$

- $\tilde{a} \to \tilde{f} f$ (squark + quark):

$$\Gamma(\tilde{a} \to \tilde{f}\bar{f} + \bar{\tilde{f}} f) \approx \frac{N_c}{16\pi}\frac{c_H^2 \mu^4}{f_a^2}\frac{m_f^2}{m_{\tilde{a}}^3}\left(1 + \frac{m_{\tilde{a}}}{\mu \tan\beta}\right)^2.$$

- $\tilde{a} \to g\tilde{g}$ (gluon + gluino):

$$\Gamma_{\tilde{a}\to g\tilde{g}} = \frac{\alpha_s^2}{8\pi^3 f_a^2} m_{\tilde{a}}^3 \left(1 - \frac{m_{\tilde{g}}^2}{m_{\tilde{a}}^2}\right)^3.$$

Axino and saxion branching fractions in the SUSY DFSZ model for the CMSSM BP (main parameters are listed in the Les Houches output in Appendix A.2.) are shown in Fig. 11.

The DFSZ model has the advantage over the KSVZ model in the context of *natural* SUSY by introducing a solution to SUSY $\mu$ problem and a solution to little hierarchy problem. Moreover, axino and saxion productions are *independent* of the reheat temperature.

### I.4.3. SUSY KSVZ Model

In the SUSY KSVZ model, a heavy PQ charged quark multiplet pair, $Q$ and $Q^c$ with mass $m_Q$, are coupled to a singlet $S$:

$$W_{\rm KSVZ} \ni \lambda\ S\ QQ^c \tag{37}$$

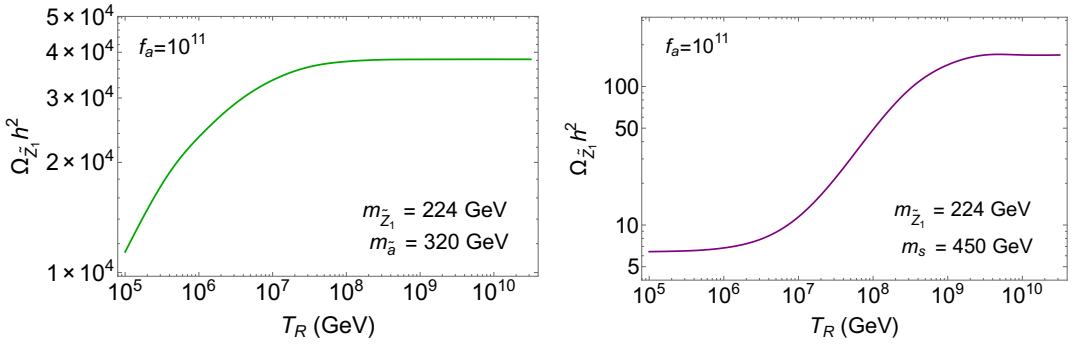


(a) (b)

Figure 12: $\Omega_{\widetilde{Z}_1}h^2$ vs. $T_R$ in PQMSSM (a) with only axino decay to neutralino (b) with only saxion to neutralino. $\Omega^{std}_{\widetilde{Z}_1}h^2 = 6.8$ without PQ sector.

After PQ symmetry breaking, the heavy quark acquires a mass $m_Q \simeq \lambda\, v_{\rm PQ}/\sqrt{2}$. In the SUSY KSVZ model, the thermal production rate of the axino is proportional to the reheat temperature [47, 48] for $m_{\tilde{a}} \ll m_{\tilde{g}}$. The reheat temperature dependent axino and saxion thermal production rates are given by [13] :

$$\begin{aligned}\frac{\rho^{\rm TP}_{\tilde{a}}}{s} &\simeq \quad 0.9\times 10^{-5} g_s^6 \ln\left(\frac{3}{g_s}\right)\left(\frac{10^{12}\ {\rm GeV}}{f_a}\right)^2\left(\frac{T_R}{10^8\ {\rm GeV}}\right) m_{\tilde{a}} \\ \frac{\rho^{\rm TP}_{s}}{s} &\simeq \ 1.3\times 10^{-5} g_s^6 \ln\left(\frac{1.01}{g_s}\right)\left(\frac{10^{12}\ {\rm GeV}}{f_a}\right)^2\left(\frac{T_R}{10^8\ {\rm GeV}}\right) m_{s}\end{aligned} \tag{38}$$

Due to axino-gluino-gluon and saxion-gluon-gluon couplings, even at low $f_a$, the neutralino can be *over*-produced at sufficiently high $T_R$ due to $\tilde{a} \to \widetilde{Z}_1 + Z/\gamma$ and $s \to \widetilde{Z}_1 + Z_j$ decays. In Fig. 12, the neutralino dark matter density enhanced by axino decays only in frame *a*) and saxion decays only in frame *b*) as a function of reheat temperature is shown for $f_a = 10^{11}$ GeV. Without axino decays, neutralino (bino-like) DM density is $\Omega^{std}_{\widetilde{Z}_1}h^2 = 6.8$. In Fig. 12 axino (saxion) mass, $m_{\tilde{a}}$ ($m_s$) is chosen so that only $\tilde{a} \to \widetilde{Z}_1 + Z$ ($s \to \widetilde{Z}_1 + \widetilde{Z}_1$) is allowed in order to show the maximum contribution to DM density. At $f_a = 10^{11}$ GeV, the thermally produced saxion starts contributing the neutralino DM at $T_R \simeq 10^6$ GeV.

The axino decays in SUSY KSVZ model are:

- $\tilde{a} \to \widetilde{Z}_i\gamma$ / $\widetilde{Z}_i$ $Z$ (neutralino + $\gamma$ / neutralino + $Z$ boson)
- $\tilde{a} \to \widetilde{W}_i^{\mp}W^{\pm}$ (chargino + $W$ boson)
- $\tilde{a} \to g\tilde{g}$ (gluon + gluino)

Typically, $\tilde{a} \to g\tilde{g}$ dominates if kinematically allowed. The saxino decays are:

- $s \to W^+W^-$ ($W$ bosons)
- $s \to ZZ$ ($Z$ bosons)
- $s \to \gamma\gamma$ (gamma pair)
- $s \to \gamma Z$ (gamma + $Z$ boson)
- $s \to \widetilde{Z}_i\widetilde{Z}_j$ / $\widetilde{W}_i\widetilde{W}_j$ (neutralino or chargino pairs)
- $s \to aa$ / $\tilde{a}\tilde{a}$ (axions / axinos)
- $s \to \tilde{g}\tilde{g}/gg$ (gluinos / gluons)

Saxion and axino branching fractions in the SUSY KSVZ model for the CMSSM benchmark point are shown in Fig. 13. Plots are for a KSVZ model with $SU(2)_L$ singlet heavy quark states so that the axion superfield only has interactions with $SU(3)_c$ and $U(1)_Y$ gauge superfields, hence the axino does not decay to a chargino pair. The coupling $\xi_s$ defined in Eq. (58), plays a crucial role in determining the dominant decay mode in saxion decays. Typically in the SUSY KSVZ model, the decays $s \to \tilde{g}\tilde{g}$ or $s \to gg$ are dominant for $\xi_s \ll 1$ [49]. In Fig. 13, $\xi_s = 1$ so $s \to \tilde{a}\tilde{a}$ (when kinematically allowed) and $s \to aa$ are the dominant decay modes.

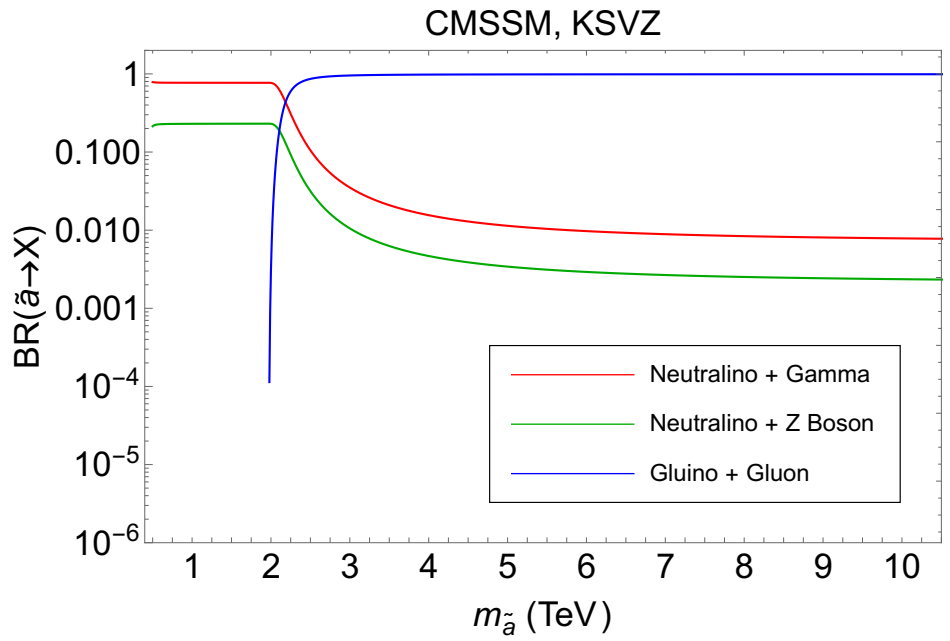


(a)

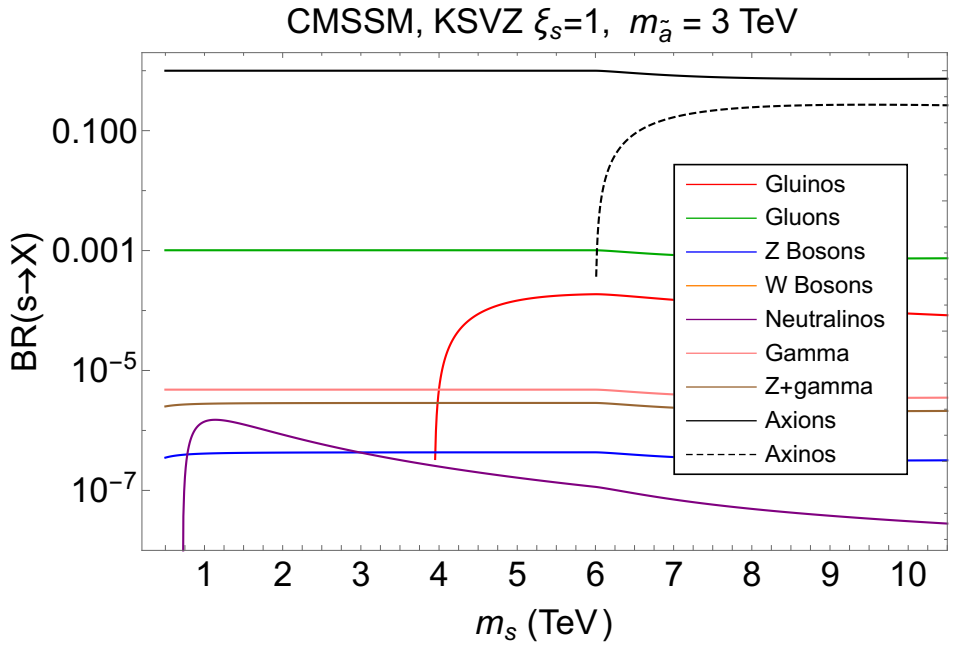


(b)

Figure 13: (a) Axino and (b) Saxion branching fractions in SUSY KSVZ model with the CMSSM benchmark point.

# II. Radiatively Broken PQ Symmetry

## II.1. SUSY $\mu$ Problem & Little Hierarchy

The supersymmetric $\mu$ term in the superpotential gives mass to the Higgs and higgsinos, and it is naively expected to be at the order of GUT or reduced Planck scale. Since $W$ and $Z$ boson masses are at around $\sim$100 GeV, phenomenologically the $\mu$ term should be roughly of order $10^2$ GeV, not bigger than $10^3$ GeV in order to allow a Higgs *vev* at the weak scale without miraculous cancellations between $\mu^2$ and soft symmetry-breaking terms [10] on the right hand side of the Eq. (27). The puzzle is called the "SUSY $\mu$ problem". Solutions that have been proposed to the problem work in a similar way; the $\mu$ term is forbidden at tree-level before supersymmetry breaking and then arises from *vev*s of some new fields. There are three popular solutions to the problem: 1. Next-to-Minimal Supersymmetric Standard Model (NMSSM) [50], 2. Giudice-Masiero [51] and 3. Kim-Nilles solution [41].

– NMSSM is an extension of the MSSM, with an additional superfield $\hat{S}$ coupled to Higgs doublets superfields:

$$\hat{f}_{\rm NMSSM} \ni \lambda_S \hat{S} \hat{H}_u \hat{H}_d \ . \tag{39}$$

The $\mu$ term arises when $\hat{S}$ develops a *vev*, $v_S$:

$$\mu = \lambda_S \ v_S \ . \tag{40}$$

However, introducing a new singlet to MSSM is problematic. Such singlets may precipitate the formation of domain walls in the early Universe

and tadpoles associated with the singlets may reintroduce quadratic divergences [53].

– In the Giudice-Masiero solution, some unknown symmetry forbids the SUSY $\mu$ term but the Higgs doublets are coupled to a hidden sector field, $\hat{h}$ in the Kahler potential:

$$K \ni \lambda_h \hat{h} \frac{\hat{H}_u \hat{H}_d}{M_{Pl}} \ . \tag{41}$$

The F-component of $\hat{h}$ develops a $vev$, $v_h \sim m^2_{hidden} \sim m_{3/2} \times M_{Pl}$ so the $\mu$ term arises as $\mu \simeq \lambda_h m_{3/2}$.

– In the Kim-Nilles solution, PQ charges of -1 are assigned to Higgs doublets $\hat{H}_u$ and $\hat{H}_d$ which forbids the usual $\mu$ term but coupled to a PQ charged superfield, $X$ in the superpotential:

$$\hat{f}_{\rm KN} \ni \lambda_\mu \frac{\hat{X}^2}{M_{Pl}} \hat{H}_u \hat{H}_d \tag{42}$$

where PQ charge of the field $\hat{X}$, $q_X$ is +1. In order to break the PQ symmetry, the superpotential also includes the term [52]:

$$\hat{f}_{\rm KN} \ni \lambda_Z \hat{Z}(\hat{X}\hat{Y} - v^2_{\rm PQ}/2) \tag{43}$$

which causes scalar components $\phi_X$ and $\phi_Y$ to gain $vev$s of order $v_{\rm PQ}/\sqrt{2}$. The Kim-Nilles solution is indeed the supersymmetrized version of the DFSZ axion model. The $\mu$ term is calculated to be $\mu \simeq \lambda_\mu \frac{v^2_{\rm PQ}}{2M_{Pl}}$.

Among these solutions, Kim-Nilles has the advantage in solving the strong CP problem and in generating a weak-scale SUSY $\mu$ term which is required for light higgsinos. However, in this solution there is an apparent hierarchy:

$\mu \ll m_{soft} (\sim m_{3/2}$ in gravity mediation) which is the hierarchy between multi-TeV SUSY particle masses and the masses of $Z$, $W^{\pm}$, $h$ and $\mu$. The *little hierarchy* is characterized by:

$$\mu \sim m_Z \ll m_{3/2} \sim \text{multi} - \text{TeV} \tag{44}$$

but actually it emerges quite naturally due to a mis-match between PQ breaking scale and hidden sector mass scale $f_a \ll m_{\text{hidden}}$. In the next chapter, a model that exhibits this behavior is studied in detail.

## II.2. MSY Model

A model which gives a solution for the SUSY $\mu$ problem and generates a little hierarchy was proposed by Murayama, Suzuki and Yanagida (MSY) [54]. In the MSY model, the PQ symmetry is broken radiatively and $\mu \ll m_{soft}$ emerges quite naturally from a mismatch between PQ and hidden sector intermediate scales $v_{\text{PQ}} \ll m_{hidden}$. The PQ breaking mechanism is similar to EWSB in the MSSM where $m_{H_u}^2$ is driven to negative values. In the MSY model, the mass term $m_X^2$ for the PQ charged field $X$ is radiatively driven to negative values resulting in breaking of PQ symmetry radiatively (RadPQB). The MSY model assumes a MSSM superpotential of the form:

$$\begin{aligned} \hat{f}_{\text{MSSM}} = \sum_{i,j=1,3} [&(\mathbf{f}_u)_{ij} \epsilon_{ab} \hat{Q}_i^a \hat{H}_u^b \hat{U}_j^c + (\mathbf{f}_d)_{ij} \hat{Q}_i^a \hat{H}_{da} \hat{D}_j^c \\ &+ (\mathbf{f}_e)_{ij} \hat{L}_i^a \hat{H}_{da} \hat{E}_j^c + (\mathbf{f}_\nu)_{ij} \epsilon_{ab} \hat{L}_i^a \hat{H}_u^b \hat{N}_j^c] \end{aligned} \tag{45}$$

where the $\hat{N}_i^c$ are the SM gauge singlet fields containing right-handed neutrinos. For matter and Higgs fields, PQ charges are assumed to be $1/2$ and $-1$ respectively. The MSSM superpotential is augmented by new PQ charged fields $\hat{X}$ and

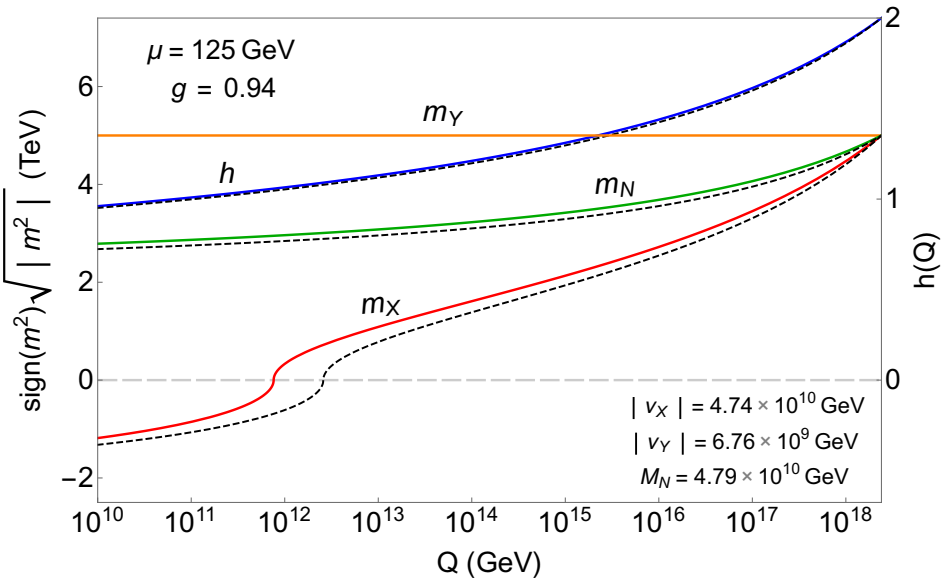


Figure 14: Plot of the running values of various soft terms and couplings versus energy scale for $h = 2$ with a common value of SUSY-breaking parameters, $m_X = m_Y = m_{N_i^c} = A_i = 5$ TeV. Black dashed lines show RG evolution without the 2-loop corrections.

$\hat{Y}$ with charges $-1$ ($\hat{X}$) and $+3$ ($\hat{Y}$):

$$\hat{f}' = \frac{1}{2}h_{ij}\hat{X}\hat{N}_i^c\hat{N}_j^c + \frac{f}{M_P}\hat{X}^3\hat{Y} + \frac{g}{M_P}\hat{X}\hat{Y}\hat{H}_u\hat{H}_d \ . \tag{46}$$

The last term in Eq. (46) gives the Kim-Nilles solution [41] to the $\mu$ problem as discussed in the previous section. The MSY model introduces a dynamical mechanism to gain *vevs* whereas in the KN solution there is no such mechanism. In the MSY model, a diagonal RH soft-breaking sneutrino mass matrix can be assumed: $h_{ij} = h_i\delta_{ij}$ and $h_i$'s are set to be equal $h_1 = h_2 = h_3 \equiv h$ for simplicity. The corresponding soft SUSY-breaking terms are given by:

$$\begin{aligned} V_{\rm soft} = \ & m_X^2|\phi_X|^2 + m_Y^2|\phi_Y|^2 + m_{N_i^c}^2|\phi_{N_i^c}|^2 \\ & + (\frac{1}{2}h_iA_i\phi_{N_i^c}^2\phi_X + \frac{f}{M_P}A_f\phi_X^3\phi_Y + \frac{g}{M_P}A_gH_uH_d\phi_X\phi_Y + h.c.) \end{aligned} \tag{47}$$

From these, the two-loop RGEs are calculated [55] following general formulae in Ref. [56]:

$$
\begin{aligned}
\frac{dh_i}{dt} =& \frac{h_i}{(4\pi)^2}(2|h_i|^2 + \frac{1}{2}\sum_j |h_j|^2) \\
& - \frac{h_i}{(4\pi)^4}(2|h_i|^4 + \sum_j |h_j|^4 + |h_i|^2 \sum_j |h_j|^2) \\
\frac{dA_i}{dt} =& \frac{2}{(4\pi)^2}(2|h_i|^2 A_i + \frac{1}{2}\sum_j |h_j|^2 A_j) \\
& - \frac{4}{(4\pi)^4}(2|h_i|^4 A_i + \sum_j |h_j|^4 A_j + \frac{1}{2}|h_i|^2 A_i \sum_j |h_j|^2 + \frac{1}{2}|h_i|^2 \sum_j |h_j|^2 A_j) \\
\frac{dm_X^2}{dt} =& \frac{1}{(4\pi)^2}\sum_i |h_i|^2 (m_X^2 + 2m_{N_i^c}^2 + |A_i|^2) \\
& - \frac{4}{(4\pi)^4}\sum_i |h_i|^4 (m_X^2 + 2m_{N_i^c}^2 + 2|A_i|^2) \\
\frac{dm_Y^2}{dt} =& \, 0 \\
\frac{dm_{N_i^c}^2}{dt} =& \frac{2|h_i|^2}{(4\pi)^2}(2m_{N_i^c}^2 + m_X^2 + |A_i|^2) \\
& - \frac{4|h_i|^4}{(4\pi)^4}(2m_{N_i^c}^2 + m_X^2 + 2|A_i|^2) - \frac{|h_i|^2}{(4\pi)^4}(2m_{N_i^c}^2 \sum_j |h_j|^2 + 2m_X^2 \sum_j |h_j|^2 \\
& + 2\sum_j m_{N_j^c}^2 |h_j|^2 + 2A_i \sum_j A_j |h_j|^2 + \sum_j |h_j|^2 |A_j|^2 + |A_i|^2 \sum_j |h_j|^2)
\end{aligned}
\tag{48}
$$

where $t = \ln(Q/M_{Pl})$. The first line of each equation corresponds to 1-loop RG evolution only and the remaining terms arise from 2-loop corrections. The effect of 2-loop corrections is shown in Fig. 14.

The essential feature of RadPQB models: $m_X^2$ gets driven radiatively to negative values when the couplings and soft terms are evolved from $Q = M_{Pl}$, the reduced Planck scale ($M_{Pl} \simeq 2.4 \times 10^{18}$ GeV) down to the scale $Q \sim v_{\rm PQ}$ of PQ

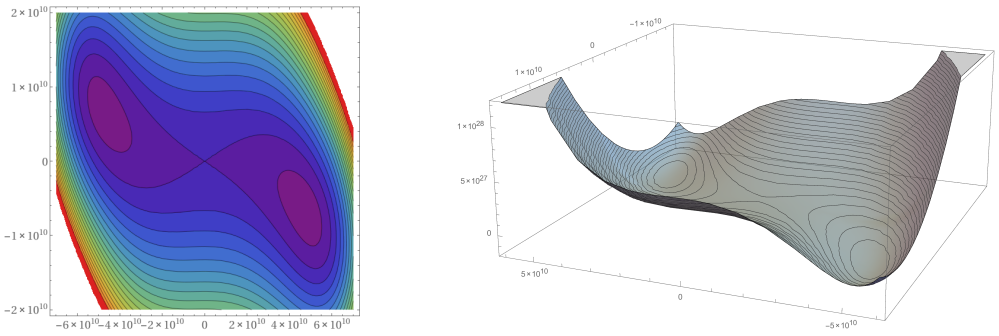

(a) (b)

Figure 15: Plot of the scalar potential $V$: (a) minima on $v_X$ vs $v_Y$ plane (b) 3-d plot of the potential $V$.

symmetry breaking. The relevant part of the scalar potential is:

$$V_F \ni \frac{|f|^2}{M_P^2}|\phi_X^3|^2 + \frac{9|f|^2}{M_P^2}|\phi_X^2\phi_Y|^2 \ . \tag{49}$$

Augmenting this with $V_{\rm soft}$, the scalar potential $V$ can be minimized at a scale $Q = v_{\rm PQ}$ to find vevs of $\phi_X$ and $\phi_Y$ ($v_X$ and $v_Y$):

$$\begin{aligned} 0 &= \frac{9|f|^2}{M_P^2}|v_X^2|^2 v_Y + f^* \frac{A_f^*}{M_{Pl}} v_X^{*3} + m_Y^2 v_Y \\ 0 &= \frac{3|f|^2}{M_P^2}|v_X^2|^2 v_X + \frac{18|f|^2}{M_P^2}|v_X|^2|v_Y|^2 v_X + 3f^* \frac{A_f^*}{M_P} v_X^{*2} v_Y^* + m_X^2 v_X \end{aligned} \tag{50}$$

The first one may be solved for $v_Y$. Substituting it into the second, the polynomial for $v_X$ can be solved for numerically. The potential has two minima in the $v_X$ and $v_Y$ plane symmetrically located with respect to the origin (see Fig. 15). When the potential develops a minimum, the Majorana neutrino mass scale is generated:

$$M_{N_i^c} = v_X \, h_i|_{Q=v_X} \tag{51}$$

along with the SUSY $\mu$ term:

$$\mu = g\frac{v_X v_Y}{M_{Pl}} \ . \tag{52}$$

After PQ symmetry is broken, the QCD axion field $a$ is the corresponding Goldstone boson of the broken PQ symmetry and is a combination of the phases of the $\phi_X$ and $\phi_Y$ fields. Along with the axion, a corresponding saxion $s$ and axino $\tilde{a}$ with masses $\sim m_{3/2}$ but with superweak couplings suppressed by $1/v_{\rm PQ}$ are generated. Since the $\mu$ term depends on an arbitrary coupling $g$, any desired value of $\mu$ can be obtained by adjusting $g$ for particular $v_X$ and $v_Y$ $vev$s. However, in case $g \gg 1$ or $g \ll 1$, an additional physical scale might be required to explain the $\mu$ term. As shown in Fig. 14, $\mu$ =125 GeV can be generated with $g \simeq 1$ with a common initial value of SUSY-breaking parameters $m_X = m_Y = m_{N_i^c} = A_i = m_{3/2} = 5$ TeV and $h|_{Q=M_{Pl}} = 2$. With such initial conditions, the value of $m_X^2$ is pushed from an initial value of 5 TeV down through zero ($Q \simeq 10^{12}$) to negative values so that PQ symmetry is radiatively broken. Solving the scalar potential minimization conditions, with $f = 1$ and $A_f = -m_{3/2}$, implies values of $v_X = 4.74 \times 10^{10}$ GeV and $v_Y = 6.76 \times 10^9$ GeV. The PQ breaking is generated $v_{\rm PQ} = \sqrt{v_X^2 + v_Y^2} = 4.79 \times 10^{10}$ GeV at an intermediate scale and the axion decay constant is $f_a = \sqrt{v_X^2 + 9v_Y^2} = 5.16 \times 10^{10}$ GeV.

RG running of the critical soft-breaking mass $m_X^2$ versus energy scale $Q$ for several initial values of $m_X = 2$, 5 and 10 TeV are shown in Fig. 16. In the figure, RG runnings with different initial values of $h_i = 2$ (dashed curves) and 4 (solid curves) show that the value of $m_X^2$ gets driven negative at exactly the same value of $Q$ independent of initial soft-breaking masses. The value of $h_i$ at $M_{Pl}$ determines the energy scale at which $m_X^2$ becomes negative. With the conditions assumed here; $m_X = m_Y = m_{N_i^c} = A_i$, $h_{ij} = h_i \delta_{ij}$ and $h_1 = h_2 =$

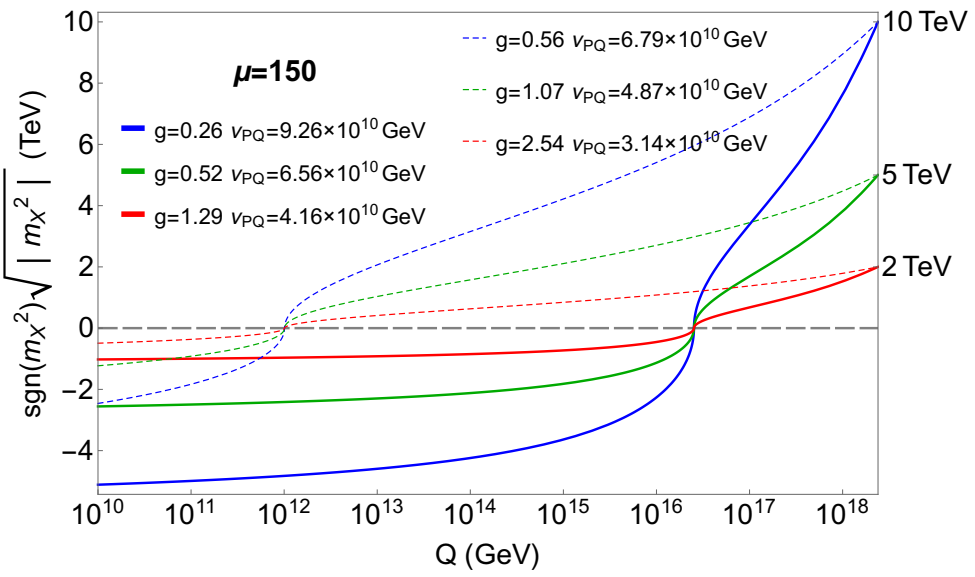


Figure 16: Plot of the running values of $m_X^2$ versus $Q$ for various values of $m_{3/2}$ and $h = 2$ (dashed) and $h = 4$ (solid), taken from Ref. [55].

$h_3 = h$, there occurs a lower bound for $h \simeq 1.7$. However, this is not an ultimate bound. For the non-unified right-handed sneutrino masses, for example, in the chaotic inflationary scenario where the right-handed sneutrino acts as an inflaton field [57], $h_1$ can be as low as $10^{-7}$ with $m_{\widetilde{N}_2} = m_{\widetilde{N}_3} \simeq m_{3/2}$. The relation between the coupling constants $g$ and $h$ for a fixed $\mu$ is shown in Fig. 17. As seen in the figure, the little hierarchy arises naturally with $g \sim 1$ and axion mass $m_a \simeq 600$ $\mu$eV for $m_{3/2} \simeq 5$ -10 TeV in the MSY model.

## II.3. Additional Models with RadPQB

Similar models with RadPQB can be written by coupling the Higgs fields with some combination of PQ-charged $X$ and $Y$ fields to generate the $\mu$ term. In the MSY model, the last term in Eq. (46) leads to $\mu$ when $X$ and $Y$ acquire *vevs*.

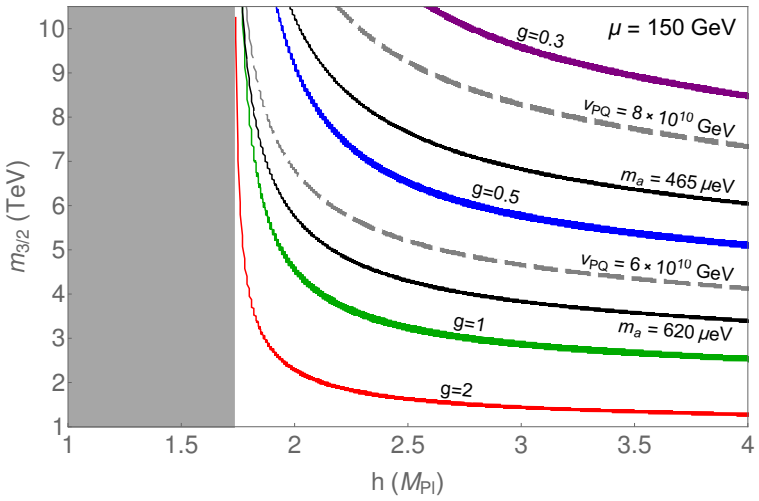


Figure 17: Values of $g$ which are needed to generate $\mu = 150$ GeV in the $h$ vs. $m_{3/2}$ plane. Dashed gray lines and black lines show contours of constant $v_{\rm PQ}$ and axion mass $m_a$, respectively. Plot taken from Ref. [55].

Choi, Chun and Kim (CCK) suggested a model with [58]:

$$W \ni \frac{g_{CCK}}{M_{Pl}} \hat{X}^2 \hat{H}_u \hat{H}_d. \tag{53}$$

Similarly, one can generate $\mu$ term with:

$$W \ni \frac{g_{Y^2}}{M_{Pl}} \hat{Y}^2 \hat{H}_u \hat{H}_d. \tag{54}$$

To summarize, additional terms to the superpotential (45) for the three models with the same RGEs can be written down:

$$\hat{f}' = \frac{1}{2} h_{ij} \hat{X} \hat{N}_i^c \hat{N}_j^c + \frac{f}{M_{Pl}} \hat{X}^3 \hat{Y} + \begin{bmatrix} \frac{g_{MSY}}{M_{Pl}} \hat{X} \hat{Y} \hat{H}_u \hat{H}_d & \to \text{MSY} \\ \frac{g_{CCK}}{M_{Pl}} \hat{X}^2 \hat{H}_u \hat{H}_d & \to \text{CCK} \\ \frac{g_{Y^2}}{M_{Pl}} \hat{Y}^2 \hat{H}_u \hat{H}_d & \to Y^2 \end{bmatrix}. \tag{55}$$

Terms with higher orders of $X$ and $Y$ generate $\mu \gg m_{3/2}$ unless more powers

| multiplet | MSY | CCK | $Y^2$ |
|---|---|---|---|
| $\tilde{H}_u$ | -1 | -1 | -3 |
| $\tilde{H}_d$ | -1 | -1 | -3 |
| $\tilde{Q}$ | +1/2 | +3/2 | +3/2 |
| $\tilde{L}$ | +1/2 | +3/2 | +5/2 |
| $\tilde{U}^c$ | +1/2 | -1/2 | +3/2 |
| $\tilde{D}^c$ | +1/2 | -1/2 | +3/2 |
| $\tilde{E}^c$ | +1/2 | -1/2 | +1/2 |
| $\tilde{N}^c$ | +1/2 | -1/2 | +1/2 |
| $\tilde{X}$ | -1 | +1 | -1 |
| $\tilde{Y}$ | +3 | -3 | +3 |

Table 3: PQ charge assignments for the various superfields of the MSY, CCK and $Y^2$ models.

| | MSY | CCK | $Y^2$ |
|---|---|---|---|
| $m_{3/2}$ (TeV) | 10 | 1.7 | 60 |

Table 4: Comparison of $m_{3/2}$ values that generates $\mu$ =150 GeV with $g = 0.3$ and $h = 3$ using MSY, CCK and $Y^2$ models.

of $M_{Pl}$ are introduced, thus such models can only explain the little hierarchy if the coupling of the term $\hat{X}^3\hat{Y}$ is suppressed by ${M_{Pl}}^n$ where $n > 1$. PQ charge assignments for all three models are listed in Table 3. Compared to the MSY model, the CCK model favors lower $m_{3/2}$ whereas the $Y^2$ model favors higher $m_{3/2}$ values for $g \sim 1$.

In Table 4, the $m_{3/2}$ values from three models that generate $\mu = 150$ GeV with same $g$ and $h$ values are shown. $Y^2$ model can accomodate a rather larger hierarchy between the soft terms and the $\mu$ term compared to the others.

In Fig. 18 $(a)$, several values of $g_{Y^2}$ that generate a $\mu$ term at 150 GeV are shown for the $Y^2$ model. For $g \simeq 1$, $m_{3/2} \simeq 20$ TeV and approaches 40 TeV as $h$ gets closer to 2. In this model, $\mu$ term is proportional to $v_Y^2$ and since $v_Y < v_x$, $g \sim 1$ favors higher $m_{3/2}$ values compared to both MSY ( $\mu \propto v_X v_Y$) and CCK ( $\mu \propto v_X^2$) models. In the region where $g_{Y^2}$ <1.5, axion mass ranges roughly from 175 to 380 $\mu$eV and $f_a$ is between $10^{11}$ GeV and $2\times10^{11}$ GeV.

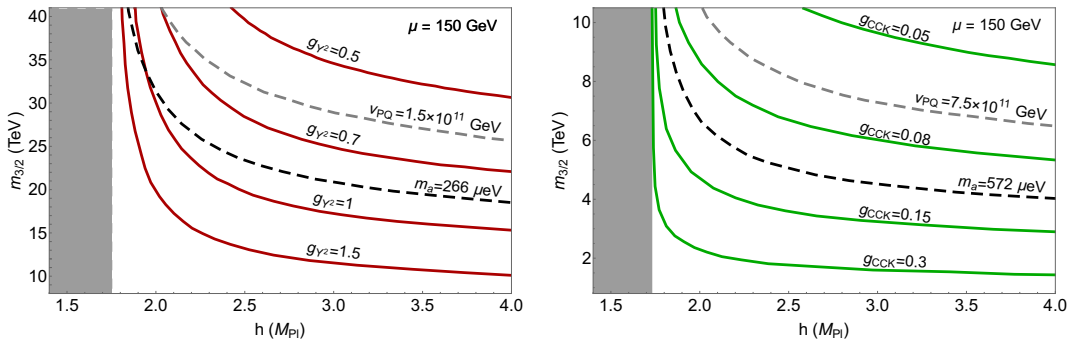


(a) (b)

Figure 18: Values of $g$ which are needed to generate $\mu = 150$ GeV in $Y^2$ model (a) and CCK model (b). Dashed gray lines and black lines show contours of constant $v_{\rm PQ}$ and axion mass $m_a$, respectively.

In Fig. 18 ($b$), the contours of $g_{CCK}$ are shown on the $h_i$ vs. $m_{3/2}$ plane. In the CCK model, $g \sim \mathcal{O}(0.1)$ for $h \simeq 2$. One expects $g$ to be around *unity* to generate $\mu$=150 GeV to avoid fine-tuning and all three models are able to successfully explain weak-scale $\mu$ in natural SUSY models with higgsino-like LSP.

# III. Mixed Axion-Neutralino Dark Matter

## III.1. Calculation

Calculation of mixed axion-neutralino dark matter relic abundance involves numerical solution of eight coupled differential equations. In the following subsections, constraints and additional parameters from PQ symmetry are explained.

### III.1.1.Cosmological Constraints

#### a) Big Bang Nucleosynthesis (BBN)

In the early Universe as temperature drops from $T \sim 1$ GeV to $T \sim 1$ MeV, the balance between neutrons and protons is maintained by the weak interactions [12]:

$$\begin{aligned} n &\longleftrightarrow p + e^- + \tilde{\nu_e}, \\ \nu_e + n &\longleftrightarrow p + e^-, \\ e^+ + n &\longleftrightarrow p + \tilde{\nu_e}. \end{aligned} \tag{56}$$

As the Universe cools down, neutrons and neutrinos are decoupled from the thermal bath (T $\sim$ 1 MeV). The neutron to proton ratio slowly decreases mostly by the dominant free neutron decay. Nucleosynthesis begins with the formation of light elements at T $\sim$ 0.1 MeV, mainly $^4He$ along with smaller quantities of $^3H$,$^3He$,$^7Li$ and $D$, deuterium. At T $\sim$ 0.01 MeV, the synthesis of light elements (Big Bang Nucleosynthesis) reach their equilibrium value.

The predictions of light elements abundance by BBN can be tested by observations of the solar system. The astrophysical data is in good agreement with BBN predictions. With the BBN, the standard cosmology is a valid description of the

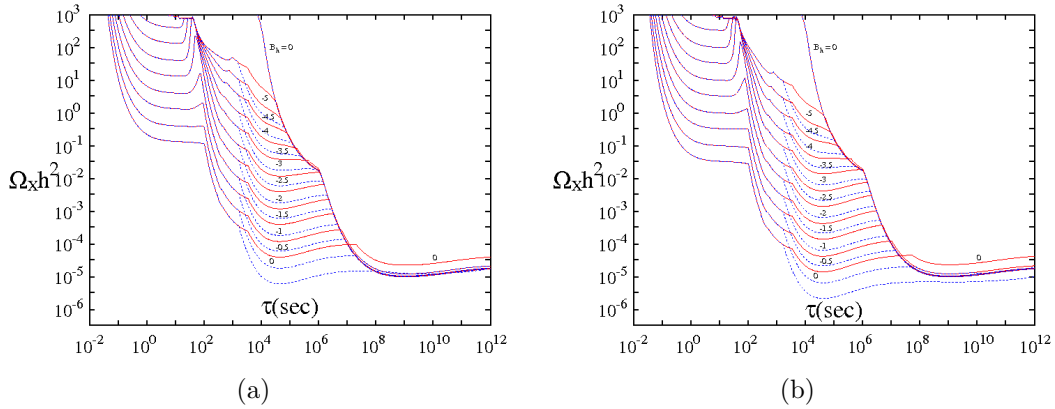


Figure 19: Constraints on the abundance of decaying neutral particle, $X$, as a function of lifetime for (a) a $M_X = 1$ TeV and (b) a $M_X = 100$ GeV particle with varying hadronic branching ratios. Plots are taken from Ref. [59]; refer to the article for details.

Universe from T$\sim$ 10 MeV ($10^{-2}$ sec.) to present. BBN predictions require the radiation-dominated Universe at T$\leq$ 1 MeV. Late-decaying particles with lifetimes ($\tau$) greater than $10^{-2}$ seconds can inject hadrons, photons and electrons into the plasma [59] which affect the nucleosynthesis by destroying light elements and might void the successful BBN calculations. In Ref. [59], BBN constraints on a hypothetical late-decaying neutral particle $X$ are shown as a function of its hadronic branching ratio, lifetime and abundance. If the late-decaying particle has a small branching ratio to hadrons, the constraint is milder. Likewise, if its abundance is small, $\tau_X$ can be as long as $10^4$ seconds or even longer if $\Omega_X h^2 \sim 10^{-6}$ as shown in Fig. 19 where $\Omega_X h^2$ is the would-be abundance of the long-lived particle $X$ had it not decayed.

A critical constraint on the calculation of mixed axion-neutralino dark matter comes from maintaining the success of the BBN. In the calculation, the validity of the results are checked by applying BBN bounds calculated by Jedamzik [59] to axino, saxion and gravitino.

**b) Dark Radiation**

The dark radiation density in the early Universe is parameterized by $N_{\text{eff}}$, number of effective neutrinos which is $\sim$3 in the SM, corresponding to three neutrino flavors. $N_{\text{eff}}$ can also be interpreted as the effective number of relativistic degrees of freedom. The *Planck* Collaboration [5] reported $N_{\text{eff}} = 3.2 \pm 0.5$ by the combined data (95%; *Planck* TT+lowP+lensing+BAO). Attempts to explain $\Delta N_{\text{eff}}$ includes thermalized massless bosons [60] and decaying particles [46, 61, 62]. In PQ augmented scenarios, $s \to aa$ decay gives rise to relativistic axions which form dark radiation [61, 44]. In the early Universe, after the unstable particles (except the axion) have decayed and the neutralino has decoupled from the thermal bath, the excess in dark radiation can be calculated as [49]:

$$\Delta N_{\text{eff}} = \frac{\rho_a(T)}{\rho_\nu} = \frac{\rho_a(T)}{T^4} \frac{120}{7\pi^2} \left(\frac{11}{4}\right)^{4/3}. \tag{57}$$

In the calculation of mixed axion-neutralino dark matter, points are checked whether they respect or not the upper bound for $N_{\text{eff}}$ reported by the *Planck* Collaboration. In Sections III.3 and III.4 points that violate the dark radiation constraint with $\Delta N_{\text{eff}} > 1$, which is excluded at greater than 99% confidence [5], are colored brown.

### III.1.2. PQ Parameters

In addition to the MSSM, PQ symmetry introduces several new parameters:

– $\xi_s$ :

The $s \to aa$ branching ratio is controlled by the axion-saxion effective coupling [63]:

$$\mathcal{L} \ni \frac{\xi_s}{f_a} s \left[(\partial_\mu a)^2 + i\bar{\tilde{a}}\partial\!\!\!/\tilde{a}\right] \tag{58}$$

where $\xi_s$ is a model dependent parameter, which can be small (or even zero) or as large as 1. Saxion decays into axions and axinos are turned off if $\xi_s = 0$ whereas $s \to aa$ and $s \to \tilde{a}\tilde{a}$ decays are allowed for $\xi_s = 1$. Since the saxion decays strongly depend on $\xi_s$, two limiting cases $\xi_s = 0$ and $\xi_s = 1$ are discussed separately in the following sections. The injected axions from saxion decay produce a significant amount of dark radiation ($\xi_s \simeq 1$). If there is no axion injection from saxion decays ($\xi_s = 0$), dark radiation constraints are always satisfied since thermally produced axions give negligible contribution to $\Delta N_{\rm eff}$.

– $f_a$ :

$f_a$ is the axion decay constant, which previously appeared in Chapter II. and in Eq. (58). For small values of $f_a$, axino and saxion couplings to matter [44] are strong enough to decay before the neutralino freeze-out. The initial axion coherent oscillation is proportional to $f_a$. The Peccei-Quinn breaking scale $v_{\rm PQ} \sim f_a$ [1] in most cases; in the Kim-Nilles mechanism $v_{\rm PQ} \sim f_a/\sqrt{2}$ so the $\mu$ term is given by $\mu \simeq \lambda_\mu f_a^2/M_{Pl}$.

– $N_{\rm DW}$ :

$N_{\rm DW}$ is the domain wall number associated with the PQ symmetry breaking [64]. In spontaneously broken symmetries, scalar field $\phi$ takes a vacuum expectation value $v_\phi = \pm\sigma$. The scalar field can make smooth transitions between two points in the ground state. The transition region between two vacua $v_\phi = \pm\sigma$, in this case $v_\phi = 0$, is called a domain wall. Domain walls arise when any discrete symmetry is broken. The number of domain wall

[1] In the literature, for example in Ref's [12, 66] Peccei-Quinn breaking scale (defined as $v_{\rm PQ}$ in this thesis) is denoted by $f_a$.

shapes the axion potential:

$$V(\theta) = m_a^2 \ f_a^2(1 - cos(\theta \ N_{\rm DW})) \tag{59}$$

The potential comes to the original value by a $\theta$ shift of $2\pi/N_{\rm DW}$. In the DFSZ model, quark doublets carry $SU(3)_c$ color charges and with three fermion generations ($N_g = 3$), $N_{\rm DW} = N_g \times 2 = 6$ so the potential has six vacua, whereas in the KSVZ model $N_{\rm DW} = 1$ which corresponds to only one vacuum state.

– $\theta_{i,s}$ :

Initial field values of coherently produced axion (axion$^{\rm CO}$) and saxion (saxion$^{\rm CO}$) are parameterized by $\theta_i = a_0/f_a$ and $\theta_s = s_0/f_a$, respectively. $\theta_i$ is known as the axion misalignment angle ($-\pi \leq \theta_i \leq \pi$) which is constant in our patch of the Universe if the Universe underwent inflation during or after PQ breaking [12]. The relic density of axion$^{\rm CO}$, ignoring possible entropy dilution effects, is given by [65]:

$$\Omega_a^{\rm CO} h^2 \simeq 0.23 f(\theta_i) \theta_i^2 \left( \frac{f_a}{10^{12} \ {\rm GeV}} \right)^{7/6} \tag{60}$$

where $f(\theta_i)$ is the anharmonicity factor, parametrized by Visinelli and Gondolo [66] as $f(\theta_i) = [\ln (e/(1 - \theta_i^2/\pi^2)]^{7/6}$. The misalignment angle is expected to be of order one, but can be small as well [67]. However, the function $f(\theta)$ is very sensitive to small changes in $\theta_i$ for $\theta_i \sim \pi$ since the term $e/(1 - \theta_i^2/\pi^2)$ diverges to infinity. Hence, the parameters that result in $\theta_i > 3$ will be treated as fine-tuned.

– $m_a$ :

The temperature-dependent axion mass is given by [66]:

$$m_a(T) = \begin{cases} 0.018\ m_a|_{T=0}(\frac{200\ \text{MeV}}{T})^4, & T \gtrsim 200\ \text{MeV}, \\ m_a|_{T=0}, & T \lesssim 200\ \text{MeV} \end{cases} \tag{61}$$

which arises through instanton effects. The axion cold DM mass, $m_a \equiv m_a|_{T=0}$ is given by:

$$m_a \simeq 620\mu\text{eV}\left(\frac{10^{10}\ \text{GeV}}{f_a}\right). \tag{62}$$

The axion mass turns on around $T \simeq 1$ GeV when the Hubble parameter reaches the axion mass, $3H(T') = m_a(T')$ and the axion begins to roll.

### III.1.3. Axion Production via Coherent Oscillation

The original motivation of the axion is to solve the Strong CP problem. Eq. (30) can be written in terms of $v_{\text{PQ}}$:

$$\mathcal{L}_{eff} \ni \bar{\theta}\frac{g_s^2}{32\pi}G_{A\mu\nu}\tilde{G}_A^{\mu\nu} + \alpha\frac{a}{v_{\text{PQ}}}\frac{g_s^2}{32\pi}G_{A\mu\nu}\tilde{G}_A^{\mu\nu} \tag{63}$$

where $\alpha$ is a model dependent constant and axion decay constant $f_a \equiv v_{PQ}/\alpha$. Naively, the offending CP-violating term is canceled when PQ symmetry is broken at a scale $v_{\text{PQ}}$:

$$a = -\bar{\theta}\ (v_{\text{PQ}}/\alpha)\ \Longrightarrow \bar{\theta} = -\frac{a}{v_{\text{PQ}}}\alpha \tag{64}$$

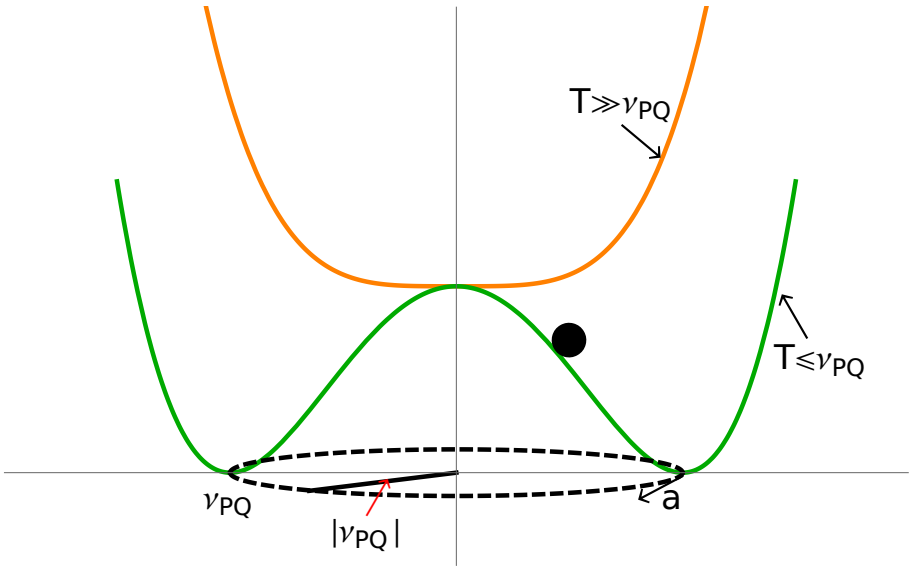


Figure 20: Potential associated with spontaneous PQ symmetry breaking. For $T \gg v_{\rm PQ}$, $U(1)_{\rm PQ}$ symmetry is not broken. When $T \simeq v_{\rm PQ}$, Peccei-Quinn symmetry is broken and Mexican hat potential (green) forms, the axion rolls down to the minimum of the potential.

The axion is the Nambu-Goldstone boson associated with $U(1)_{\rm PQ}$ breaking and can be identified as the phase of the PQ scalar, $X$:

$$X = |X|e^{i\theta_x} \xrightarrow{\cancel{U(1)_{\rm PQ}}} |v_{\rm PQ}|e^{i\ a/v_{\rm PQ}} \tag{65}$$

The charge of the field $X$ due to $U(1)_{\rm PQ}$ symmetry assumed to be *unity*. Spontaneous breaking of PQ symmetry via a Mexican hat potential ensures that the phase of the field $X$, $\theta_x$ is between 0 and $2\pi$. The axion field arises when $X$ gets a *vev*, $|X| \simeq v_{\rm PQ}$ and has a periodicity $2\pi v_{\rm PQ}$. In Fig. 20, the form of the potential responsible for the spontaneous breaking of the PQ symmetry [68], $V(X) \ni \kappa(X^2 - v_{\rm PQ}^2)^2$ , is shown for $T \gg v_{\rm PQ}$ (orange) and $T \lesssim v_{\rm PQ}$ (green). The axion rolls down to the minimum of the potential, shown by the black disk. The azimuthal direction denoted by $a$ is the direction of the oscillation of the axion field. $U(1)_{\rm PQ}$ breaking occurs at $T \simeq v_{PQ}$ and cosmic strings are formed.

The axion starts to oscillate at a much lower scale, $\Lambda_{\rm QCD} \lesssim 1$ GeV. There exists a hierarchy between the scale at which cosmic strings are formed, $v_{\rm PQ}$, and the scale at which domain walls are formed, $\Lambda_{\rm QCD}$. At $T \simeq 1$ GeV, the axion potential is not flat anymore and domain walls are formed [68]. The vacua which are separated by domain walls are the local minima of the axion potential, given by:

$$V(a) = m_a^2 (v_{PQ}/N_{\rm DW})^2 (1 - cos(a\ N_{\rm DW}/v_{\rm PQ})). \tag{66}$$

$\theta_a$, the axion misalignment angle is defined as $a/f_a$ and can take values from 0 to $2\pi N_{\rm DW}$. Then the constant $\alpha$ in Eq. (63) is identified as the domain wall number, $N_{\rm DW}$. Using[2] $v = f_a \times N_{\rm DW}$ and $\theta_a = a/f_a$, both Eq's. (63,66) can be written in terms of $\theta_a$:

$$\begin{aligned} \mathcal{L}_{eff} \ni\ & \bar{\theta} \frac{g_s^2}{32\pi} G_{A\mu\nu} \tilde{G}_A^{\mu\nu} - \theta_a \frac{g_s^2}{32\pi} G_{A\mu\nu} \tilde{G}_A^{\mu\nu} \\ V(a) =\ & m_a^2 f_a^2 (1 - cos(\theta_a)). \end{aligned} \tag{67}$$

The potential is symmetric under the axion field shift $a \to a + 2\pi k f_a$ since vacua are degenerate. For $T \gg 1$ GeV the axion potential is flat. When $T \sim 1$ GeV, the axion field begins to roll down to one of the minima located at $a/f_a = 2\pi$ as in Fig. 21. In the figure, the x-axis represents the axion field which is the azimuthal direction in Fig. 20. The vacua in terms of the phase of the PQ-charged $X$ field, are located at: $\theta_{x_{min}}$:

$$\theta_{x_{min}} = \frac{2\pi k}{N_{\rm DW}}, \text{ where } k = 0, 1, \ldots, N_{\rm DW} - 1. \tag{68}$$

For $N_{\rm DW} = 1$, the potential has only one vacuum ($k$=0) and the domain wall is located at $\theta_x = \pi$. The form of the potential is represented in Fig. 22(a). The

[2]This relation holds if PQ charge of the field $X$ is unity and $v_X \simeq v_{\rm PQ}$. The exact relation between $f_a$, $v_{\rm PQ}$ and PQ fields $X_i$'s with charges $q_i$ is given by $f_a = \sqrt{2 \sum_i q_i^2 v_i^2}/N_{\rm DW}$ [69].

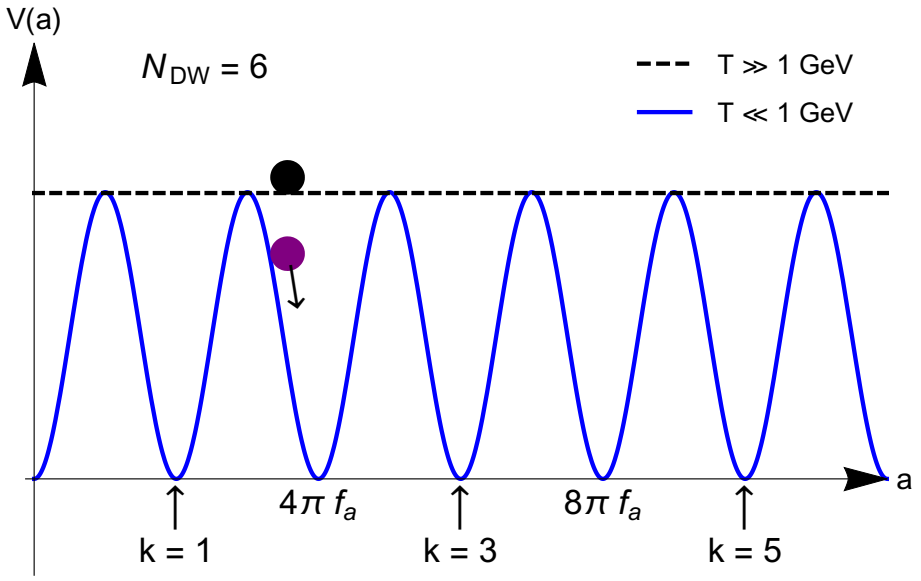


Figure 21: Axion potential, $V(a)$ for $N_{\rm DW} = 6$. The black dashed line shows the form of potential for $T \gg 1$ GeV and the blue curve shows the potential which forms when $T \sim 1$ GeV. The axion, shown by the purple disk, starts rolling down to a minimum at $T \lesssim 1$ GeV and $Z_{N_{\rm DW}}$ symmetry breaks down.

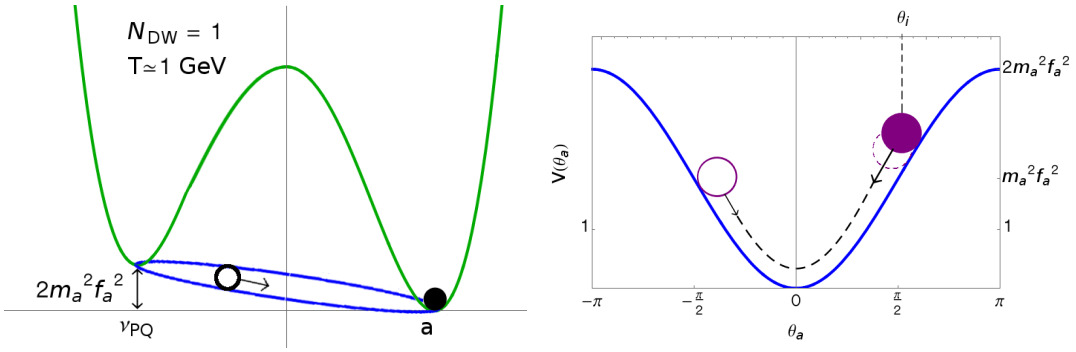


(a) (b)

Figure 22: (a) Plot of the effective axion potential, $V_{eff}$ for $N_{\rm DW} = 1$ after both $U(1)_{\rm PQ}$ and $Z_{\rm N_{DW}}$ symmetries are broken. The axion (black disk) sits at the minimum of the potential, $\theta_x = \theta_a = \theta_i = 0$. The black circle shows the initial position of the axion ($\theta_i \simeq 3\pi/4$) before it starts to oscillate. In frame (b) the plot of the axion potential, $V(\theta_a)$ is shown. The axion starts to oscillate by rolling down from initial misalignment angle, $\theta_i$.

axion (black disk) is sitting at the minimum of the potential. It does not start to oscillate if initially it sits at $\theta_i = 0$ which is the same position as $\theta_x = 0$ since $N_{\rm DW} = 1$. The black circle represents an axion with an initial misalignment angle bigger than 0. Once the temperature drops below 1 GeV, $U(1)_{\rm PQ}$ symmetry is broken into $Z_{\rm N_{DW}}$ symmetry so the potential is not flat anymore and a domain wall forms at $\theta_x = \pm\pi$. The axion starts to oscillate around $\theta_x = 0$ on the blue contour. In $\theta_a$ space, the oscillation can be pictured as in Fig. 22(b). $\theta_i$ is defined as the initial value of $\theta_a$ where the axion starts rolling down and oscillates which results in significant axion$^{\rm CO}$ abundance [66]. According to the misalignment mechanism the axion density at the temperature $T_{\rm osc}$, where $T_{\rm osc}$ is defined by $m_a(T_{\rm osc}) = 3H(T_{\rm osc})$, is given by [12, 66]:

$$\rho_a^{\rm mis} = 1.44\ m_a(T_{\rm osc}) f_a^2 \theta_i^2 f(\theta_i) \tag{69}$$

where $f(\theta_i)$ is defined as $f(\theta_i) = \left[\ln\left(e/(1-\theta_i^2/\pi^2)\right)\right]^{7/6}$.

If PQ symmetry is broken after inflation, topological defects such as strings and domain walls are formed. If $N_{\rm DW} = 1$ as in the KSVZ model, domain walls are short lived and collapse quickly [64]. However, for $N_{\rm DW} > 1$ strings attached to domain walls are formed and domain walls eventually overclose the Universe [68]. In case PQ symmetry is broken during or before inflation (and not restored after inflation), strings are diluted during the inflationary era so domain walls do not overclose the Universe. For the calculation of mixed axion-neutralino dark matter in the SUSY DFSZ model ($N_{\rm DW} = 6$), the latter scenario is assumed to be the correct description of PQ symmetry breaking and inflation scales so that in the remainder of this thesis, cosmic string effects can be neglected.

### III.1.4. Coupled Boltzmann Equations

The goal is to numerically solve the coupled Boltzmann equations which track the number and energy densities of neutralinos $\widetilde{Z}_1$, gravitinos $\tilde{G}$, saxions $s$, axinos $\tilde{a}$, axions $a$ and radiation as a function of time starting at the reheat temperature $T = T_R$ at the end of inflation until today. Coherently produced axion and saxion components (axion$^{\rm CO}$ and saxion$^{\rm CO}$) are separately included in the computation. In the KSVZ model, considered in Ref. [70], the thermal production of saxions, axions and axinos is maximal at $T \sim T_R$, resulting in a thermal yield proportional to the reheat temperature [47, 48], as seen in Fig. 12. Also, since the axino/saxion decay widths are suppressed by the loop factor as well as by the PQ scale, their decays tend to take place at temperatures $T \ll m_{\tilde{a},s}$. Hence the thermal production and decay processes can be safely treated as taking place at distinct time scales. Furthermore, the inverse decay process ($a + b \to \tilde{a}, s$) is always Boltzmann-suppressed when the decay term becomes sizable ($\Gamma \sim H$), thus inverse decay contributions can be neglected.

In the DFSZ scenario, the tree-level couplings between the axion supermultiplet and the Higgs superfields modify the thermal scatterings of saxions, axions and axinos and can significantly enhance their decay widths. The scattering cross section (in the supersymmetric limit) can be estimated by [42]:

$$\sigma_{(I+J\to\tilde{a}+\cdots)}(s) \sim \frac{1}{16\pi s}\,|\mathcal{M}|^2 \sim \frac{g^2 c_H^2\,|T_{ij}(\Phi)^a|^2}{2\pi s}\frac{M_\Phi^2}{v_{PQ}^2}, \tag{70}$$

where $\Phi$ is a PQ- and gauge-charged matter supermultiplet, $g$ the corresponding gauge coupling constant, $T_{ij}(\Phi)^a$ is the gauge-charge matrix of $\Phi$ and $M_\Phi$ its mass. For the DFSZ SUSY axion model, the heaviest PQ charged superfields are the Higgs doublets, so $g$ is the $SU(2)$ gauge coupling, $M_\Phi = \mu$, and $|T_{ij}(\Phi)^a|^2 = (N^2-1)/2 = 3/2$. The rate for the scattering contribution of axino (or saxion)

production can be obtained from the integration formula [71]:

$$\langle \sigma_{(I+J\to\tilde{a}(s)+\cdots)} v\rangle n_I n_J \simeq \frac{T^6}{16\pi^4}\int_{M/T}^{\infty} dx K_1(x) x^4 \sigma(x^2 T^2) \tag{71}$$

where $K_1$ is the modified Bessel function, $M$ is the threshold energy for the process; also, both the higgsino or saxion/axino mass and number densities $n_{I,J}$ are proportional to $T^3$. Integrating over the Bessel function, the axino (or saxion) production rate is found to be proportional to [42]:

$$\langle \sigma_{(I+J\to\tilde{a}(s)+\cdots)} v\rangle \propto \left(\frac{\mu}{f_a}\right)^2 \frac{M^2}{T^4} K_2\left(M/T\right) \tag{72}$$

Production is maximal at $T \simeq M/3 \ll T_R$. Hence most of the thermal production of axinos and saxions takes place at $T \sim M$, resulting in thermal yields which are independent of $T_R$ (unlike the KSVZ case). This behavior is similar to the freeze-in mechanism [72], where a weakly interacting (and decoupled) dark matter particle becomes increasingly coupled to the thermal bath as the Universe cools down. However, in the current scenario, the "frozen-in" species (axinos and saxions) are not stable and their decays will contribute to the neutralino relic abundance if they take place after neutralino freeze-out (for $f_a \gtrsim 10^{10}$ GeV) and will also contribute to the dark radiation (saxion decays). The coupling in Eq. (35) enhances the axino/saxion decay width for large $\mu$ values, since the coupling to Higgs/higgsinos is proportional to $\mu/f_a$. As a result, saxions and axinos may decay at much earlier times (higher temperatures) when compared to the KSVZ scenario. If their decay temperatures are of order of their masses, then inverse decay process such as $\widetilde{Z}_1 + h \to \tilde{a}$ or $h + h \to s$ cannot be neglected. As shown in Ref. [44], the decay temperatures can be larger than the axino or saxion mass, so the inverse decay process can be significant. The main effect

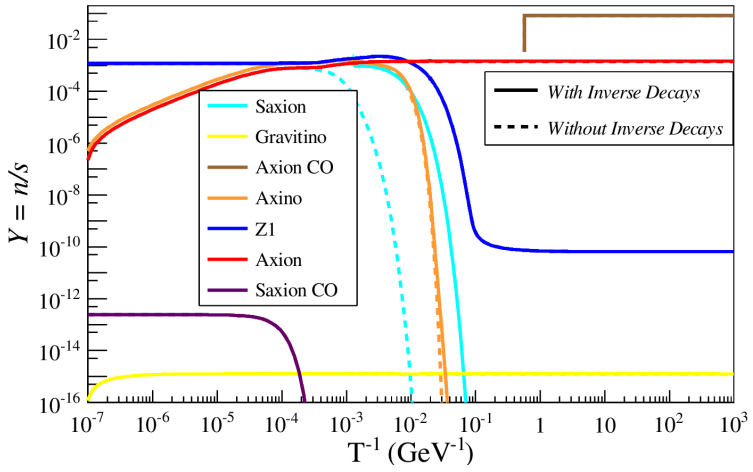


Figure 23: Evolution of the axion, saxion, axino, neutralino and gravitino yields for the SOA benchmark case in Ref. [43] with $f_a = 10^{10}$ GeV, $m_{\tilde{G}} = 10$ TeV, $m_a = 1$ TeV, $m_s = 500$ GeV, $\theta_s = \theta_i = 1$ and $\xi_s = 1$, taken from Ref. [43].

of including the inverse decay process is to delay the axino/saxion decay. This effect cannot be accounted for in the sudden decay approximation and requires the numerical solution of the Boltzmann equations. Fig. 23 shows the evolution of the yields ($n_i/s$) versus the inverse of the temperature with and without (dashed line) inverse decay. As expected in the DFSZ case, saxion and axino yields (non-CO) increase as the temperature is reduced since their production is maximal at $T \sim m_{\tilde{a}/s}$, reaching the maximal value just before their decay. The axion is (effectively) stable; its yield remains constant after the thermal production becomes suppressed at $T \lesssim \mu$. Gravitinos are produced through thermal scatterings as well. However, their production cross-section peaks at $T \sim T_R$, much like the saxion/axino production in the KSVZ case. As seen in Fig. 23, the inclusion of inverse decays delays the decay of saxions and axinos, with the effect being larger for saxions, since they tend to decay earlier. Nonetheless, the neutralino and axion relic densities are unchanged. The inverse decay process is only relevant for $T_{\rm decay} \gtrsim m_{\tilde{a}/s}$ since if the decay happens at lower temperatures,

it is Boltzmann-suppressed. As a result, the inverse decay process is only relevant for the cases where axinos and saxions decay before neutralino freeze-out (since $T_{Fr} \sim m_{\tilde{Z}_1}/20 \ll m_{\tilde{a}/s}$). Although such decays have minimal contribution to the neutralino relic abundance, it is essential to include them in the Boltzmann equations for consistency. With the inverse decay process, the Boltzmann equations for the number ($n$)'s and energy ($\rho_i$) densities of a thermal species $i$ ($= a, s$ or $\tilde{a}$) read:

$$\begin{aligned}\frac{dn_{\tilde{Z}_1}}{dt} =& -3Hn_{\tilde{Z}_1} + \sum_{j\in\text{MSSM}} \left(\bar{n}_{\tilde{Z}_1}\bar{n}_j - n_{\tilde{Z}_1}n_j\right)\langle\sigma v\rangle_{\tilde{Z}_1 j} \\ &+ \sum_x \Gamma_x \mathcal{B}_{\tilde{Z}_1} m_x \frac{n_x}{\rho_x}\left(n_x - \bar{n}_x \sum_{x\to\tilde{Z}_1+y} \frac{\mathcal{B}_{\tilde{Z}_1 y}}{\mathcal{B}_{\tilde{Z}_1}} \frac{n_{\tilde{Z}_1} n_y}{\bar{n}_{\tilde{Z}_1}\bar{n}_y}\right)\end{aligned}$$

$$\begin{aligned}\frac{dn_a}{dt} =& -3Hn_a + \sum_{j\in\text{MSSM}} (\bar{n}_a\bar{n}_j - n_a n_j)\langle\sigma v\rangle_{aj} \\ &- \Gamma_a m_a \frac{n_a}{\rho_a}\left(n_a - \bar{n}_a \sum_{a\to x+y} \mathcal{B}_{xy} \frac{n_x n_y}{\bar{n}_x\bar{n}_y}\right) \\ &+ \sum_x \Gamma_x \mathcal{B}_a m_x \frac{n_x}{\rho_x}\left(n_x - \bar{n}_x \sum_{x\to a+y} \frac{\mathcal{B}_{ay}}{\mathcal{B}_a} \frac{n_a n_y}{\bar{n}_a\bar{n}_y}\right)\end{aligned}$$

$$\frac{dn_a^{\text{CO}}}{dt} = -3Hn_a^{\text{CO}} - \Gamma_a m_a n_a^{\text{CO}} \frac{n_a^{\text{CO}}}{\rho_a^{\text{CO}}}$$

$$\begin{aligned}\frac{dn_s}{dt} =& -3Hn_s + \sum_{j\in\mathrm{MSSM}} \left(\bar{n}_s\bar{n}_j - n_s n_j\right)\langle\sigma v\rangle_{sj} \\ &- \Gamma_s m_s \frac{n_s}{\rho_s}\left(n_s - \bar{n}_s \sum_{s\to x+y} \mathcal{B}_{xy}\frac{n_x n_y}{\bar{n}_x\bar{n}_y}\right) \\ &+ \sum_x \Gamma_x \mathcal{B}_s m_x \frac{n_x}{\rho_x}\left(n_x - \bar{n}_x \sum_{x\to s+y}\frac{\mathcal{B}_{sy}}{\mathcal{B}_s}\frac{n_s n_y}{\bar{n}_s\bar{n}_y}\right)\end{aligned}$$

$$\frac{dn_s^{\mathrm{CO}}}{dt} = -3Hn_s^{\mathrm{CO}} - \Gamma_s m_s n_s^{\mathrm{CO}}\frac{n_s^{\mathrm{CO}}}{\rho_s^{\mathrm{CO}}}$$

$$\begin{aligned}\frac{dn_{\tilde{a}}}{dt} =& -3Hn_{\tilde{a}} + \sum_{j\in\mathrm{MSSM}} \left(\bar{n}_{\tilde{a}}\bar{n}_j - n_{\tilde{a}} n_j\right)\langle\sigma v\rangle_{\tilde{a}j} \\ &- \Gamma_{\tilde{a}} m_{\tilde{a}} \frac{n_{\tilde{a}}}{\rho_{\tilde{a}}}\left(n_{\tilde{a}} - \bar{n}_{\tilde{a}} \sum_{\tilde{a}\to x+y} \mathcal{B}_{xy}\frac{n_x n_y}{\bar{n}_x\bar{n}_y}\right) \\ &+ \sum_x \Gamma_x \mathcal{B}_{\tilde{a}} m_x \frac{n_x}{\rho_x}\left(n_x - \bar{n}_x \sum_{x\to \tilde{a}+y}\frac{\mathcal{B}_{\tilde{a}y}}{\mathcal{B}_{\tilde{a}}}\frac{n_{\tilde{a}} n_y}{\bar{n}_{\tilde{a}}\bar{n}_y}\right)\end{aligned}$$

$$\begin{aligned}\frac{dn_{\widetilde{G}}}{dt} =& -3Hn_{\widetilde{G}} + \sum_{j\in\mathrm{MSSM}} \left(\bar{n}_{\widetilde{G}}\bar{n}_j - n_{\widetilde{G}} n_j\right)\langle\sigma v\rangle_{\widetilde{G}j} \\ &- \Gamma_{\widetilde{G}} m_{\widetilde{G}} \frac{n_{\widetilde{G}}}{\rho_{\widetilde{G}}}\left(n_{\widetilde{G}} - \bar{n}_{\widetilde{G}} \sum_{\widetilde{G}\to x+y} \mathcal{B}_{xy}\frac{n_x n_y}{\bar{n}_x\bar{n}_y}\right)\end{aligned}$$

$$\frac{d\rho_i}{dt} + 3H(\rho_i + P_i) = \sum_{j\in \mathrm{MSSM}} \left(\bar{n}_i \bar{n}_j - n_i n_j\right) \langle \sigma v \rangle_{ij} \frac{\rho_i}{n_i}$$
$$- \Gamma_i m_i \left( n_i - \bar{n}_i \sum_{i\to x+y} \mathcal{B}_{xy} \frac{n_x n_y}{\bar{n}_x \bar{n}_y} \right)$$
$$+ \sum_x \Gamma_x \mathcal{B}_i \frac{m_x}{2} \left( n_x - \bar{n}_x \sum_{x\to i+y} \frac{\mathcal{B}_{iy}}{\mathcal{B}_i} \frac{n_i n_y}{\bar{n}_i \bar{n}_y} \right)$$

where $\mathcal{B}_{xy} \equiv BR(i \to x + y)$, $\mathcal{B}_{iy} \equiv BR(x \to i + y)$, $\mathcal{B}_i \equiv \sum_y \mathcal{B}_{iy}$, $\bar{n}_i$ is the equilibrium density of particle species $i$ and the $\Gamma_i$ are the zero temperature decay widths. Here subscript $j$ denotes the MSSM particles that interact with axion, saxion and axino. It is also convenient to use the above results to obtain a simpler equation for $\rho_i/n_i$ (again $i = a, s$ or $\tilde{a}$):

$$\frac{d\left(\rho_i/n_i\right)}{dt} = -3H\frac{P_i}{n_i} + \sum_x \mathcal{B}_i \frac{\Gamma_x m_x}{n_i} \left(\frac{1}{2} - \frac{n_x}{\rho_x}\frac{\rho_i}{n_i}\right) \left( n_x - \bar{n}_x \sum_{x\to i+y} \frac{\mathcal{B}_{iy}}{\mathcal{B}_i} \frac{n_i n_y}{\bar{n}_i \bar{n}_y} \right) \quad (73)$$

where $P_i$ is the pressure density ($P_i \simeq 0$ ($\rho_i/3$) for non-relativistic (relativistic) particles). As discussed in Ref. [70], the CO-produced components of the axion and saxion fields are tracked separately since CO components are assumed not to have scattering contributions. Under this approximation, the equations for the CO-produced fields (axions and saxions) read:

$$\frac{dn_i^{\mathrm{CO}}}{dt} + 3Hn_i^{\mathrm{CO}} = -\Gamma_i m_i \frac{dn_i^{\mathrm{CO}}}{\rho_i^{\mathrm{CO}}} n_i^{\mathrm{CO}} \quad \text{and} \quad \frac{d(n_i^{\mathrm{CO}}/\rho_i^{\mathrm{CO}})}{dt} = 0. \quad (74)$$

The amplitude of the coherent oscillations is defined by the initial field values, which for the case of PQ breaking before the end of inflation is a free parameter for both the axion and saxion fields, are parametrized by $\theta_i = a_0/f_a$ and $\theta_s = s_0/f_a$. In the post-inflation cosmology where PQ breaking occurs after inflation, $\theta_i$ is not a free parameter but the $rms$ average of a uniform distribution of initial values from $-\pi$ to $+\pi$, $\theta_i|_{rms} = \pi/\sqrt{3}$ [12, 73].

Finally, the above set of simplified Boltzmann equations must be supplemented with an equation for the entropy of the thermal bath:

$$\frac{dS}{dt} = \frac{R^3}{T} \sum_i BR(i,X)\Gamma_i m_i \left( n_i - \bar{n}_i \sum_{i \to x+y} \mathcal{B}_{xy} \frac{n_x n_y}{\bar{n}_x \bar{n}_y} \right) \tag{75}$$

where $R$ is the scale factor and $BR(i,X)$ is the fraction of energy injected in the thermal bath from $i$ decays.

Saxion and axino partial widths, branching fractions and annihilation cross sections appearing in the above equations have been calculated in Ref.'s [44, 70] while the gravitino widths are computed in Ref. [77]. The MSSM particles are mostly in thermal equilibrium: a further approximation as $n_j \simeq \bar{n}_j$ in Boltzmann equations is made to solve eight coupled differential equations simultaneously. The value of $\langle \sigma v \rangle_{\tilde{a}}$ for thermal axino production is given in Ref. [42], while $\langle \sigma v \rangle_{\widetilde{Z}_1}$ for neutralino annihilation is extracted from IsaRed [74, 75]. Since supersymmetry assures the same dimensionless couplings, it is reasonable to expect annihilation/production rates similar to the axino's for thermal saxion and axion production. Hence the result for axino thermal production from Ref's [52, 42] applies also to saxions and axions. For the gravitino thermal production, the result in Ref. [76] is used to calculate $\langle \sigma v \rangle_{\tilde{G}}$.

### III.1.5. Initial Conditions of the Early Universe

As previously stated in section I.3.1, the Universe can be in matter or radiation or vacuum-dominated states. The early Universe after *reheat* was radiation dominated. After inflation, the inflaton decays into relativistic particles (vacuum dominated → matter dominated → radiation dominated) and the Universe is reheated to the temperature $T_R$, calculated as in Eq. (15). As the Universe cools down, the saxion or axino can become the dominant form of energy if it

is produced at large rates at $T = T_R$ since the energy density of radiation, $\rho_{\rm rad}$ decreases as $\rho_{\rm rad} \sim R^{-4}$ while for the density of non-relativistic (or CO) particles $\rho_{\tilde{a}/s} \sim R^{-3}$. The axion is stable so it cannot be responsible for the matter-dominated phase, otherwise it will violate BBN constraints. In order to preserve BBN predictions, axino/saxion has to decay before light elements start to form at $T \sim 1$ MeV. Initial energy densities at $T = T_R$ for radiaton and saxion$^{\rm CO}$ are calculated as [70]:

$$\begin{aligned} \rho_{\rm rad} &= \frac{\pi^2}{30} g_*(T_R) T_R^4 \\ \rho^0_{s^{\rm CO}} &= 2.1 \times 10^{-9} \left( \frac{2\pi^2 g_*(T_R) T_R^3}{45} \right) \left( \frac{T_R}{10^5} \right) \left( \frac{s_0}{10^{12}} \right)^2 \end{aligned} \tag{76}$$

where it is assumed that saxion$^{\rm CO}$ starts oscillating at a temperature $T_{s^{\rm CO}}$ when the Universe is inflaton-dominated ($T_{s^{\rm CO}} > T_R$). This assumption is valid for the parameter choices in the SUSY DFSZ model where $T_R \lesssim 10^9$ GeV in order to avoid dark matter overproduction from gravitino production and BBN constraints [33]. Saxion oscillation starts at [78]:

$$T_{s^{\rm CO}} \simeq \sqrt{M_{Pl} m_s} \left( \frac{5}{4\pi^3} \frac{1}{g_*(T_{s^{\rm CO}})} \right)^{1/4} \tag{77}$$

which is larger than the reheat temperature considered even for $m_s \sim 100$ GeV. Hence at $T = T_R$, $\rho_{\rm rad} > \rho^0_{s^{\rm CO}}$ as required. An example for a BBN safe scenario is shown in Fig. 24. In the upper frame evolution of radiation, saxion$^{\rm CO}$, axino and gravitino energy density along with temperature vs. the scale factor $R/R_0$ is shown whereas in the lower frame such evolutions are plotted vs. temperature. A high $f_a = 10^{16}$ GeV is chosen to show an intermediate matter-dominated era [79]. $s_0$ is set to be equal to $f_a$ so the saxion$^{\rm CO}$ is produced in a large amount before reheating. As seen in the figure, the Universe is radiation-dominated at $T = T_R$.

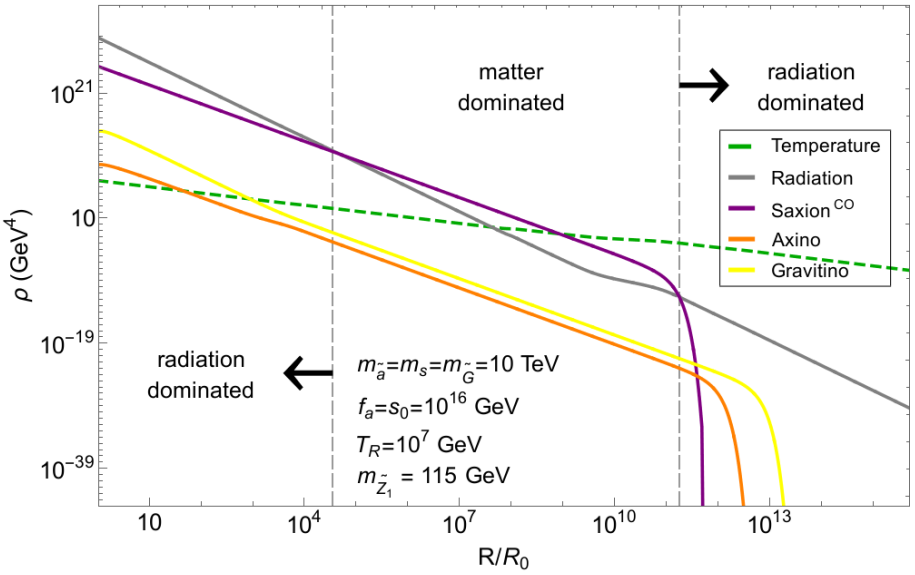


(a)

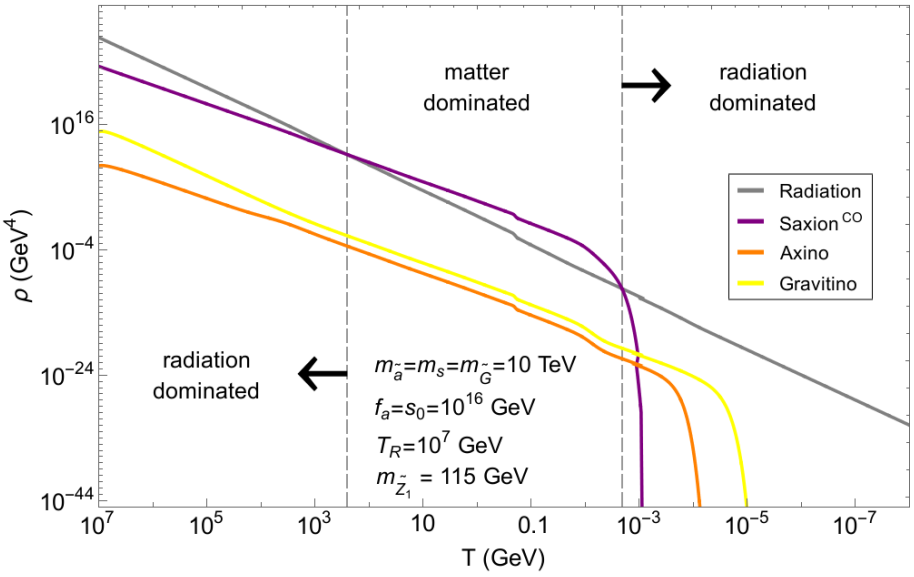


(b)

Figure 24: Evolution of various energy densities (a) vs. scale factor ($R/R_0$) and (b) vs. temperature (T) for the RNS benchmark point with $\xi_s = 1$, $s_0 = f_a = 10^{16}$ GeV and other parameters as indicated in the figure. Matter-dominated intermediate era is shown between the vertical dashed lines.

As the Universe cools down, the saxion starts to dominate the energy density at around $T \simeq 250$ GeV (or $R/R_0 \simeq 3.6 \times 10^4$). The saxion starts decaying when the temperature reaches down to $\simeq$10 MeV and injects entropy in the thermal bath. Entropy production can be seen as the increase in the radiation curve at $R/R_0 \simeq 3 \times 10^9$ (upper frame). The radiation dominated era resumes at $T \simeq 2$ MeV and saxion is completely decayed at $T \simeq 0.5$ MeV. Although the gravitino is long-lived and decays at $T \simeq 0.01$ MeV, its abundance is quite small, hence it does not violate BBN constraints. However, the point is excluded due to overproduction of neutralino DM: $\Omega_{\widetilde{Z}_1} h^2 = 2517$ due to enhanced $s \to \widetilde{Z}_i \widetilde{Z}_j$ decays.

### III.1.6. General Procedure

Axion-neutralino mixed dark matter can be calculated by solving the eight coupled differential equations. As a first step, the SUSY spectrum is generated with Isajet [75] and $\langle \sigma_{ann}.v \rangle(T)$ for neutralino annihilation is extracted from IsaRed [74]. In all the calculations, $\theta_s$ is chosen to be 1 so that $s_0 = f_a$ since it is expected to be around unity. As mentioned before, in the SUSY DFSZ scenario thermal production of axion, axino and saxion are independent of the reheat temperature and for the values of $T_R$ less than $10^9$ GeV, the gravitino problem is avoided. For the SUSY DFSZ model, $T_R$ is set to $10^7$ GeV. The evolution of number densities are tracked from the end of inflation, from $T_R$ until today. For each parameter set which yields an allowable value of $\Omega_{\widetilde{Z}_1} h^2 < 0.12$, the axion misalignment angle $\theta_i$ will be adjusted using Eq. (60) such that $\Omega_{\widetilde{Z}_1} h^2 + \Omega_a h^2 = 0.12$, *i.e.* the summed DM abundance saturates the measured value by adjusting the initial axion field strength parameter $\theta_i$. With the calculated $\theta_i$ that satisfies the DM constraint and fixing other parameters, the coupled Boltzmann equations are re-solved in order to precisely compute the effect of entropy dilution on the

neutralino density.

If the axino and saxion are decayed before the neutralino freeze-out, $\Omega_{\widetilde{Z}_1}h^2$ takes its standard value, $\Omega^{std}_{\widetilde{Z}_1}h^2$, computed by IsaRed which is independent of the PQ parameters. Since axion supermultiplet interactions are proportional to $\mu$ in DFSZ model, such a scenario can be realized for a low value of $f_a$ as shown in Fig. 25(a) (generated using the RNS benchmark point) where only neutralino, axion$^{\rm CO}$, saxion, saxion$^{\rm CO}$ and axino energy densities are shown for simplicity. Axinos and saxions decay more slowly with increasing $f_a$. Saxion (and axino) decays enhance the neutralino dark matter density ($s \to \widetilde{Z}_1\widetilde{Z}_1$ or $s \to ... \to \widetilde{Z}_1\widetilde{Z}_1$) only if it is long-lived. In the SUSY DFSZ case for $f_a \lesssim 10^{13}$ GeV, the neutralino DM abundance is enhanced mostly by both axino and saxion decays whereas for $f_a \gtrsim 10^{13}$ GeV saxion$^{\rm CO}$ is highly produced and its decay mainly contributes to the neutralino abundance. In Fig. 25(b), an example scenario where axino decays after neutralino freeze-out is presented. Here the axino mass is chosen to be 1 TeV so that it is long-lived whereas the saxion mass is set to 10 TeV. The saxion decays before freeze-out since the coherently produced saxions at $f_a = 10^{12}$ GeV are short-lived unless $m_s \lesssim$1 TeV. However, choosing a light saxion mass may lower the neutralino relic abundance by injecting entropy. In frame (b), $\theta_i \simeq 1.3$ so that $\Omega_{\widetilde{Z}_1}h^2 + \Omega_a^{\rm CO}h^2 = 0.12$ and dark matter is composed of axions and neutralino with almost equal abundance. Axino decays into $\widetilde{Z}_1 + ...$ right after the neutralino freeze-out as seen by the blue curve, hence they augment $\Omega_{\widetilde{Z}_1}h^2$.

## III.2. Axion-Higgsino Dark Matter

For the mixed axion-higgsino dark matter calculation, an RNS benchmark point with $\mu = 125$ GeV is used to generate the SUSY spectrum. The SUSY KSVZ model with higgsino-like neutralino has been studied in Ref. [49] as an example for SUSY models with a standard underabundance (SUA) neutralino density.

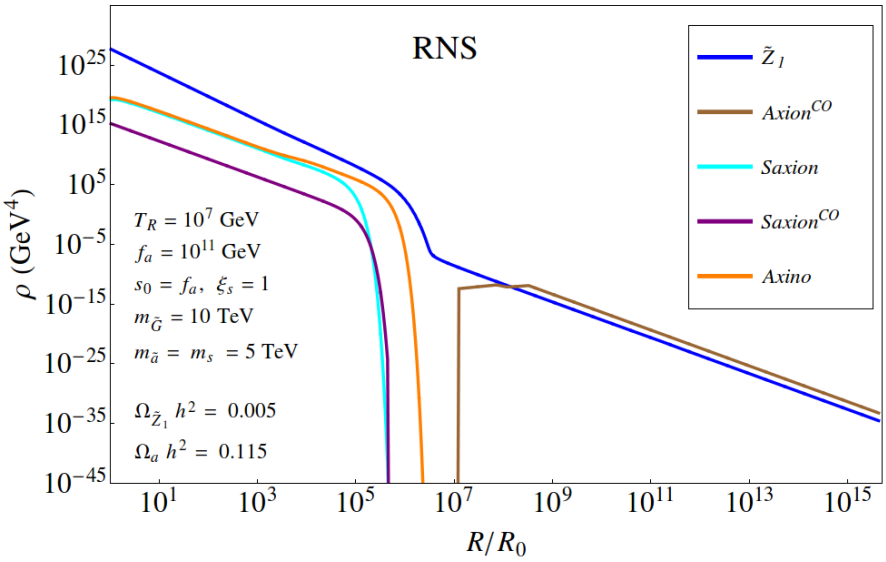


(a)

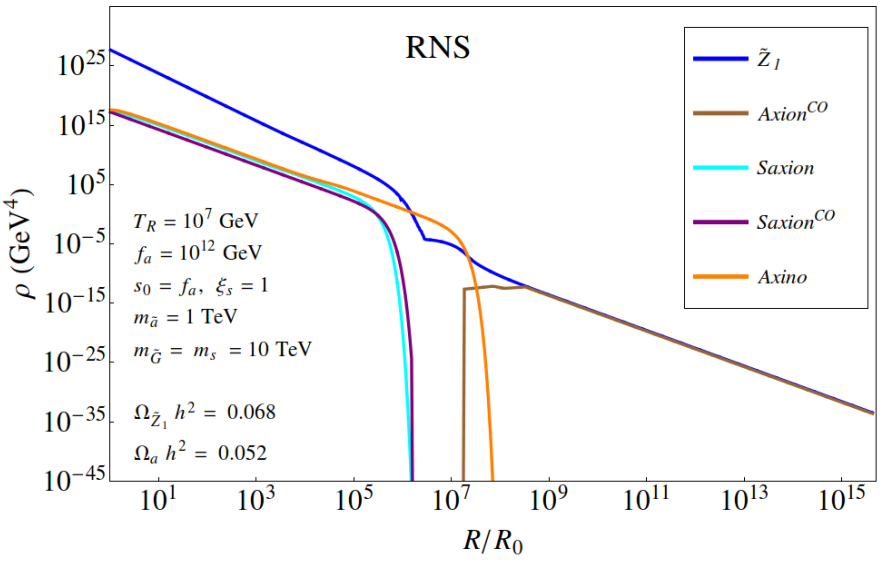


(b)

Figure 25: Evolution of axino, axion$^{\rm CO}$, saxion, saxion$^{\rm CO}$ and neutralino energy densities for (a) $f_a = 10^{11}$ GeV and (b) $f_a = 10^{12}$ GeV with RNS benchmark point. Other parameters are listed on the figure. For $f_a = 10^{11}$ GeV, axion and saxion decay *before* neutralino freeze-out so $\Omega_{\tilde{Z}_1} h^2 = 0.005$ and dark matter density is mostly composed of axions (a). For $f_a = 10^{12}$ GeV and with $m_{\tilde{a}} = 1$ TeV, axion continues to decay even *after* the neutralino freeze-out so neutralino abundance is enhanced by axino decays (b).

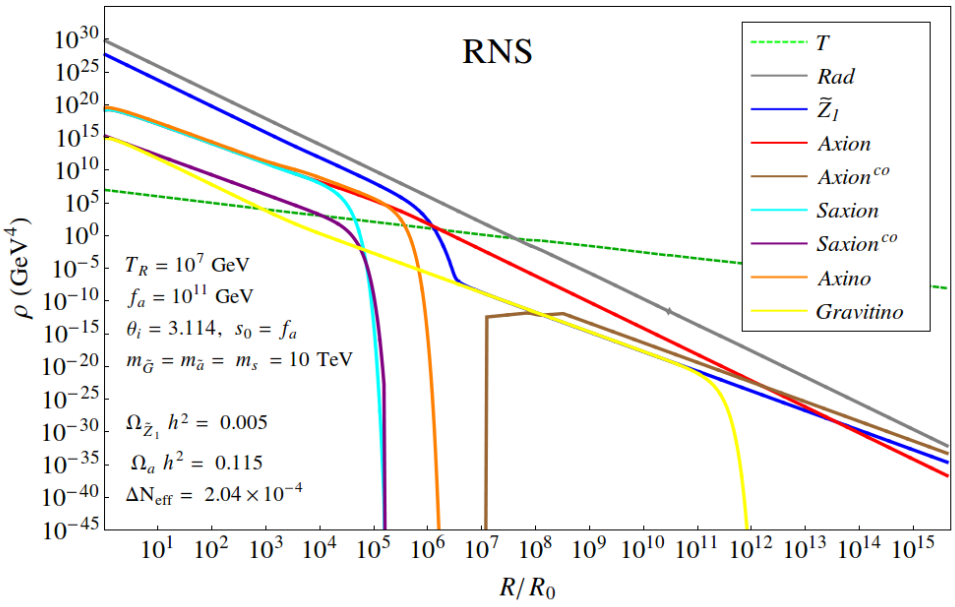


Figure 26: Evolution of various energy densities vs. scale factor $R/R_0$ for the RNS benchmark case with parameters as indicated in the figure.

The focus of this section is the SUSY DFSZ scenario with an RNS benchmark point. The calculation and results are very similar to those of SUA benchmark point in Ref. [43]. In Fig. 26, the solution of the Boltzmann equations is shown for the RNS point with $T_R = 10^7$ GeV, $f_a = 10^{11}$ GeV, $m_{\tilde{G}} = m_{\tilde{a}} = m_s = 10$ TeV, $\theta_s = 1$ and $\theta_i = 3.11$. The evolution of the energy densities of axions and saxions (both CO- and thermally produced), axinos, neutralinos and gravitinos as a function of the scale factor of the Universe $R/R_0$ ($R_0$ is the scale factor at $T = T_R$) are presented. For this parameter set, the final neutralino abundance is $\Omega_{\tilde{Z}_1} h^2 = 0.005$ while the axion abundance is $\Omega_a h^2 = 0.115$, resulting in a total dark matter relic abundance within the measured value. It is seen that at $T = T_R$ (where $R/R_0 \equiv 1$) the Universe is radiation-dominated with smaller abundances of neutralinos, axions, axinos and saxions, and even smaller abundances of saxion$^{\rm CO}$ and thermally/decay produced gravitinos. The saxion$^{\rm CO}$ evolve as a non-relativistic matter fluid and so its density diverges from

the relativistic gravitino abundance as $R$ increases. Both thermal and coherent populations of saxions begin to decay around $R/R_0 \sim 10^5$, at temperatures ($T \sim 10^2$ GeV) well below their masses. Somewhat later, but still before neutralino freeze-out, the axino population decays. Since these decays happen before neutralino freeze-out, the neutralino population is unaffected. The axion mass turns on around $T \sim 1$ GeV so that the axion field begins to oscillate around $R/R_0 \simeq 2 \times 10^7$. The axion$^{\rm CO}$ field evolves as DM and ultimately dominates the Universe at a value of $R/R_0$ somewhat off the plot. The behavior of the DFSZ axinos and saxions –in that they tend to decay before neutralino freeze-out– is typical of this model for the lower range of $f_a \lesssim 10^{12}$ GeV with TeV-scale values of $m_{\tilde{a}}$ and $m_s$ [44].

Finally, gravitinos are long-lived and decay well after the neutralino freeze-out, at $T \sim \mathcal{O}(100)$ keV. However, for $T_R = 10^7$ GeV, gravitinos typically have a small number density and contribute marginally to the final neutralino relic abundance. Also– due to their small energy density– the gravitino decays do not have any significant impact on Big Bang nucleosynthesis.

### III.2.1. Branching Fractions

The SUSY spectra for the RNS benchmark point is given in Appendix.A.1. The point has $m_h = 125$ GeV, a low electroweak fine-tuning $\Delta_{\rm EW} = 19.6$, a higgsino-like neutralino with mass $m_{\widetilde{Z}_1} = 117.5$ GeV and standard thermal neutralino abundance $\Omega^{std}_{\widetilde{Z}_1}h^2 = 0.005$, low by a factor ∼25 from the measured DM density. Since the point has a low $\mu$ ($\mu = 125$ GeV), the axion supermultiplet couplings are not strong so axino decays do not contribute to the DM density at low $f_a$ compared to models with a higher $\mu$ term [43]. Saxion branching ratios with the decays $s \to aa$ / $\tilde{a}\tilde{a}$ turned off ($\xi_s = 0$) for the RNS benchmark point is shown in Fig. 27. For $\xi = 0$ and a large saxion mass ($m_s \gtrsim 1.5$ TeV), the most

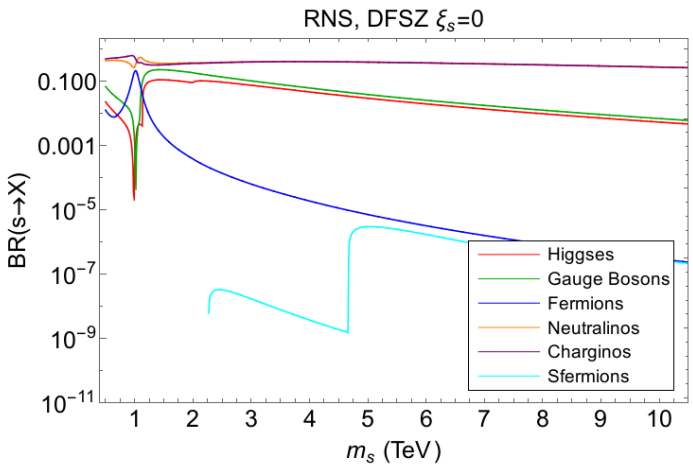


Figure 27: Saxion branching fractions in SUSY DFSZ model with $\xi_s = 0$ for the RNS benchmark point.

important decays are into charginos and neutralinos (the curves almost overlap). Decays into gauge bosons and Higgs particles are subdominant, one or two orders of magnitude smaller than the neutralino and chargino modes since the partial decay widths are inversely proportional to $m_s$ for the decays into gauge and Higgs states, while they are proportional to $m_s$ for the decay to neutralinos and charginos [44]. In Fig. 28 saxion branching ratios, with the saxion decays to axion and neutralino pairs allowed ($\xi_s = 1$), are shown for the RNS benchmark point. Since $s \to \tilde{a}\tilde{a}$ is one of the dominant decay modes, $m_{\tilde{a}} = 3$ TeV is chosen to show its branching ratio for $m_s > 6$ TeV. The most dominant mode is $s \to aa$ where the $BR(s \to aa)$ is a few orders of magnitude larger than MSSM modes for a large $m_s$ since the decay into axion pairs is proportional to the third power of the saxion mass, $m_s^3$, while the other decays are proportional to $m_s$ or $1/m_s$ [44]. As the saxion mass gets larger, $BR(s \to \text{SM})$ gets smaller. For $m_s = 8$ TeV, $BR(s \to \text{SM}) \lesssim 10^{-4}$ hence $BR(s \to aa)$ and $BR(s \to \tilde{a}\tilde{a})$ are strongly dominant. As a consequence, the constraint from dark radiation becomes stronger due to $s \to aa$ decay and the decays $s \to \tilde{a}\tilde{a} \to \widetilde{Z}_1 + ...$ might

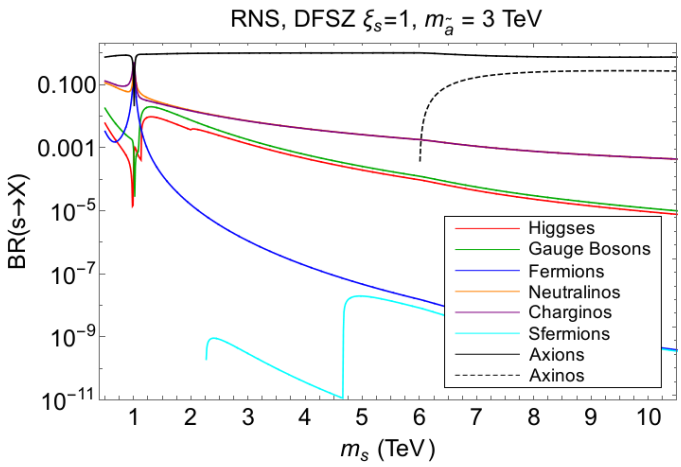


Figure 28: Saxion branching fractions in SUSY DFSZ model with $\xi_s = 1$ for the RNS benchmark point.

become the dominant source of the neutralino dark matter for large saxion mass. For smaller saxion mass, $m_s \lesssim 1$ TeV, the branching ratios into SUSY and SM channels become larger but still $BR(s \to \text{SUSY/SM}) \lesssim 0.1$ so that the constraint from dark radiation becomes less important.

Fig. 29 shows axino branching fractions as a function of $m_{\tilde{a}}$ for the RNS benchmark point. For $m_{\tilde{a}} \lesssim 8$ TeV, the branching fractions for decay to $\widetilde{Z}_i + h\ /H\ /A$, $\widetilde{W}_i^{\pm} + H^{\mp}$, $\widetilde{Z}_i + Z$ and $\widetilde{W}_i^{\pm} + W^{\mp}$ are all comparable while decays to $f + \tilde{f}$ are suppressed. $BR(\tilde{a} \to g + \tilde{g})$ is proportional to $m_{\tilde{a}}^3(1 - m_{\tilde{g}}^2/m_{\tilde{a}}^2)^3$ so the branching ratio gets larger as $m_{\tilde{a}}$ increases and dominates other modes for $m_{\tilde{a}} \gtrsim 10$ TeV.

### III.2.2. Neutralino DM from Axino and Saxion Decays

Neutralino dark matter is enhanced from its standard thermal value by $\tilde{a} \to \widetilde{Z}_1 + ...$, $s \to ... \to \widetilde{Z}_1\widetilde{Z}_1$ and $s \to \widetilde{Z}_1\widetilde{Z}_i$ decays. For $f_a \lesssim 10^{12}$ GeV (or $f_a \lesssim 10^{13}$ GeV for the $\xi_s = 1$ case) mostly axino decays augment neutralino abundance from its standard value; in higher $f_a$ region saxion$^{\text{CO}}$ decays become more im-

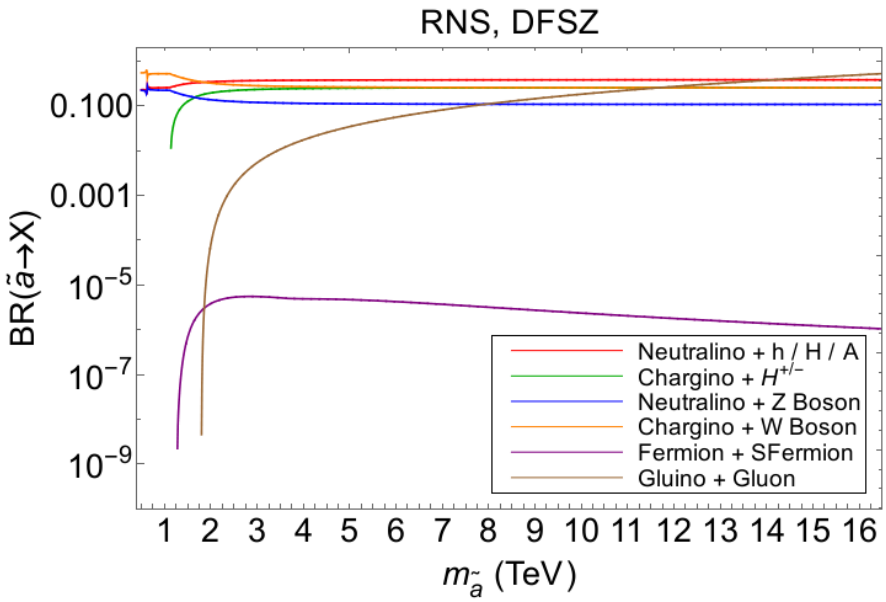


Figure 29: Axino branching fractions in SUSY DFSZ model for the RNS benchmark point.

portant. Fig. 30 shows $\Omega_{\widetilde{Z}_1}h^2$ vs $f_a$ from a scan over 0.4 TeV$< m_{\tilde{a},s} <$ 20 TeV with the saxion$^{\rm CO}$ component turned off. For $f_a \lesssim 3\times 10^{10}$ GeV, axino and saxion (thermally produced) decay before neutralino freeze-out so their decay does not contribute to the neutralino abundance. As $f_a$ increases, the neutralino abundance increases, mostly from axino decays, up to $f_a \simeq 3\times 10^{13}$ GeV. In the region with higher $f_a \gtrsim 10^{14}$ GeV, axino/saxion decays are suppressed since their thermal yields are proportional to $1/f_a^2$ [48] hence the neutralino relic density decreases and reaches its standard value at $f_a \simeq 10^{16}$ GeV.

The red dashed lines show how the relic density would be affected by saxion$^{\rm CO}$ which is the general case presented in the next section. Figures 30(a) and 30(b) slightly differ from each other due to thermally produced saxion decays into axino and axion pairs controlled by the parameter $\xi_s = 1$. In Fig. 30(b), $\xi_s = 1$ so the decays $s \to aa/\tilde{a}\tilde{a}$ are allowed and $s \to aa$ mostly dominates over the other decays (see Fig. 28) suppressing $BR(s \to ... \to \widetilde{Z}_1\widetilde{Z}_1)$, hence for the

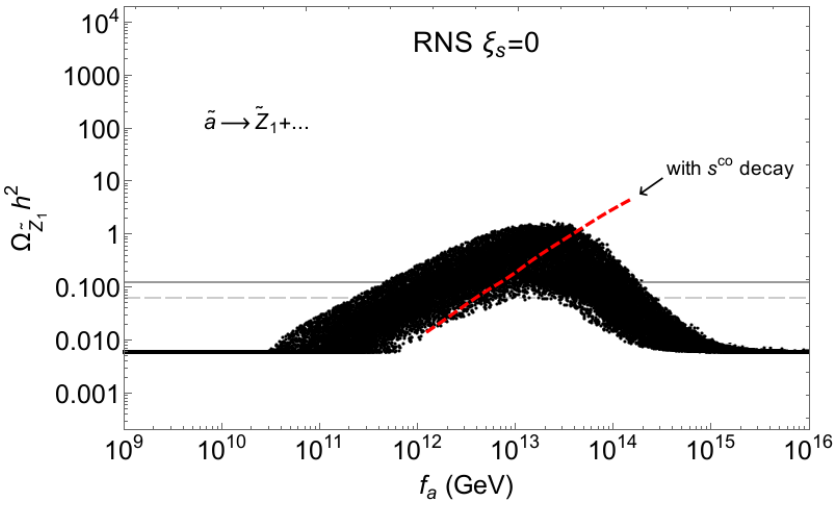


(a)

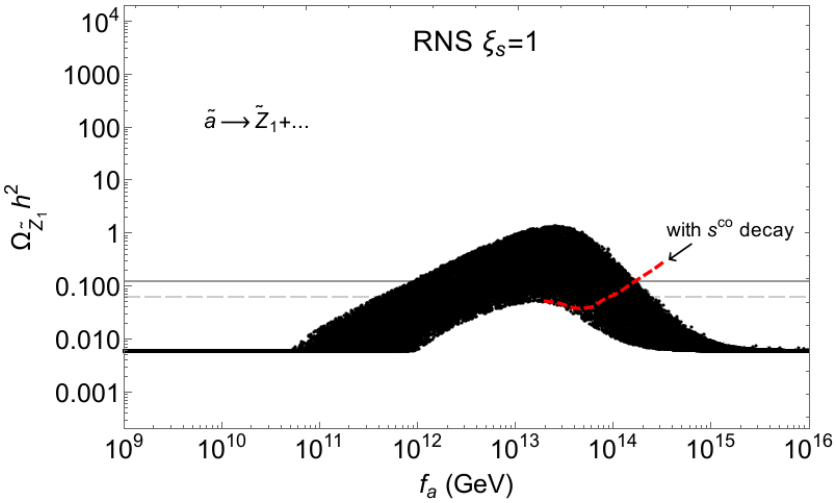


(b)

Figure 30: Neutralino dark matter abundance from axino decays (an illustrative scenario without saxion$^{\rm CO}$) in SUSY DFSZ model with (a) $\xi_s = 0$ and (b) $\xi_s = 1$ for the RNS benchmark point. Dashed red lines show the lower limit on $\Omega_{\tilde{Z}_1} h^2$ with saxion$^{\rm CO}$ contribution.

same parameter choices the neutralino relic density is smaller compared to the case $\xi_s = 0$. For the same reason, the neutralino relic density starts to rise at $f_a = 2 \times 10^{10}$ GeV for $\xi_s = 0$ but at $f_a = 5 \times 10^{10}$ GeV for $\xi_s = 1$. In both figures thermally produced saxions with $m_s \simeq 0.4$ TeV shapes the upper curve up to $f_a$ a few $\times 10^{13}$ GeV whereas in the region with higher $f_a$, $m_{\tilde{a}} \simeq 0.4$ TeV sets the boundary.

## III.3. Scan Results

In the following subsections, neutralino and axion relic abundances for $\xi_s = 0$ and $\xi_s = 1$ are computed separately through the numerical integration of the Boltzmann equations. In order to be as general as possible, the scan is over the following SUSY DFSZ parameters:

$$\begin{aligned} 10^9 \text{ GeV} < \ & f_a < 10^{16} \text{ GeV}, \\ 0.4 \text{ TeV} < \ & m_{\tilde{a}} < 20 \text{ TeV}, \\ 0.4 \text{ TeV} < \ & m_s < 20 \text{ TeV}. \end{aligned}$$

For simplicity, the initial saxion field strength is fixed at $s_0 = f_a$ ($\theta_s \equiv s_0/f_a = 1$) with $m_{\widetilde{G}} = 10$ TeV. Since the axion, axino and saxion thermal production rates are independent of the reheat temperature $T_R$, the bulk of the scan results do not depend on $T_R$. Nonetheless, the gravitino thermal abundance is proportional to $T_R$, and since gravitinos are long-lived they may affect BBN if $T_R$ is sufficiently large. In order to avoid the BBN constraints on gravitinos, $T_R = 10^7$ GeV is chosen. $T_R \ll 10^{11}$ GeV results in a sufficiently small (would-be) gravitino abundance, hence they typically do not contribute significantly to the neutralino abundance.

### III.3.1. $\xi_s = 0$

In this section, the scan result for the RNS benchmark with no direct coupling between saxions and axions/axinos ($\xi_s = 0$) is presented. In Fig. 31(a), $\Omega_{\widetilde{Z}_1}h^2$ vs. $f_a$ is shown for a scan over the parameter space defined in Eq. 78. Since for large $f_a$ values, saxions and axinos may decay during BBN, the BBN constraints using the bounds from Jedamzik [59] with extrapolations for intermediate values of $m_X$ other than those shown in his plots are applied. These constraints depend on the lifetime of the decaying state, its energy density before decaying and the fraction of energy injected as hadrons or color-charged states ($R_h$). In the DFSZ scenario, the dominant decays of saxions are into neutralinos,charginos, Higgs states or gauge bosons. Also, axinos decay into neutralinos or charginos plus gauge bosons or Higgs states. Thus the branching ratio for $s \to$ hadrons must be similar to $BR(W/Z \to \text{quarks})$ or $BR(\text{Higgs} \to \text{quarks})$, resulting in $R_h \sim 1$. So $R_h$ is conservatively taken as $R_h = 1$ for saxion and axino decays. In Fig. 31(a) the red points violate BBN bounds on late-decaying neutral relics, while the blue points are BBN safe. The points below the solid black line at $\Omega_{\widetilde{Z}_1}h^2 = 0.12$ are DM-allowed, whilst those above the line overproduce neutralinos and so would be ruled out. The dashed gray line denotes the level of equal axion-neutralino DM densities, each at 50% of the measured abundance. Since, as previously discussed, the thermal production of axions gives a negligible contribution to $\Delta N_{\text{eff}}$ and, for $\xi_s = 0$, there is no axion injection from saxion decays so the dark radiation constraints are always satisfied in this case.

For low values of $f_a \sim 10^9 - 10^{10}$ GeV, $\Omega_{\widetilde{Z}_1}h^2$ takes on its standard thermal value: 0.005. This is because with such a small value of $f_a$, the axino and saxion couplings to matter are sufficiently strong that they always decay before neutralino freeze-out. In this region, DM is mainly composed of axion with

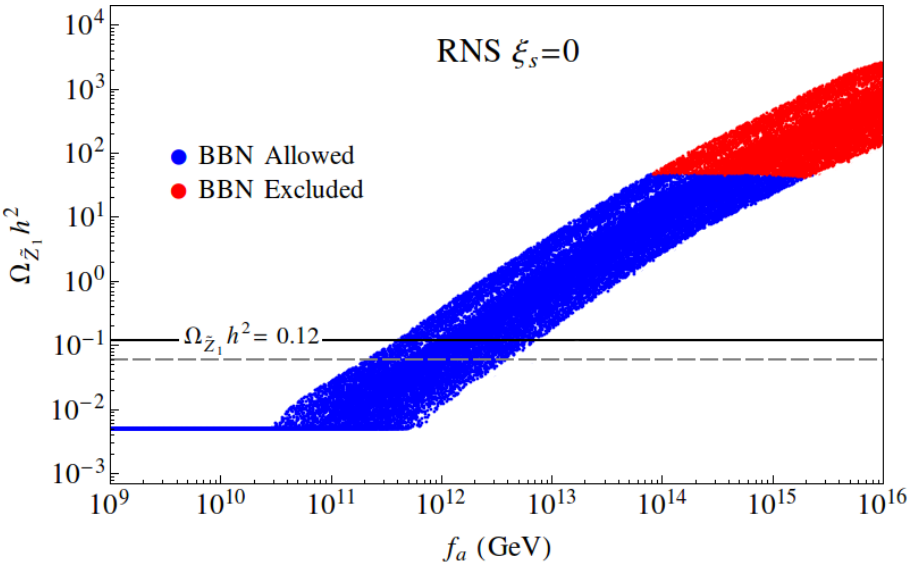


(a)

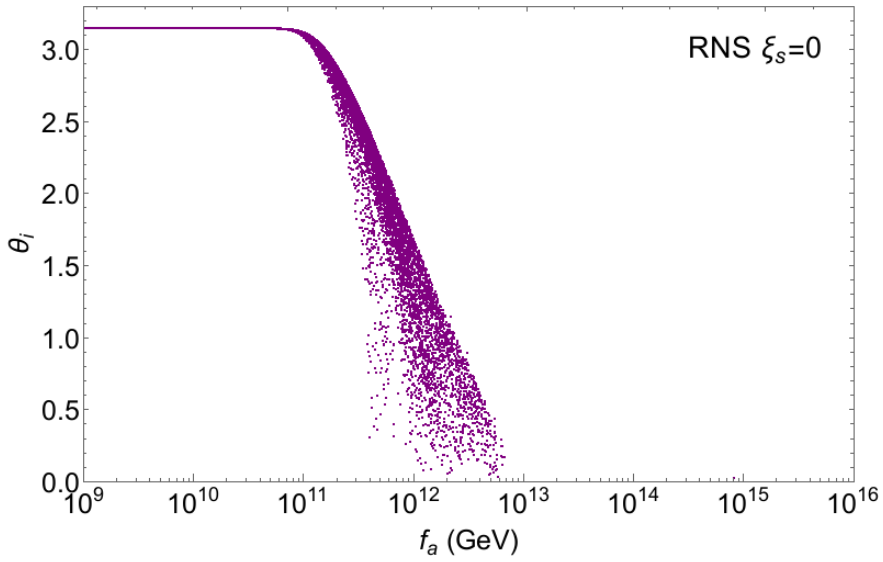


(b)

Figure 31: In (a), neutralino relic density from a scan over SUSY DFSZ parameter space for the RNS benchmark case with $\xi_s = 0$ is shown. The grey dashed line shows the points where DM consists of 50% axions and 50% neutralinos. In (b), the initial axion misalignment angle $\theta_i$ needed to saturate the dark matter relic density $\Omega_{\tilde{Z}_1+a}\ h^2 = 0.12$ is plotted.

$\sim 5-10\%$ contribution of higgsino-like WIMPs [80]. As $f_a$ increases, saxions and axinos decay more slowly, often after neutralino freeze-out. Late decays increase the neutralino density. If the injection of neutralinos from saxion/axino decays is sufficiently large, the 'supersaturated' decay-produced neutralinos re-annihilate, reducing their density. Although re-annihilation can reduce the neutralino density by orders of magnitude, its final value is always larger than the freeze-out density in the standard MSSM cosmology [81].

As $f_a$ increases, the thermal production of axinos and saxions decreases, while the density of saxion$^{\rm CO}$ increases (since $\theta_s = s_0/f_a = 1$). For $f_a \lesssim 10^{12}$ GeV, axinos and saxions are mostly thermally produced and $\Omega_{\widetilde{Z}_1}h^2$ rises steadily with $f_a$ mainly due to the increase of axino and saxion lifetimes, resulting in a late injection of neutralinos well after their freeze-out. On the other hand, for $f_a \gtrsim 5\times 10^{12}$ GeV, the thermal production of axions and axinos becomes suppressed and the main contribution to the neutralino abundance comes from coherently produced saxions and their decay. As seen in Fig. 31(a), once axinos and saxions start to decay after the neutralino freeze-out ($f_a \gtrsim 3\times 10^{10}$ GeV), $\Omega_{\widetilde{Z}_1}h^2$ always increases with $f_a$; this is due to the increase in saxion and axino lifetimes and also due to the increase in rate of CO-produced saxions in the region where $f_a \gtrsim 10^{13}$ GeV.

By the time $f_a$ exceeds $10^{13}$ GeV, then always too much neutralino DM is produced and the model is excluded. BBN constraints do not kick in until $f_a$ exceeds $\sim 10^{14}$ GeV. For a given $f_a$ value, the minimum value of $\Omega_{\widetilde{Z}_1}h^2$ seen in Fig. 31 happens for the largest saxion/axino masses considered in the scan (20 TeV). This is simply due to the fact that the lifetime decreases with the saxion/axino mass, resulting in earlier decays. As a result, neutralinos are injected earlier on and can re-annihilate more efficiently, since their annihilation rate increases with temperature. Hence, an increase in the axino/saxion mass

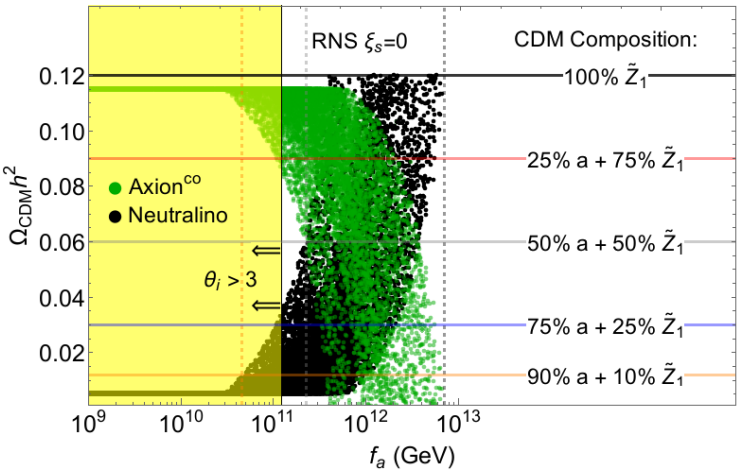


Figure 32: Axion (green points) and neutralino (black points) for the RNS benchmark case with $\xi_s = 0$ on Linear-Log plane with the same parameters in Fig. 31(a). Horizontal lines show the points that are composed of the given axion and neutralino percentage. $\theta_i > 3$ in the yellow shaded region.

usually implies a decrease in the neutralino relic abundance for a fixed $f_a$ value.

The axion misalignment angle $\theta_i$ which is needed to obtain $\Omega_{\widetilde{Z}_1}h^2+\Omega_a h^2 = 0.12$ is shown in Fig. 31(b). For low $f_a$ values ($\sim 10^9 - 10^{11}$ GeV), rather large values of $\theta_i \sim \pi$ are required to bolster the axion abundance into the range of the measured DM density. For values of $f_a \sim 10^{11} - 10^{12}$ GeV, then values of $\theta_i \sim 2$ are required. For $f_a \geq 4 \times 10^{12}$ GeV, axions tend to get overproduced by CO-production and so a small value of $\theta_i \lesssim 0.5$ is required for suppression. For even higher $f_a$ values, too many neutralinos are produced, so the models are all excluded.

Neutralino and axion DM abundances as a function of $f_a$ for the allowed points are shown together in Fig. 32 in a Linear-Log plane. For $f_a < 3 \times 10^{10}$ GeV, it is seen that axions make up more than 90% of the total dark matter abundance. Axions and neutralinos may contribute to dark matter density in equal amounts, 50% axino and 50% neutralino, within the region bounded by $2 \times 10^{11}$ GeV$< f_a < 4 \times 10^{12}$ GeV. Note that this does not imply that for a

given $f_a$ value in that region there is equal amount of axion and neutralino dark matter, but this is the region where the condition $\Omega_{\widetilde{Z}_1}h^2 = \Omega_a h^2$ can be satisfied. The neutralino becomes strictly the dominant DM component within a small $f_a$ region from $f_a \simeq 4\times 10^{12}$ GeV to $f_a \simeq 10^{13}$ GeV after which the whole parameter space is excluded by overproduction of dark matter. The yellow shaded region indicates the range of $f_a$ where $\theta_i > 3$ and can be considered to be fine-tuned in axion$^{\rm CO}$ production process.

### III.3.2. $\xi_s = 1$

In this section, the scan result for the RNS benchmark with a non-vanishing saxion-axion/axino coupling is presented. For simplicity, $\xi_s$ is fixed to 1, where $\xi_s$ is defined in Eq. (58). In this case saxions can directly decay to axions and axinos when kinematically allowed (if $m_s > 2m_{\tilde{a}}$). The $s \to aa$ decay usually dominates over the other decays as shown in Fig. 28, suppressing $BR(s \to \ldots \to \widetilde{Z}_1\widetilde{Z}_1)$ and significantly reducing the neutralino injection from saxion decays. As a result, the neutralino relic abundance is usually smaller (for the same choice of PQ parameters) than the $\xi_s = 0$ case. Furthermore, the saxion lifetime is reduced (due to the large $s \to aa$ width) and saxions tend to decay earlier when compared to the $\xi_s = 1$ case.

In Fig. 33(a), once again $\Omega_{\widetilde{Z}_1}h^2$ vs. $f_a$ for the RNS SUSY benchmark but now for $\xi_s = 1$ is plotted. As just discussed, in this case the saxion lifetime is reduced, so the region of $f_a$ where saxions/axinos always decay before freeze-out is extended beyond the values generated for the $\xi_s = 0$ case. Since $BR(s \to \ldots \to \widetilde{Z}_1\widetilde{Z}_1)$ is suppressed in the $\xi_s = 1$ case, saxions do not significantly contribute to $\Omega_{\widetilde{Z}_1}h^2$ except when $f_a \gtrsim 10^{14}$ GeV where saxion$^{\rm CO}$ has such large densities that –even though their branching ratio to neutralinos is at the 0.1% level– their decay still enhances the neutralino relic density. For $10^{11}$ GeV $\lesssim f_a \lesssim 10^{14}$

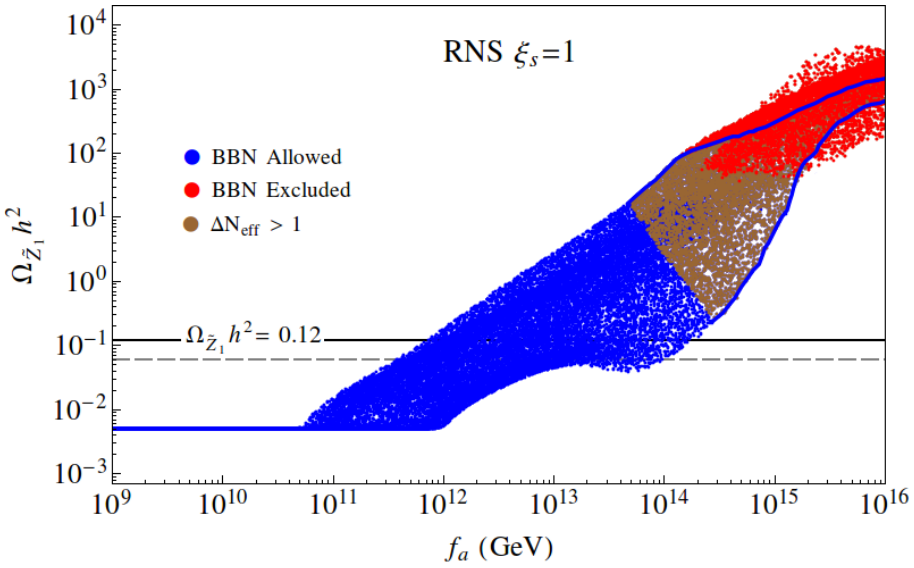


(a)

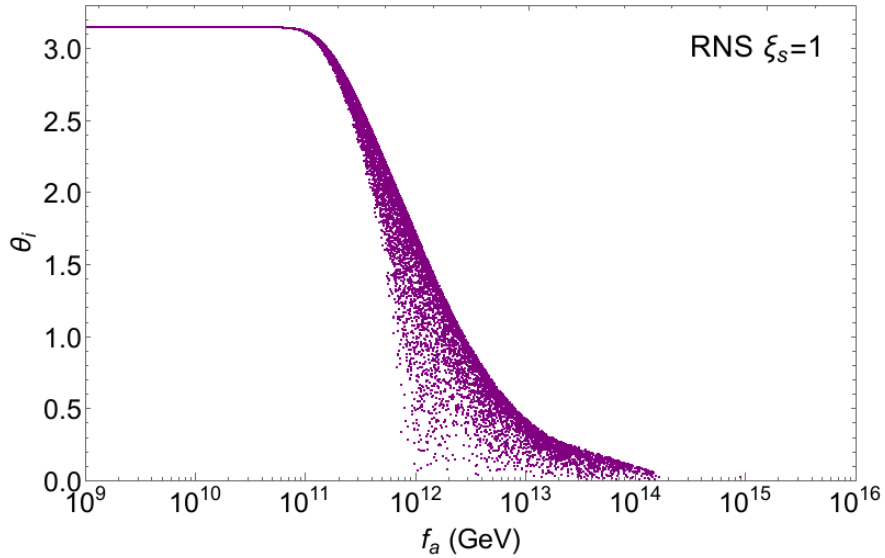


(b)

Figure 33: In (a), neutralino relic density from a scan over SUSY DFSZ parameter space for the RNS benchmark case with $\xi_s = 1$ is shown. The grey dashed line shows the points where DM consists of 50% axions and 50% neutralinos. The red BBN-forbidden points occur at $f_a \gtrsim 10^{14}$ GeV and above. Brown points are excluded by too much dark radiation $N_{\rm eff} > 4$. In (b), the initial axion misalignment angle $\theta_i$ needed to saturate the dark matter relic density $\Omega_{\tilde{Z}_1+a}\ h^2 = 0.12$ is plotted.

GeV however, $\Omega_{\widetilde{Z}_1}h^2$ is dominated by the thermal axino contribution and the neutralino relic density increases with $f_a$, as in the $\xi_s = 0$ case. Once $f_a \gtrsim 10^{13}$ GeV, the thermal production of axinos becomes strongly suppressed and despite decaying well after neutralino freeze-out, their contribution to $\Omega_{\widetilde{Z}_1}h^2$ starts to decrease as $f_a$ increases. This is seen by the turn over of $\Omega_{\widetilde{Z}_1}h^2$ around $f_a \sim 10^{13}$ GeV. Parameters that show this behavior have $m_s < 2m_{\tilde{a}}$ so the decay $s \to \tilde{a}\tilde{a} \to \widetilde{Z}_1\widetilde{Z}_1$ is not allowed hence decay contribution to neutralino DM is minimal. As $f_a$ increases past $10^{14}$ GeV, saxions$^{\rm CO}$ start to contribute to the neutralino relic density, which rises with $f_a$. The blue lines show the borders of BBN-allowed points that are hidden under brown and red coloration. Unlike the $\xi_s = 0$ case, there are BBN-allowed points for all $f_a$ values due to shorter lifetime of saxion$^{\rm CO}$, even at $f_a \sim 10^{16}$ GeV.

Another important difference in the $\xi_s = 1$ case is the large injection of relativistic axions from saxion decays. For large values of $f_a$, where the density of saxions$^{\rm CO}$ is enhanced, the injected axions have a non-negligible contribution to $\Delta N_{\rm eff}$. In particular, for $f_a \gtrsim 10^{14}$ GeV, saxion$^{\rm CO}$ decays produce too much dark radiation, so this region (shown by brown points in Fig. 33(a) is excluded by the cosmic microwave background (CMB) constraints [5] on dark radiation ($\Delta N_{\rm eff} < 1$). These points are also excluded by overproduction of neutralinos and violation of BBN bounds.

In Fig. 33(b), the $\theta_i$ value which is needed by axions so that one matches the measured abundance of DM, is shown. Once again, at low $f_a$, $|\theta_i| \sim \pi$ is required, while for high $f_a$ values ($\gtrsim 10^{13}$ GeV), low $|\theta_i|$ is required in order to suppress axion$^{\rm CO}$ production. Furthermore, since $\Omega_{\widetilde{Z}_1}h^2$ is usually smaller in the $\xi_s = 1$ case for the same $f_a$ values (when compared to $\xi_s = 0$), the axion$^{\rm CO}$ contribution to DM can be larger and higher values of $\theta_i$ are usually allowed, as seen in Fig. 33(b).

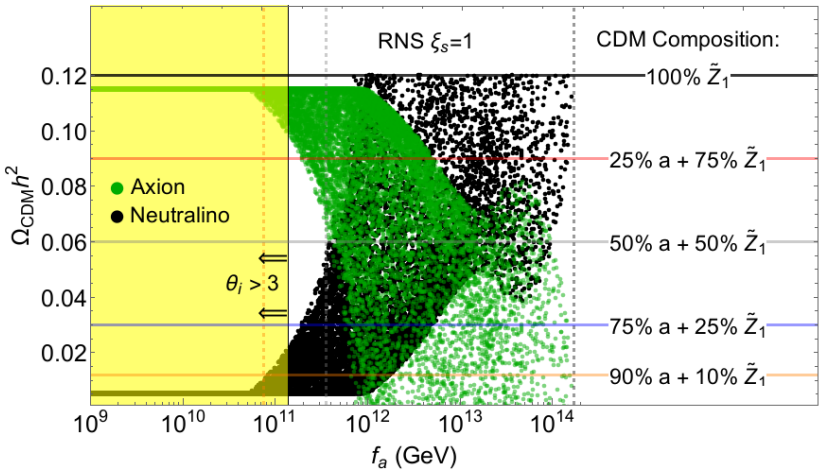


Figure 34: Axion (green points) and neutralino (black points) for the RNS benchmark case with $\xi_s = 1$ on Linear-Log plane with the same parameters in Fig. 33(a). The horizontal lines show the points that are composed of the given axion and neutralino percentage. $\theta_i > 3$ in the yellow shaded region.

Finally, in Fig. 34, the neutralino and axion DM abundances as a function of $f_a$ for the allowed points are shown together in a Linear-Log plane for $\xi_s = 1$. The axion makes up more than 90% of the total dark matter abundance for $f_a \leq 8 \times 10^{10}$ GeV which is slightly higher compared to the $\xi_s = 0$ case due to the additional decay modes as discussed before. Equal amounts of DM components; 50% axino and 50% neutralino can exist in a more spread region bounded by $4 \times 10^{11}$ GeV$\leq f_a \leq 10^{14}$ GeV. For $f_a \gtrsim 2 \times 10^{14}$ GeV, the region is excluded by over production of DM. $\theta_i > 3$ in the yellow shaded region which is considered to be fine-tuned.

In this section, results for axion-higgsino mixed DM are presented. However, the results do not strictly depend on the benchmark point chosen. A scan for a benchmark point with similar thermal neutralino density (underabundance), $m_{\tilde{Z}_1}$ (or $2m_{\tilde{Z}_1} < m_s|_{min}$) and $\mu$ would give similar results on $f_a$ vs. $\Omega_{\tilde{Z}_1}h^2$. For example, the RNS model with wino LSP generates similar results to the SUSY DFSZ scenario [82].

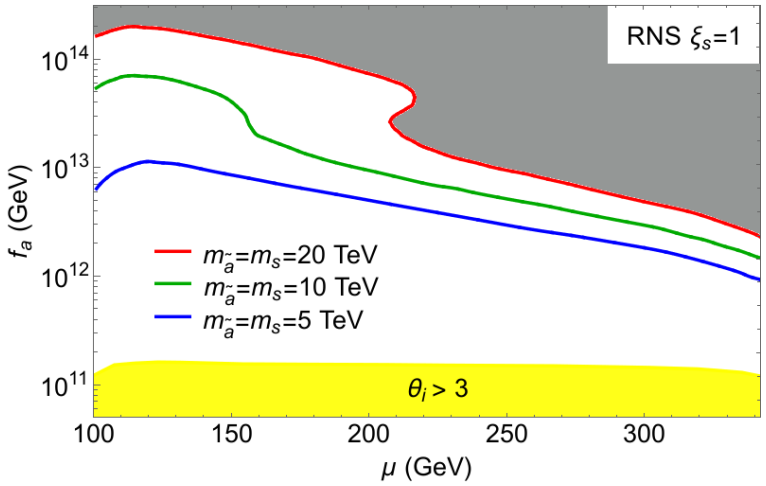


Figure 35: Contours of allowed $f_a$ region as $\mu$ varies along the RNS benchmark model parameters with $\xi_s = 1$. The region covered with black stripes is excluded due to overproduction of dark matter and/or $\Delta N_{\rm eff} > 1$ and/or BBN constraints.

In order to see how sensitive the allowed $f_a$ region is to the $\mu$ parameter, contour lines for a given axino and saxion mass in the $f_a$ vs $\mu$ plane are shown in Fig. 35. Keeping other parameters $(m_0, m_{1/2}, A_0, tan\beta, m_A, \theta_s, T_R)$ set at the RNS DFSZ benchmark model, $\mu$ is varied between 100 GeV and 342 GeV. For $\mu > 342$ GeV, the neutralino becomes bino-like and when $\mu \simeq 360$ GeV, the thermal neutralino relic abundance (without PQ sector) reaches the observed value: $\Omega^{std}_{\tilde{Z}_1}h^2 = \Omega_{\rm CDM}h^2 = 0.12$. With increasing $\mu$, $\Omega^{std}_{\tilde{Z}_1}h^2$ increases so there is less room for axion dark matter even at low $f_a$.

Contour lines in Fig. 35 show allowed $f_a$ values by all constraints for $m_{\tilde{a}} = m_s = 5$ (blue), 10 (green) and 20 (red) TeV. Mixed axion-higgsino dark matter can exist in the region below the contour lines, the lower limit of $f_a$ is $\sim 10^9$ GeV based on astrophysical observations or higher for *natural* $\theta_i$ values. The $f_a$ region where $\theta_i > 3$ is needed is also shown in Fig. 35 as the yellow shaded region which can be interpreted as *unnatural* so it defines a lower naturalness bound on $f_a$. For a fixed $\mu$, as axino and saxion mass increase, $f_a$ can take higher values since

their lifetime gets shorter. For the chosen parameters, the boundaries are only determined by the dark matter density as BBN and dark radiation constraints become more important at higher $f_a$ where the model is already excluded due to overproduction of DM as in Fig. 33.

## III.4. Axion-Bino Dark Matter

In this section, the scan results for the mixed axion-bino dark matter using the CMSSM benchmark point are presented. As in the previous case, the SUSY spectrum is generated using Isajet. The CMSSM point has $\mu = 3110$ GeV and $m_{\tilde{g}} = 1970$ GeV which is beyond LHC gluino mass constraints [83, 84]. A similar SUSY DFSZ scenario has been studied in Ref. [43] with a benchmark point with standard overabundance (SOA) neutralino density.

For this benchmark point, the lightest neutralino is mainly bino-like with $m_{\widetilde{Z}_1} = 359.9$ GeV, and the standard neutralino thermal abundance is found to be $\Omega^{std}_{\widetilde{Z}_1} h^2 \simeq 24.5$, a factor of $\sim 200$ above the measured value. Due to its large $\mu$ parameter, this point has high electroweak finetuning $\Delta_{\rm EW} = 2327$ but for the same reason axino and saxion decay rates, which are porportional to some power of $\mu$, are bolstered. With a higher $\mu$ value, axino and saxion decay temperatures are one or two orders of magnitude larger compared to the RNS DFSZ model, so their lifetime is shorter for the CMSSM DFSZ scenario.

For the axion-bino DM calculation, SUSY DFSZ parameters are chosen as follows:

$$10^9 \text{ GeV} < \ f_a < 10^{16} \text{ GeV},$$

$$0.5 \text{ TeV} < \ m_{\tilde{a}} < 20 \text{ TeV},$$

$$0.5 \text{ TeV} < \ m_s < 20 \text{ TeV}.$$

As in the RNS DFSZ scenario, the initial saxion field strength is fixed at $s_0 = f_a$

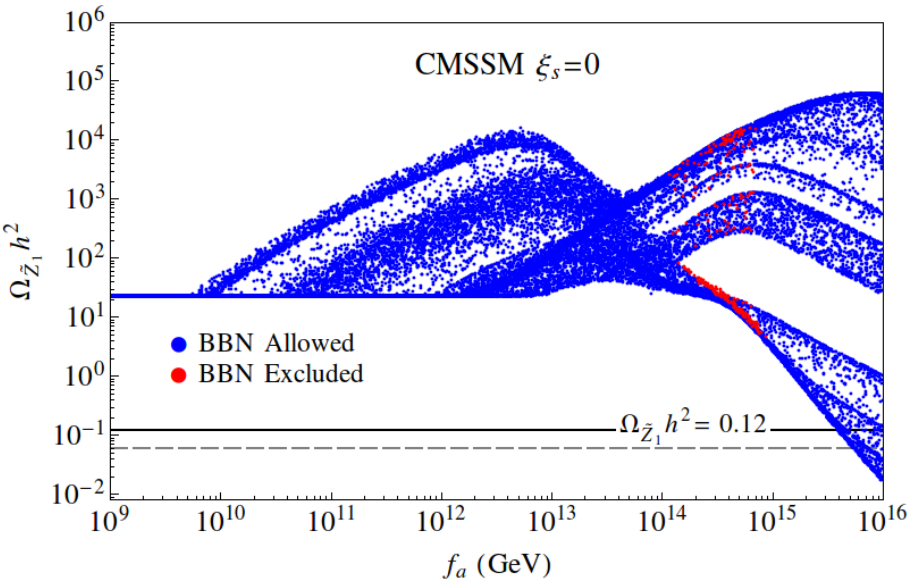


Figure 36: Neutralino relic density from a scan over SUSY DFSZ parameter space for the CMSSM benchmark case with $\xi_s = 0$. The solid black line shows measured relic density and the grey dashed line shows the points where DM consists of 50% axions and 50% neutralinos.

($\theta_s \equiv s_0/f_a = 1$) and $m_{\tilde{G}} = 10$ TeV. For the CMSSM benchmark point, the lower limit for the $m_a = m_s$ is set to 0.5 TeV so that $\tilde{a} \to \widetilde{Z}_1 + h$ ($m_{\widetilde{Z}_1} \simeq 360$ GeV) is kinematically allowed as in the mixed axion-higgsino calculation.

### III.4.1. $\xi_s = 0$

The first scan results are shown in Fig. 36 for the CMSSM benchmark point with $\xi_s = 0$. Unlike the axion-higgsino scenario, there are BBN-allowed points for all $f_a$ values. A few points with $m_{\tilde{a}} < 700$ GeV violate BBN constraints at $f_a \gtrsim 10^{14}$ GeV but when $f_a$ reaches up to $10^{15}$ GeV, axinos are underproduced and do not violate BBN constraints. Moreover, the saxion decays before BBN starts since the $\mu$ term enhances its decay to Higgs pairs and to vector bosons even at large $f_a$.

For low values of $f_a$, $f_a \lesssim 5 \times 10^9$ GeV axinos and saxions decay before

neutralino freeze-out so $\Omega_{\widetilde{Z}_1}h^2$ takes its standard value. When $f_a$ is in between $\sim 10^{10-13}$ GeV, there are distinct branches that enhance the neutralino relic density. For the RNS benchmark point, neutralino and chargino masses are less than $\mathcal{O}(1)$ TeV so there are no distinct branches due to the decay modes. These branches due to axino decays can be classified into three groups:

- The uppermost branch corresponds to $m_{\tilde{a}} \lesssim 780$ GeV $\simeq (m_{\widetilde{Z}_2}) + (m_Z)$. For the low $m_{\tilde{a}}$, the open decay channels are $\tilde{a} \to \widetilde{Z}_1 + Z/h$ so the axinos mostly decay into neutralinos.

- Points with 780 GeV$\lesssim m_{\tilde{a}} \lesssim$3300 GeV form the middle branch since additional decay channels are now open: $\tilde{a} \to \widetilde{Z}_2 + Z/h$ and $\tilde{a} \to \widetilde{W}_1^{(\pm)} + W^{(\mp)}$ so the decays into neutralino dark matter are diminished.

- For $m_{\tilde{a}} \gtrsim$3200 GeV, there are three additional decay channels since $m_{\widetilde{Z}_3} \simeq m_{\widetilde{Z}_4} \simeq m_{\widetilde{W}_2}$. Neutralino dark matter is not enhanced till $f_a \simeq 10^{12}$ GeV due to $\tilde{a} \to \widetilde{W}_2^{(\pm)} + W^{(\mp)}$ and $\widetilde{Z}_{3/4} + Z/h$ decays.

In the large $f_a$ region, there is a visible gap (for a fixed $f_a$ value) between the branch with a suppression of $\Omega_{\widetilde{Z}_1}h^2$ and the one with an enhanced value of $\Omega_{\widetilde{Z}_1}h^2$. The lower branch (with $\Omega_{\widetilde{Z}_1}h^2 \lesssim 1$) corresponds to points with low saxion masses, where $BR(s \to \ldots \widetilde{Z}_1\widetilde{Z}_1) \ll 1$, so saxion decays mostly dilute the neutralino relic density. Once $m_s > 2m_{\tilde{t}_1}$, the $s \to \tilde{t}_1\bar{\tilde{t}}_1$ channel becomes kinematically allowed and there is a sudden increase in $\Omega_{\widetilde{Z}_1}h^2$, resulting in the gap seen in Fig. 36. For $f_a < 4 \times 10^{15}$ GeV, the model is excluded due to overproduction of dark matter.

Axino and saxion decays increase neutralino relic density for the $f_a$ values up to $\sim 2 \times 10^{14}$ GeV. At higher $f_a$, the majority of points show a different behavior and the neutralino relic abundance actually decreases with increasing $f_a$ since

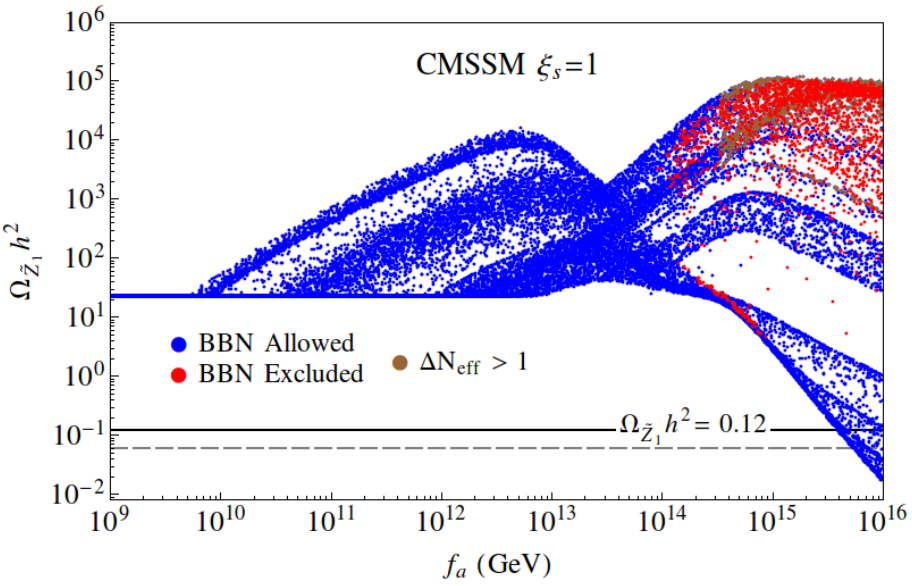


Figure 37: Neutralino relic density from a scan over SUSY DFSZ parameter space for the CMSSM benchmark case with $\xi_s = 1$. The solid black line shows measured relic density and the grey dashed line shows the points where DM consists of 50% axions and 50% neutralinos.

the only effect of saxion decays ($\xi_s = 0$ so $s \to aa$ is not allowed) is to inject entropy into the early Universe. There is a huge rate for saxion production via coherent oscillations and the entropy injection from saxion decays which reduce the neutralino density. The neutralino relic abundance even decreases below the measured value for a subset of points with $m_s \lesssim 1.3$ TeV (lower limit for $m_s$ during the scan is 0.5 TeV). This behavior is studied in the subsection III.4.3.

### III.4.2. $\xi_s = 1$

Scan results for the CMSSM benchmark point with $\xi_s = 1$ is shown in Fig. 37. Unlike the RNS scenario, decays to axions are not always dominant, since $\Gamma(s \to aa) \sim m_s^3/f_a^2$, while $\Gamma(s \to WW/ZZ, hh) \sim \mu^4/(m_s f_a^2)$. Hence saxions dominantly decay to gauge bosons/higgses, except for $m_s \gg \mu$. The low $f_a$ behavior of $\Omega_{\tilde{Z}_1} h^2$ is much the same as in the $\xi_s = 0$ case: the neutralino abundance is

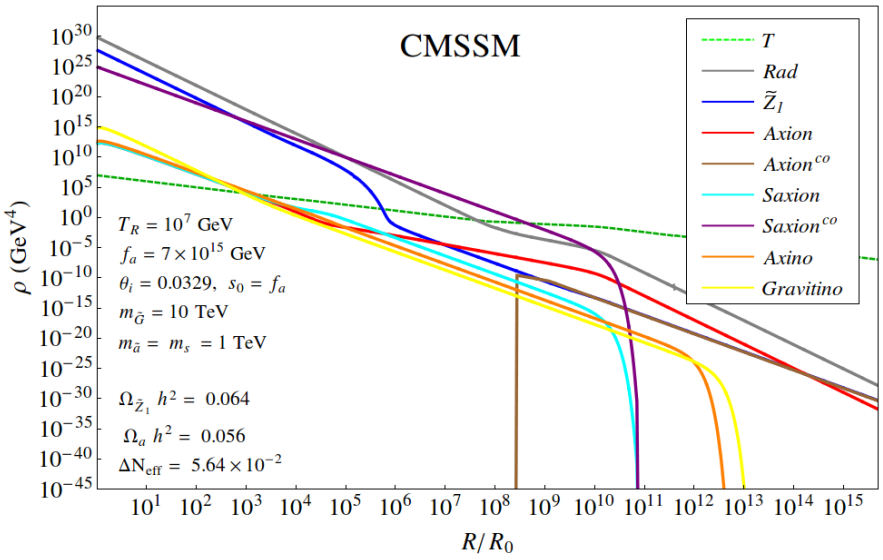


Figure 38: Evolution of various energy densities vs. scale factor $R/R_0$ for the CMSSM benchmark scenario with parameters as indicated in the figure.

only bolstered to even higher values and thus remains excluded by overproduction of WIMPs. As in the $\xi_s = 0$ case, there again exists a set of points with $f_a \gtrsim 4 \times 10^{15}$ GeV and with $m_s \lesssim 1.3$ TeV which is allowed by all constraints. This is possible in the $\xi_s = 1$ case, since, for $m_s \ll \mu$, saxions mainly decay to higgses and gauge bosons, thus injecting enough entropy to dilute $\Omega_{\tilde{Z}_1} h^2$. Points with $m_s \gg \mu$, however, have $BR(s \to aa) \simeq 1$, resulting in a large injection of relativistic axions and a suppression of entropy injection. In this case many models start to become excluded by overproduction of dark radiation (brown points). It can be concluded that the SUSY DFSZ model with large $\mu$ and either small or large $\xi_s$ along with small $m_s$ is able to reconcile the expected value of Peccei-Quinn scale from string theory [85] (where $f_a$ is expected $\sim m_{\rm GUT}$) with dark matter abundance, dark radiation and BBN constraints.

### III.4.3. $\Omega_{\widetilde{Z}_1} h^2 \leq 0.12$

The allowed region for the CMSSM benchmark point is $f_a \gtrsim 4 \times 10^{15}$ GeV due to high saxion$^{\rm CO}$ production which results in entropy injection. A specific example is shown in Fig. 38, where the evolution of the energy density of various species as a function of the Universe scale factor is presented for $f_a = 7 \times 10^{15}$ GeV and $m_s = m_{\tilde{a}} = 1$ TeV. For this choice of parameters, the neutralino relic abundance is highly suppressed ($\Omega_{\widetilde{Z}_1} h^2 = 0.064$) but does approximately comprise 50% of the total DM abundance. The remaining ∼50% is composed of axions although these require a somewhat small value of the axion misalignment angle ($\theta_i = 0.0329$) in order to suppress the axion$^{\rm CO}$ production. From Fig. 38 it is seen that the saxion$^{\rm CO}$ energy density dominates over the radiation energy density at $R/R_0 \sim 10^5$ and decays at $R/R_0 \sim 10^{11}$, so that the Universe is saxion-dominated during this period. In this case, saxions dominantly decay into SM particles, since the rate for saxion → neutralinos is highly suppressed by the kinematic phase space factor in $BR(s \to \widetilde{Z}_1 \widetilde{Z}_1) \sim 10^{-8}$ at this point. Therefore, a huge amount of entropy is produced that can be seen from the radiation curve (grey), while the neutralino density (blue) is almost unaffected by the saxion decay. As a result, the final neutralino density is given by $\Omega_{\widetilde{Z}_1} h^2 = 0.064$ and this can be a viable model, even though the PQ scale is very large. The axino and gravitino decay at a later time than the saxion but they do not violate the BBN constraint since their abundance is small.

Only the points with $m_s \lesssim 1.3$ TeV can meet the dark matter constraint since for higher saxion mass, the decays $s \to \widetilde{Z}_1 \widetilde{Z}_j$ and $s \to ... \to \widetilde{Z}_1 + ...$ greatly enhances neutralino dark matter density. Scan results only for the set of parameters that result in $\Omega_{\widetilde{Z}_1} h^2 \leq 0.12$ are shown in Fig. 39(a). The lower limit of the branch with $\Omega_{\widetilde{Z}_1} h^2 \leq 0.12$ has $m_s < 2 \times \widetilde{Z}_1$ so the saxion decays do

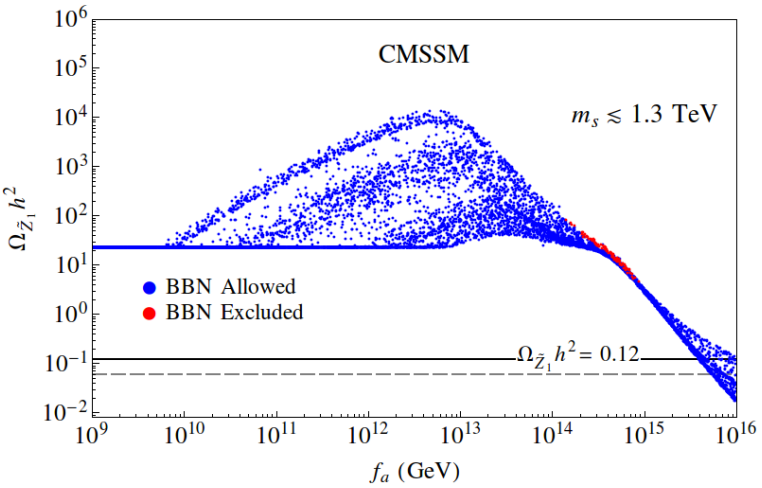


(a)

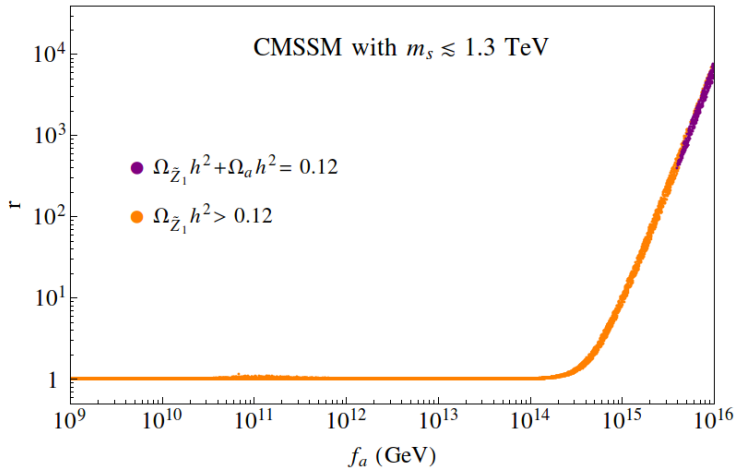


(b)

Figure 39: In (a), the neutralino relic density vs $f_a$ for the scan over the SUSY DFSZ parameter space for the CMSSM benchmark case with $m_s \lesssim 1.3$ TeV is shown. The grey dashed line shows the points where DM consists of 50% axions and 50% neutralinos. In (b) the dilution factor $r$ vs. $f_a$ is plotted.

not directly or indirectly contribute to neutralino abundance but inject entropy to the Universe. For higher values of $m_s$, the neutralino abundance increases for a fixed $f_a$. The saxion mass is $\simeq$1.3 TeV on the upper limit of the branch. For even higher saxion mass, $m_s \simeq 1.4$ TeV, which is the threshold mass for the decays $s \to \widetilde{Z}_2\widetilde{Z}_2$ and $s \to \widetilde{W}_1^{\pm}\widetilde{W}_1^{\mp}$, another distinct branch forms as seen in Fig. 36 and in Fig. 37 but such points overproduce DM.

Fig. 39(b) shows how the entropy dilution factor ($r \equiv S_f/S_0$) increases with $f_a$, reaching values as high as $10^4$, for $f_a \sim 10^{16}$ GeV. For other branches at high $f_a$ that violate the dark matter constraint, the dilution factor shows a similar behavior as in Fig. 39(b).

The results for axion-bino mixed DM for the CMSSM benchmark point are presented in this section. For CMSSM models that satisfy Higgs mass and LHC constraints, the neutralino (bino LSP) relic abundance without PQ symmetry can range from $\mathcal{O}(1)$ to $\mathcal{O}(10^5)$ [86] so $\Omega_{\widetilde{Z}_1}h^2$ vs. $f_a$ plots for different benchmark points would have some major differences in terms of dark matter abundance in the region $\Omega_{\widetilde{Z}_1}h^2 > 0.12$. However, since the entropy dilution due to saxion decays does not occur for $f_a$ less than $\sim 10^{14}$ GeV, the points that are allowed by the dark matter constraints would again be in the high $f_a$ region, $f_a \gtrsim 10^{15}$ GeV, for a benchmark point with standard neutralino overabundance.

# IV. WIMP and Axion Searches

## IV.1. Implications for WIMP Detection

Pure neutralino dark matter and its implications for searches in deflected AMSB scenario and in CMSSM/NUHM models have been studied in Ref [87] and in Ref. [88, 89, 90] respectively. In Chapter III., mixed axion-neutralino dark matter models with over- and under-abundant neutralino DM are considered for the specific benchmark points: RNS and CMSSM. The focus of this chapter is to study the implications of 2 component dark matter for WIMP searches with a broader range of parameters. The results are not based on a single benchmark point with fixed parameters but with a general scan over SUSY parameters. Scan results for both bino- and higgsino-like neutralinos are required to obey the following constraints:

- The neutralino $\widetilde{Z}_1$ is the lightest MSSM particle,
- $m_h$ =125±2 GeV (±2 GeV to account for computational uncertainty),
- $-2.3 \times 10^{-9} < \Delta\mathrm{Br}(B_s \to \mu^+\mu^-) < 0.6 \times 10^{-9}$
  and $-3.6 \times 10^{-5} < \Delta\mathrm{Br}(b \to s\gamma) < 9.2 \times 10^{-5}$ [91],
- $m_{\widetilde{W}_1^{\pm}} > 103.5$ GeV [18],
- $m_{\tilde{g}} > 1.8$ TeV [83],
- $m_{\widetilde{Z}_1}$ vs. $m_{\tilde{t}_1}$ boundaries [92] are respected.

Only the results that satisfy all the constraints are shown on the reach plots.

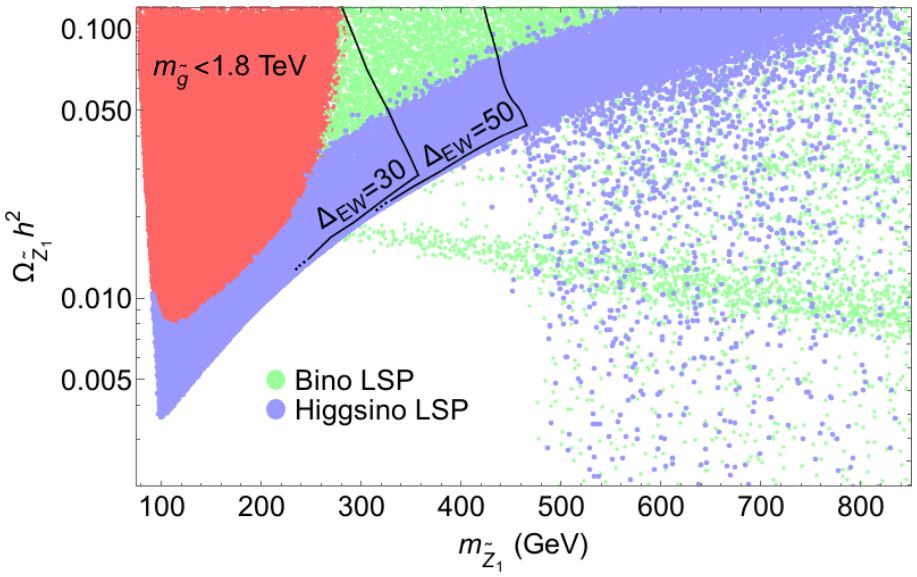


Figure 40: Plot of standard thermal neutralino abundance $\Omega^{std}_{\tilde{Z}_1}h^2$ vs. $m_{\tilde{Z}_1}$ from a scan over NUHM2 parameter space.

### IV.1.1. Higgsino-Like Neutralino

In RNS models, higgsino-like neutralino dark matter is underproduced. Indeed, even in the SUGRA-19 model higgsino- and wino-like neutralino, DM is underproduced for $m_{\tilde{Z}_1} < 500$ GeV [27]. Results presented in this section are generated with a scan over the following NUHM2 parameters:

$$\begin{aligned} 2 \text{ TeV} < \ & m_0 < 10 \text{ TeV}, \\ 0.65 \text{ TeV} < \ & m_{1/2} < 2 \text{ TeV}, \\ -3 \ < \ & A_0/m_0 < 3, \\ 3 \ < \ & \tan\beta < 60, \\ 0.1 \text{ TeV} < \ & \mu < 1.1 \text{ TeV}, \\ 1 \text{ TeV} < \ & m_A < 10 \text{ TeV}. \end{aligned}$$

In Fig. 40, standard thermal neutralino abundance $\Omega^{std}_{\widetilde{Z}_1}h^2$ vs. neutralino LSP mass up to $m_{\widetilde{Z}_1} = 850$ GeV is plotted. The ATLAS working group has excluded the region $m_{\tilde{g}} \lesssim 1.8$ TeV for $m_{\widetilde{Z}_1} < 0.8$ TeV [83]. The excluded region, which assumes $\tilde{g} \to b\bar{b}\widetilde{Z}_1$ decay, is shown in red color. Parameters that result in a bino-like LSP are marked in green color. Points with bino-like LSP in SUSY DFSZ model that generate standard underabundance neutralino density would show a different behavior than higgsino-like LSP since $m_{\widetilde{Z}_1} \ll \mu$ and so will not be considered in this section. $\Delta_{\rm EW} = 50$ contour shows the natural SUSY boundary where $m_{\widetilde{Z}_1}$ is allowed up to $\simeq 460$ GeV. When $\Delta_{\rm EW}$ reaches 50, $\mu \simeq 450$ GeV in order to cancel out a somewhat large $C(H_u)$ term in Eq. 28. A more severe naturalness limit dictates $\Delta_{\rm EW} < 30$ which only allows 3% fine-tuning and sets an upper limit to $\mu \lesssim 300$ GeV. The $\Delta_{\rm EW}$ contours are drawn to show the upper limit on $m_{\widetilde{Z}_1}$ by naturalness. The NUHM2 model is considered as fine-tuned when $m_{\widetilde{Z}_1} \geq 650$ GeV where $\Delta_{\rm EW} > 100$. There is an apparent blue band that increases with increasing $m_{\widetilde{Z}_1}$; this band corresponds to a mostly pure higgsino state. Points which are below the band have smaller $\Omega^{std}_{\widetilde{Z}_1}h^2$ due to highly mixed higgsino-bino states due to coannihilation mostly through $A-$resonance.

WIMP searches by the collaborations DARWIN, LUX, LZ (joint LUX & ZEPLIN) and XENON set limits on spin-(in)dependent neutralino-proton scattering rate in cm$^2$ for a given $m_{\widetilde{Z}_1}$. Current (LUX(2015) [93] and XENON100 [94]) and projected (DARWIN [95], LZ [96] and XENON [97]) reach of experiments by the collaborations are plotted in Fig. 41. $\sigma^{\rm SI}(\widetilde{Z}_1, p)$ for the NUHM2 model is calculated using the updated IsaReD [74]. The result is rescaled by a factor $\xi = \min[1, \Omega^{\rm std}_{\widetilde{Z}_1}h^2/0.12]$ to account for the fact that the local relic abundance might be less than the usually assumed value $\rho_{\rm local} \simeq 0.3$ GeV/cm$^3$, as suggested by Bottino *et al.* [98].

Results from a scan over NUHM2 parameters are shown in Fig. 41. Probed

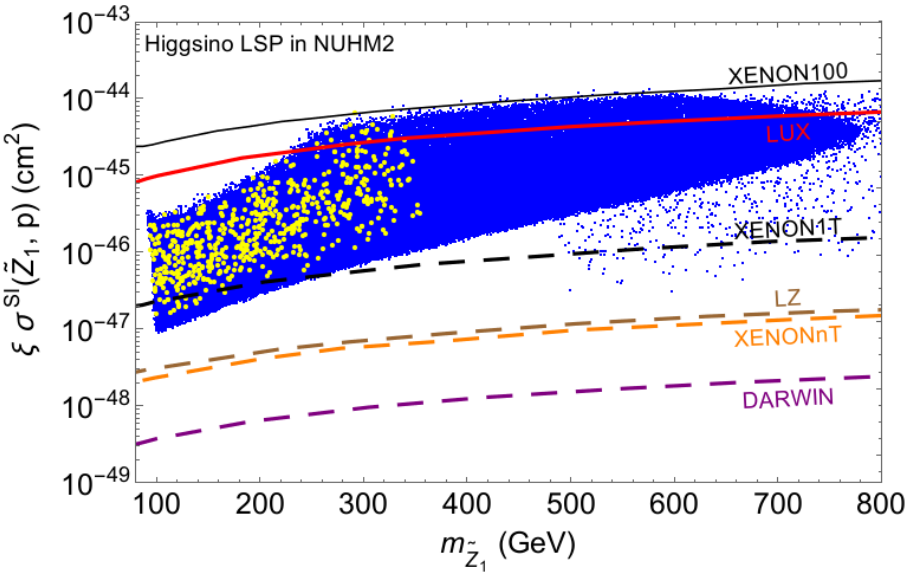


Figure 41: Plot of rescaled higgsino-like WIMP spin-independent direct detection rate $\xi\sigma^{\rm SI}(\widetilde{Z}_1, p)$ versus $m_{\widetilde{Z}_1}$ from a scan over NUHM2 parameter space with $\Delta_{\rm EW} < 30$ colored yellow. The current reach from the XENON100(2012) and LUX(2015) experiment and projected reaches of XENON1T, LZ and Darwin are shown.

cross section values with no observation of dark matter are shown with continous lines whereas projected reaches are indicated by dashed lines. The missing region within $m_{\widetilde{Z}_1} \lesssim 250$ GeV and $\sigma^{\rm SI}(\widetilde{Z}_1 p) \gtrsim 4\times 10^{-46}$ cm$^2$ is from LHC13 constraints on gluino mass. Results with pure bino state (not shown in the figure) are all excluded by LUX(2015) experiment. Although points with mixed higgsino-bino states are beyond the reach of LUX, such models will be totally probed by LZ and XENONnT. LUX collaboration results from 2015 data [93] show that a small fraction of NUHM2 parameter space has already been probed. The projected reach of the XENON1T detector covers nearly all the predicted parameter space points by NUHM2 model. LZ collaboration, an update of LUX, aims to probe parameter space points beyond that which NUHM2 predicts. The entire set of points generated by the scan will be probed by LZ, XENONnT and DARWIN. Since deployment of these ton-scale detectors is ongoing, it seems that direct

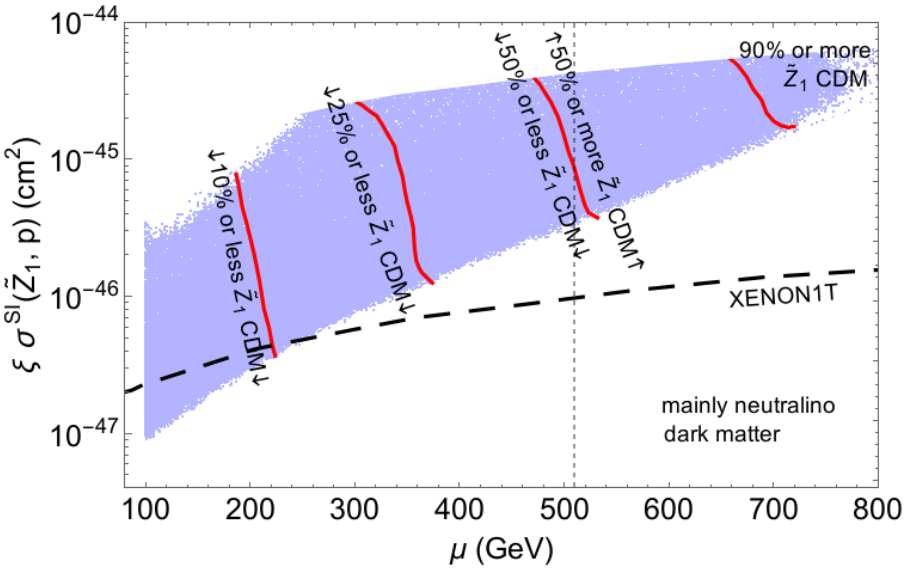


Figure 42: Plot of rescaled higgsino-like WIMP spin-independent direct detection rate $\xi\sigma^{\rm SI}(\widetilde{Z}_1, p)$ versus $\mu$ from a scan over NUHM2 parameter space. Only the results that are not excluded by LUX are shown.

WIMP search experiments may either verify or exclude RNS models in the near future [99, 90].

In Fig. 42, the spin-independent (SI) direct detection cross section is shown, this time versus the $\mu$ parameter in the horizontal axis with only non-excluded points from LUX results. Furthermore, points with highly mixed higgsino-bino states are removed. With the scan results, approximate boundaries ($\pm$10 GeV) for the composition of CDM can be drawn. The only region that XENON1T will not be able to probe has a small neutralino abundance: $\Omega^{std}_{\widetilde{Z}_1}h^2/\Omega_{\rm CDM}h^2 < 0.1$. These results are from a scan over NUHM2 parameter space which accounts for only one component of the dark matter. For the mixed axion-neutralino DM scenario, when the neutralino abundance is not enhanced from axino or saxion decays (either $f_a$ is low or axino and saxion are heavy (short-lived axino and saxion)), percentage values roughly indicate the contribution of neutralino DM to total $\Omega_{\rm CDM}h^2$. However, additional (axino and saxion) decays to neutralino

can bolster the neutralino abundance to much higher values even at $\mu < 200$ GeV, for example $\Omega^{std}_{\widetilde{Z}_1}h^2 \rightarrow \Omega_{\widetilde{Z}_1}h^2 \simeq 0.12$ at $f_a \simeq 10^{12}$ GeV as seen in Fig. 34.

### IV.1.2. Bino-Like Neutralino

A scan over CMSSM parameter space results in bino-like neutralino DM since $M_1^{weak} \sim m_{\widetilde{Z}_1}$ unlike the NUHM2 model where $\mu \sim m_{\widetilde{Z}_1}$. In CMSSM, $m_{H_u} = m_{H_d} = m_0$ at GUT scale so the $\mu$ term is adjusted to satisfy the EWSB condition (Eq. 27) and is greater than 0.5 TeV within the parameter space that is not excluded by the LHC. The hypothesis of thermally produced neutralino only CDM used to be one of the most favorite scenarios until the LHC excluded the most lucrative regions (stau or stop co-annihilation, $A$ or $h$ resonance annihilation and mixed higgsino annihilation) that satisfy CDM relic density constraint from WMAP [86]. In order to show experimental reach plots, a scan over CMSSM parameter space is performed by using the following ranges of parameters:

$$\begin{aligned} 2 \text{ TeV} < \ & m_0 < 20 \text{ TeV}, \\ 0.65 \text{ TeV} < \ & m_{1/2} < 8 \text{ TeV}, \\ -3 \ < \ & A_0/m_0 < 3, \\ 3 \ < \ & \tan\beta < 60. \end{aligned}$$

Since neutralino dark matter is mostly overproduced in CMSSM, $\Omega^{std}_{\widetilde{Z}_1}h^2 < 0.12$ is not required. Hence, $m_0$ or $m_{1/2}$ can be chosen as high as possible unless naturalness is a consideration. An additional naturalness constraint might arise from the dilution mechanism. In a PQMSSM scenario where late time saxion decays cause entropy dilution, a measure of naturalness in the PQ sector would be the value of $\theta_s$. A very high $\Omega^{std}_{\widetilde{Z}_1}h^2$ would require $\theta_s \gg 1$. $\sigma^{\rm SI}(\widetilde{Z}_1, p)$ for the CMSSM model is again calculated using IsaReD and rescaled by the factor $\xi$.

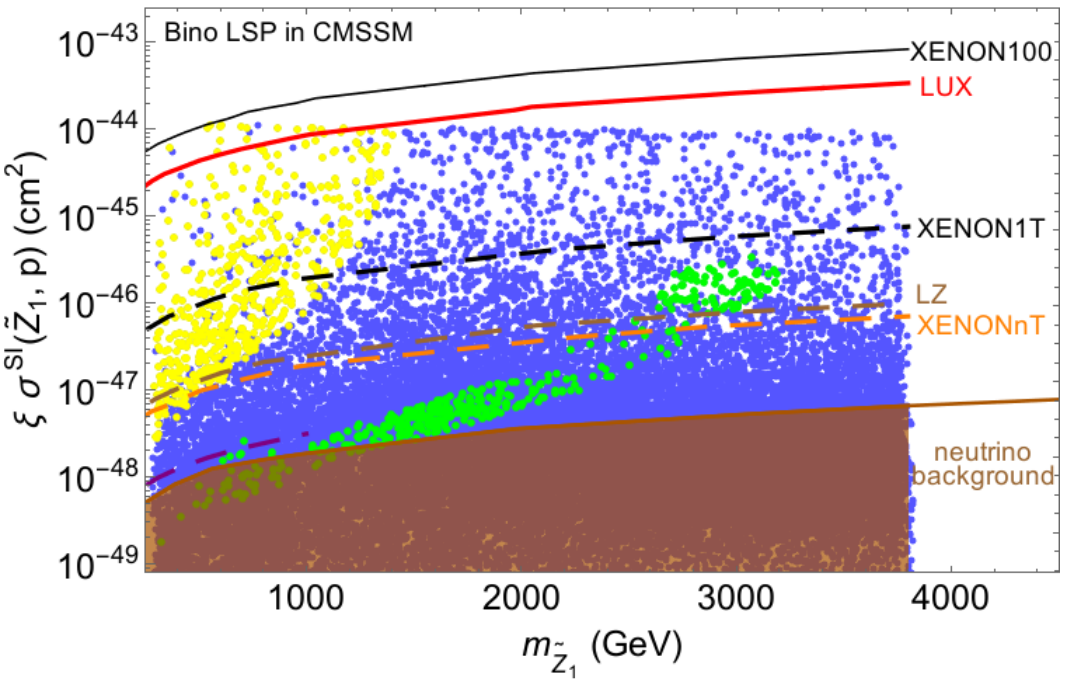


Figure 43: Plot of rescaled bino-like WIMP spin-independent direct detection rate $\xi\sigma^{\rm SI}(\widetilde{Z}_1, p)$ versus $m_{\widetilde{Z}_1}$ from a scan over CMSSM parameter space. Current and projected reaches (dashed lines) from the experiments are plotted. Yellow points have $\Delta_{\rm EW} < 500$ and green points might show similar behavior as the CMSSM benchmark point in mixed DM calculation with appropriate PQ parameter choices. Astrophysical neutrino background dominates in the brown region.

Results from a scan over CMSSM parameters are shown in Fig. 43. The first observation is $m_{\widetilde{Z}_1} \gtrsim 300$ GeV due to LHC bounds on $m_0$ vs $m_{1/2}$ plane. Yellow points have rather low $\Delta_{\rm EW}$, $\Delta_{\rm EW} < 500$. All points with $\Delta_{\rm EW} < 200$ are within the reach of XENON1T. The brown region shows the neutrino discovery limit where the astrophysical neutrino dominates [100]. Green points have a $\mu$ term between $3 - 3.5$ TeV, and $\Omega^{std}_{\widetilde{Z}_1} h^2 = 10 - 50$ that are similar to the ones in the CMSSM benchmark point used to calculate mixed bino-neutralino DM. The bulk of CMSSM parameters with $|A_0/m_0| > 2$ falls under the neutrino detection limit since the LSP is almost pure bino with heavy squarks; as a consequence the SI cross section is small. It is unlikely to exclude CMSSM with direct DM searches in case $\Omega^{std}_{\widetilde{Z}_1} h^2 = 0.12$ is not required as in the mixed axion-bino DM scenario. However, if purely neutralino dark matter is considered, CMSSM parameter space is limited by $\tan\beta \lesssim 5$ [90] which generate SI cross sections that are accesible to future LZ and XENONnT experiments.

## IV.2. Implications for Axion Detection

The axion is a very attractive dark matter candidate since it emerges from a solution to the strong CP problem. Although there is a wide range of technologies used in axion detection, high precision is required since the axion is weakly coupled to photons ($g_{a\gamma\gamma} \sim 1/f_a$). The experimental landscape of the axion and historical bounds from the searches involving a variety of techniques are shown in Fig. 44. The cold dark matter axion mass lies in the mass range from 1 to 100 $\mu$eV whereas the QCD axion can be as heavy as 1 meV [101, 102]. The ADMX (Axion Dark Matter eXperiment) collaboration will start probing the axion CDM mass range defined by KSVZ and DFSZ type of axion models. The projected reach by year 2020 is to probe axion mass up to 40 $\mu$eV [103]. The computation of mixed axion-higgsino dark matter puts an upper limit on the

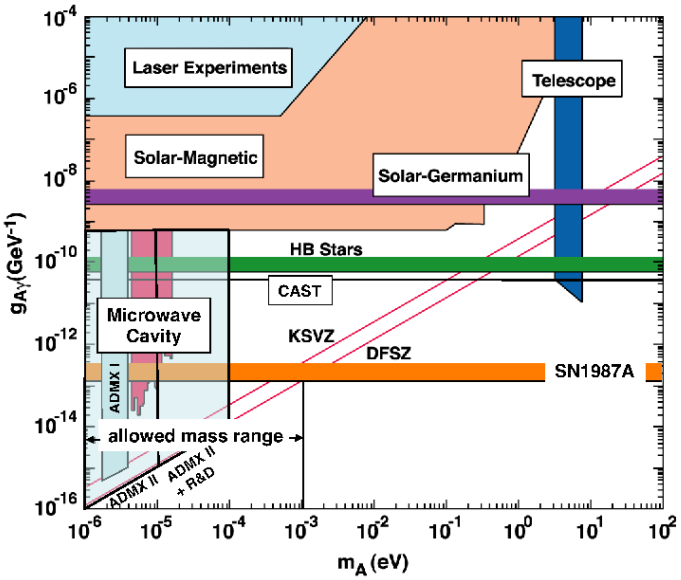


Figure 44: The landscape of axion searches. The vertical axis is the axion's coupling to two photons. The horizontal axis is the axion's mass. Plot taken from Ref. [101].

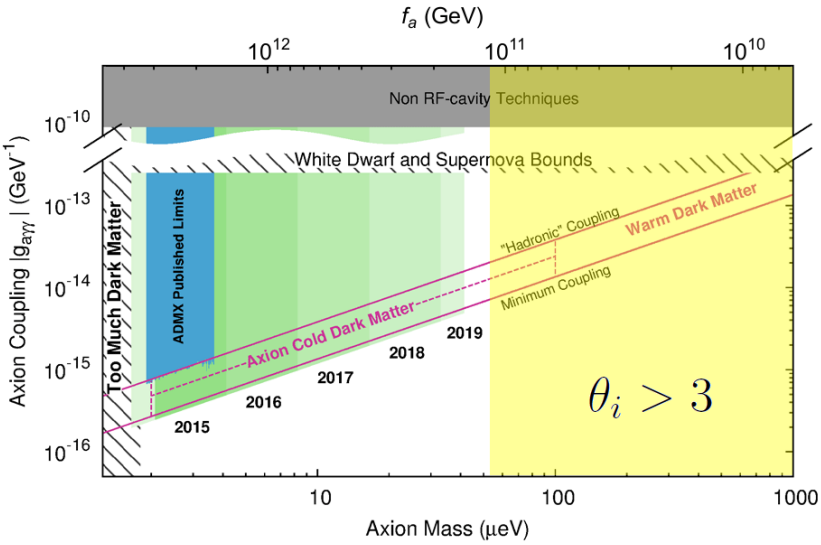


Figure 45: The projected sensitivity of ADMX experiment after the dilution refrigerator is added. Axion parameter space already excluded by the ADMX experiment is shown in blue. Plot reproduced from Ref. [104]. Upper ticks show corresponding $f_a$ values. $f_a$ range with $\theta_i > 3$ in mixed axion-higgsino calculation is shown in yellow.

axion decay constant $f_a \lesssim 2 \times 10^{14}$ GeV for $\xi_s = 1$ and $f_a \lesssim 7 \times 10^{12}$ GeV for $\xi_s = 0$. The lower limit for $f_a$, $f_a \gtrsim 10^{11}$ GeV is defined by the naturalness condition: $\theta_i < 3$. In the case of mixed axion-bino dark matter in the CMSSM model, $f_a$ is bounded below due to overproduction of dark matter: $f_a \gtrsim 4 \times 10^{15}$ GeV. The axion decay constant and axion mass are related to each other by Eq. (62) so a finite $f_a$ range implies a finite axion mass range.

The projected sensitivity of the ADMX experiment is shown in Fig. 45. The upper red line denoted by "Hadronic Coupling" shows the KSVZ type of axion coupling whereas the lower one ("Minimum Coupling") shows the DFSZ type of axion to photons coupling. A wide $f_a$ region ($10^{11} \lesssim f_a/\text{GeV} \lesssim 5 \times 10^{12}$) predicted by natural SUSY DFSZ models is accessible to ADMX projected sensitivity by 2020.

# V. Summary

The lack of discovery of supersymmetry at the LHC has raised questions as to the nature of and existence of weak scale SUSY [105] since most of the sparticle mass predictions in pre-LHC era were based on naturalness as defined in Ref. [21]. It has been argued that the *old* naturalness definition ignores correlations between dependent quantities [22], and some variants of the MSSM model are still natural with low EW fine-tuning within certain parameter ranges. SUSY indeed has been challenged and yet survived three times [106]: $m_h \lesssim 135$ GeV, gauge coupling unification and $m_t \sim 100 - 200$ GeV for a successfull EWSB. It is still known as the best solution for the hierarchy problem of the weak scale.

The CMSSM parameter space after LHC, which is mostly still highly fine-tuned in $\Delta_{\rm EW}$ measure, can only satisfy the correct relic abundance within a narrow band on the $m_0$ vs. $m_{1/2}$ plane. The model barely remains phenomenologically viable and favors $\sim 1$ TeV higgsino DM [107]. In the CMSSM, the neutralino is mostly overproduced and bino-like so an additional moduli field is needed to dilute the DM density. In the PQMSSM scenario, entropy dilution is realized by saxion decays at high $f_a$ values. However, natural values of the $\theta_s$ parameter with $s_0 \simeq f_a$ and $f_a \simeq 10^{16}$ GeV constrains highly neutralino overabundant MSSM models.

On the other hand, the NUHM2 models with low $\mu$ parameter (RNS) have low electroweak fine-tuning, $\Delta_{\rm EW} \lesssim 30$ and give $\Omega^{std}_{\widetilde{Z}_1}h^2 < 0.12$ in most of the parameter space. In a typical RNS mass spectrum, the lightest neutralino and chargino lie not too far from the weak scale and squarks are at the multi-TeV scale. The higgsino-like neutralino is mostly underabundant and the DM is composed of both neutralino and axion. In the SUSY DFSZ model, Higgs doublets superfields carry PQ charges so the $\mu$ term is generated upon breaking of the PQ

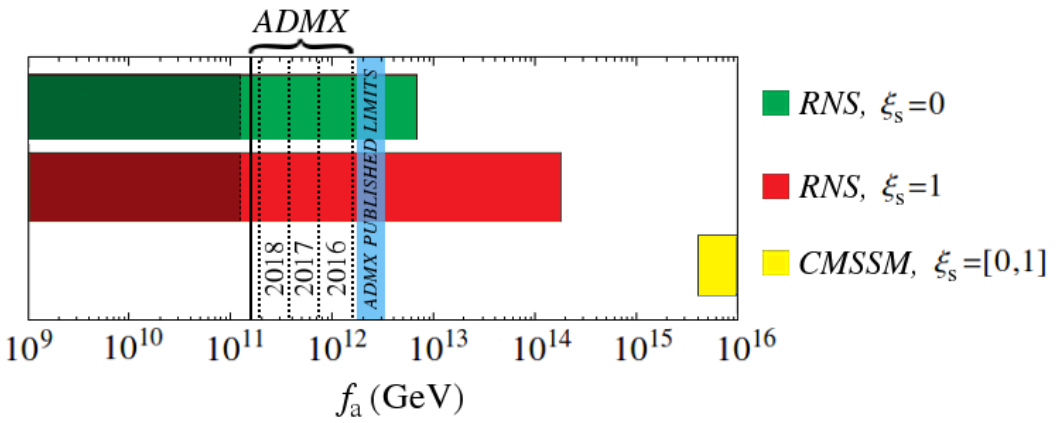


Figure 46: Range of $f_a$ which is allowed in each PQMSSM scenario for the RNS and CMSSM benchmark models. The shaded regions indicate range of $f_a$ where $\theta_i > 3$. ADMX future reach by years and published limits are shown on $f_a$ plane. For both scenarios, $\theta_s$ is taken to be 1.

symmetry. The little hierarchy between the $\mu$ term and the soft masses can be explained as a consequence of the mismatch between the PQ scale $v_{PQ}$ and the hidden scale $m_{\text{hidden}}$ with $v_{PQ} \ll m_{\text{hidden}}$. The $\mu$ term can naturally be generated by breaking the PQ symmetry radiatively with $\mu \ll m_{3/2}$.

The solution of the eight coupled Boltzmann equations gives allowed $f_a$ ranges as seen in Fig. 46. ADMX will be probing the region without entropy dilution. Natural SUSY models with mainly axion DM favors $f_a \sim 10^{11} - 10^{12}$ GeV which is within the ADMX projected reach. The SUSY DFSZ model with the CMSSM benchmark point is allowed in a narrow $f_a$ region. It should be noted that during computation, $\theta_s$ is taken to be 1. Higher $\theta_s$ values can pull the lower limit of $f_a$ down to $\sim 10^{15}$ GeV in the CMSSM scenario by creating a huge entropy dilution. A CMSSM benchmark point with lower $\Omega^{std}_{\tilde{Z}_1} h^2$ would also result in a couple of magnitudes lower $f_a$ limit [43].

Introducing the axion as the second component of the dark matter in a SUSY model has the advantage of solving the strong CP problem. For both overabundant CMSSM and underabundant NUHM2 models, the initial axion misalign-

ment angle $\theta_i$ can be adjusted so that $\Omega_{\widetilde{Z}_1+a}h^2 = 0.12$. The ADMX experiment will be probing the axion mass spectrum predicted by the RNS models within the next 3 years. Discovery of the axion would tell us where to look for the neutralino dark matter in a SUSY DFSZ scenario.

Radiative natural SUSY models are already being probed by the LHC (gluino mass bound) and the LUX(2015) DM detection experiment has excluded a small region of the RNS parameter space. With the high luminosity LHC data, RNS models will either be confirmed or excluded with 95%CL [108]. The XENON1T experiment is also expected to confirm or rule out the RNS model by the year 2020.

In natural SUSY DFSZ models, both an axion and a WIMP (higgsino) detection is ultimately expected within this decade.

# References


[1] G. Aad *et al.* [ATLAS Collaboration], Phys. Lett. B **716**, 1 (2012).

[2] S. Chatrchyan *et al.* [CMS Collaboration], Phys. Lett. B **716**, 30 (2012).

[3] G. Aad *et al.* [ATLAS and CMS Collaborations], Phys. Rev. Lett. **114**, 191803 (2015) doi:10.1103/PhysRevLett.114.191803 [arXiv:1503.07589 [hep-ex]].

[4] F. Englert and R. Brout, Phys. Rev. Lett. **13**, 321 (1964). doi:10.1103/PhysRevLett.13.321; P. W. Higgs, Phys. Lett. **12**, 132 (1964). doi:10.1016/0031-9163(64)91136-9.

[5] P. A. R. Ade *et al.* [Planck Collaboration], arXiv:1502.01589 [astro-ph.CO].

[6] G. Hinshaw *et al.* [WMAP Collaboration], Astrophys. J. Suppl. **208**, 19 (2013) doi:10.1088/0067-0049/208/2/19 [arXiv:1212.5226 [astro-ph.CO]].

[7] K. A. Olive *et al.* [Particle Data Group Collaboration], Chin. Phys. C **38**, 090001 (2014). doi:10.1088/1674-1137/38/9/090001

[8] R. D. Peccei, Lect. Notes Phys. **741**, 3 (2008) doi:10.1007/978-3-540-73518-2 [hep-ph/0607268].

[9] T. Yanagida, Conf. Proc. C **7902131**, 95 (1979); P. Minkowski, Phys. Lett. B **67**, 421 (1977). doi:10.1016/0370-2693(77)90435-X.

[10] S. P. Martin, Adv. Ser. Direct. High Energy Phys. **21**, 1 (2010) [Adv. Ser. Direct. High Energy Phys. **18**, 1 (1998)] doi:10.1142/9789812839657, 10.1142/9789814307505 [hep-ph/9709356].

[11] H. P. Nilles, Phys. Rept. **110**, 1 (1984). doi:10.1016/0370-1573(84)90008-5

[12] E. W. Kolb, M. S. Turner, "The Early Universe", 1990, Addison-Wesley, Frontiers in Physics, 69.

[13] H. Baer, K. Y. Choi, J. E. Kim and L. Roszkowski, Phys. Rept. **555**, 1 (2014) doi:10.1016/j.physrep.2014.10.002 [arXiv:1407.0017 [hep-ph]].

[14] H. Baer and X. Tata, *Weak Scale Supersymmetry: From Superfields to Scattering Events*, (Cambridge University Press, 2006).

[15] L. J. Hall and M. Suzuki, Nucl. Phys. B **231**, 419 (1984). doi:10.1016/0550-3213(84)90513-3; R. N. Mohapatra, Nucl. Instrum. Meth. A **284**, 1 (1989). doi:10.1016/0168-9002(89)90237-4.

[16] T. Hambye and K. Riesselmann, Phys. Rev. D **55**, 7255 (1997) doi:10.1103/PhysRevD.55.7255 [hep-ph/9610272].

[17] M. Carena and H. E. Haber, Prog. Part. Nucl. Phys. **50**, 63 (2003) doi:10.1016/S0146-6410(02)00177-1 [hep-ph/0208209].

[18] R. Barate *et al.* [LEP Working Group for Higgs boson searches and ALEPH and DELPHI and L3 and OPAL Collaborations], Phys. Lett. B **565**, 61 (2003) doi:10.1016/S0370-2693(03)00614-2

[19] A. H. Chamseddine, R. L. Arnowitt and P. Nath, Phys. Rev. Lett. **49**, 970 (1982). doi:10.1103/PhysRevLett.49.970

[20] S. Cassel, D. M. Ghilencea, S. Kraml, A. Lessa and G. G. Ross, JHEP **1105**, 120 (2011) doi:10.1007/JHEP05(2011)120 [arXiv:1101.4664 [hep-ph]].

[21] J. R. Ellis, K. Enqvist, D. V. Nanopoulos and F. Zwirner, Mod. Phys. Lett. A **1**, 57 (1986). doi:10.1142/S0217732386000105; R. Barbieri and G. F. Giudice, Nucl. Phys. B **306**, 63 (1988). doi:10.1016/0550-3213(88)90171-X

[22] H. Baer, V. Barger and D. Mickelson, Phys. Rev. D **88**, no. 9, 095013 (2013) doi:10.1103/PhysRevD.88.095013 [arXiv:1309.2984 [hep-ph]].

[23] H. Baer, V. Barger, P. Huang, A. Mustafayev and X. Tata, Phys. Rev. Lett. **109**, 161802 (2012) doi:10.1103/PhysRevLett.109.161802 [arXiv:1207.3343 [hep-ph]].

[24] H. Baer, V. Barger, P. Huang, D. Mickelson, A. Mustafayev and X. Tata, Phys. Rev. D **87**, no. 3, 035017 (2013) doi:10.1103/PhysRevD.87.035017 [arXiv:1210.3019 [hep-ph]].

[25] J. Ellis, F. Luo, K. A. Olive and P. Sandick, Eur. Phys. J. C **73**, no. 4, 2403 (2013) doi:10.1140/epjc/s10052-013-2403-0 [arXiv:1212.4476 [hep-ph]].

[26] H. Baer, V. Barger and A. Mustafayev, Phys. Rev. D **85**, 075010 (2012) doi:10.1103/PhysRevD.85.075010 [arXiv:1112.3017 [hep-ph]].

[27] H. Baer, A. D. Box and H. Summy, JHEP **1010**, 023 (2010) doi:10.1007/JHEP10(2010)023 [arXiv:1005.2215 [hep-ph]].

[28] G. Aad *et al.* [ATLAS Collaboration], JHEP **1510**, 054 (2015) doi:10.1007/JHEP10(2015)054 [arXiv:1507.05525 [hep-ex]].

[29] J. R. Ellis, K. A. Olive and Y. Santoso, Phys. Lett. B **539**, 107 (2002) doi:10.1016/S0370-2693(02)02071-3 [hep-ph/0204192]; J. R. Ellis, T. Falk, K. A. Olive and Y. Santoso, Nucl. Phys. B **652**, 259 (2003) doi:10.1016/S0550-3213(02)01144-6 [hep-ph/0210205].

[30] G. F. Giudice and R. Rattazzi, Nucl. Phys. B **757**, 19 (2006) doi:10.1016/j.nuclphysb.2006.07.031 [hep-ph/0606105]; Y. Nomura and D. Poland, Phys. Lett. B **648**, 213 (2007) doi:10.1016/j.physletb.2007.03.012 [hep-ph/0611249].

[31] J. L. Feng, K. T. Matchev and T. Moroi, Phys. Rev. Lett. **84**, 2322 (2000) doi:10.1103/PhysRevLett.84.2322 [hep-ph/9908309].

[32] H. Baer, V. Barger, M. Savoy and H. Serce, doi:10.1016/j.physletb.2016.05.010 arXiv:1602.07697 [hep-ph].

[33] K. J. Bae, H. Baer, H. Serce and Y. F. Zhang, JCAP **1601**, 012 (2016) doi:10.1088/1475-7516/2016/01/012 [arXiv:1510.00724 [hep-ph]].

[34] L. Randall and S. D. Thomas, Nucl. Phys. B **449**, 229 (1995) doi:10.1016/0550-3213(95)00228-K [hep-ph/9407248].

[35] S. Weinberg, Phys. Rev. D **11**, 3583 (1975). doi:10.1103/PhysRevD.11.3583

[36] G. 't Hooft, Phys. Rev. Lett. **37**, 8 (1976). doi:10.1103/PhysRevLett.37.8

[37] R. D. Peccei and H. R. Quinn, Phys. Rev. Lett. **38**, 1440 (1977). doi:10.1103/PhysRevLett.38.1440

[38] S. Weinberg, Phys. Rev. Lett. **40**, 223 (1978). doi:10.1103/PhysRevLett.40.223; F. Wilczek, Phys. Rev. Lett. **40**, 279 (1978). doi:10.1103/PhysRevLett.40.279.

[39] M. Dine, W. Fischler and M. Srednicki, Phys. Lett. B **104**, 199 (1981). doi:10.1016/0370-2693(81)90590-6; A. R. Zhitnitsky, Sov. J. Nucl. Phys. **31**, 260 (1980) [Yad. Fiz. **31**, 497 (1980)].

[40] J. E. Kim, Phys. Rev. Lett. **43**, 103 (1979). doi:10.1103/PhysRevLett.43.103; M. A. Shifman, A. I. Vainshtein and V. I. Zakharov, Nucl. Phys. B **166**, 493 (1980). doi:10.1016/0550-3213(80)90209-6.

[41] J. E. Kim and H. P. Nilles, Phys. Lett. B **138**, 150 (1984). doi:10.1016/0370-2693(84)91890-2

[42] K. J. Bae, K. Choi and S. H. Im, JHEP **1108**, 065 (2011) doi:10.1007/JHEP08(2011)065 [arXiv:1106.2452 [hep-ph]].

[43] K. J. Bae, H. Baer, A. Lessa and H. Serce, JCAP **1410**, no. 10, 082 (2014) doi:10.1088/1475-7516/2014/10/082 [arXiv:1406.4138 [hep-ph]].

[44] K. J. Bae, H. Baer and E. J. Chun, JCAP **1312**, 028 (2013) doi:10.1088/1475-7516/2013/12/028 [arXiv:1309.5365 [hep-ph]].

[45] H. Baer, S. Kraml, A. Lessa and S. Sekmen, JCAP **1104**, 039 (2011) doi:10.1088/1475-7516/2011/04/039 [arXiv:1012.3769 [hep-ph]].

[46] P. Graf and F. D. Steffen, JCAP **1302**, 018 (2013) doi:10.1088/1475-7516/2013/02/018 [arXiv:1208.2951 [hep-ph]].

[47] L. Covi, H. B. Kim, J. E. Kim and L. Roszkowski, JHEP **0105**, 033 (2001) doi:10.1088/1126-6708/2001/05/033 [hep-ph/0101009].

[48] A. Strumia, JHEP **1006**, 036 (2010) doi:10.1007/JHEP06(2010)036 [arXiv:1003.5847 [hep-ph]].

[49] K. J. Bae, H. Baer and A. Lessa, JCAP **1304**, 041 (2013) doi:10.1088/1475-7516/2013/04/041 [arXiv:1301.7428 [hep-ph]].

[50] U. Ellwanger, C. Hugonie and A. M. Teixeira, Phys. Rept. **496**, 1 (2010) doi:10.1016/j.physrep.2010.07.001 [arXiv:0910.1785 [hep-ph]].

[51] G. F. Giudice and A. Masiero, Phys. Lett. B **206**, 480 (1988). doi:10.1016/0370-2693(88)91613-9

[52] K. J. Bae, E. J. Chun and S. H. Im, JCAP **1203**, 013 (2012) doi:10.1088/1475-7516/2012/03/013 [arXiv:1111.5962 [hep-ph]].

[53] K. R. Dienes and C. F. Kolda, hep-ph/9712322.

[54] H. Murayama, H. Suzuki and T. Yanagida, Phys. Lett. B **291**, 418 (1992). doi:10.1016/0370-2693(92)91397-R

[55] K. J. Bae, H. Baer and H. Serce, Phys. Rev. D **91**, no. 1, 015003 (2015) doi:10.1103/PhysRevD.91.015003 [arXiv:1410.7500 [hep-ph]].

[56] S. P. Martin and M. T. Vaughn, Phys. Rev. D **50**, 2282 (1994) [Phys. Rev. D **78**, 039903 (2008)] doi:10.1103/PhysRevD.50.2282, 10.1103/PhysRevD.78.039903 [hep-ph/9311340].

[57] T. Gherghetta and G. L. Kane, Phys. Lett. B **354**, 300 (1995) doi:10.1016/0370-2693(95)00620-Z [hep-ph/9504420].

[58] K. Choi, E. J. Chun and J. E. Kim, Phys. Lett. B **403**, 209 (1997) doi:10.1016/S0370-2693(97)00465-6 [hep-ph/9608222].

[59] K. Jedamzik, Phys. Rev. D **74**, 103509 (2006) doi:10.1103/PhysRevD.74.103509 [hep-ph/0604251].

[60] S. Weinberg, Phys. Rev. Lett. **110**, no. 24, 241301 (2013) doi:10.1103/PhysRevLett.110.241301 [arXiv:1305.1971 [astro-ph.CO]].

[61] D. Hooper, F. S. Queiroz and N. Y. Gnedin, Phys. Rev. D **85**, 063513 (2012) doi:10.1103/PhysRevD.85.063513 [arXiv:1111.6599 [astro-ph.CO]].

[62] K. Ichikawa, M. Kawasaki, K. Nakayama, M. Senami and F. Takahashi, JCAP **0705**, 008 (2007) doi:10.1088/1475-7516/2007/05/008 [hep-ph/0703034 [HEP-PH]]; J. Hasenkamp and J. Kersten, JCAP **1308**, 024 (2013) doi:10.1088/1475-7516/2013/08/024 [arXiv:1212.4160 [hep-ph]].

[63] E. J. Chun and A. Lukas, Phys. Lett. B **357**, 43 (1995) doi:10.1016/0370-2693(95)00881-K [hep-ph/9503233].

[64] S. M. Barr, K. Choi and J. E. Kim, Nucl. Phys. B **283**, 591 (1987). doi:10.1016/0550-3213(87)90288-4

[65] L. F. Abbott and P. Sikivie, Phys. Lett. B **120**, 133 (1983); J. Preskill, M. B. Wise and F. Wilczek, Phys. Lett. B **120**, 127 (1983). doi:10.1016/0370-2693(83)90637-8; M. Dine and W. Fischler, Phys. Lett. B **120**, 137 (1983). doi:10.1016/0370-2693(83)90639-1; M. S. Turner, Phys. Rev. D **33**, 889 (1986). doi:10.1103/PhysRevD.33.889.

[66] L. Visinelli and P. Gondolo, Phys. Rev. D **80**, 035024 (2009) doi:10.1103/PhysRevD.80.035024 [arXiv:0903.4377 [astro-ph.CO]].

[67] J. E. Kim and G. Carosi, Rev. Mod. Phys. **82**, 557 (2010) doi:10.1103/RevModPhys.82.557 [arXiv:0807.3125 [hep-ph]].

[68] M. Kawasaki, K. Saikawa and T. Sekiguchi, Phys. Rev. D **91**, no. 6, 065014 (2015) doi:10.1103/PhysRevD.91.065014 [arXiv:1412.0789 [hep-ph]]; T. Hiramatsu, M. Kawasaki, K. Saikawa and T. Sekiguchi, JCAP **1301**, 001 (2013) doi:10.1088/1475-7516/2013/01/001 [arXiv:1207.3166 [hep-ph]].

[69] K. Ishiwata, JHEP **1409**, 122 (2014) doi:10.1007/JHEP09(2014)122 [arXiv:1407.1827 [hep-ph]].

[70] H. Baer, A. Lessa and W. Sreethawong, JCAP **1201**, 036 (2012) doi:10.1088/1475-7516/2012/01/036 [arXiv:1110.2491 [hep-ph]].

[71] K. Choi, K. Hwang, H. B. Kim and T. Lee, Phys. Lett. B **467**, 211 (1999) doi:10.1016/S0370-2693(99)01156-9 [hep-ph/9902291].

[72] L. J. Hall, K. Jedamzik, J. March-Russell and S. M. West, JHEP **1003**, 080 (2010) doi:10.1007/JHEP03(2010)080 [arXiv:0911.1120 [hep-ph]].

[73] M. P. Hertzberg, M. Tegmark and F. Wilczek, Phys. Rev. D **78**, 083507 (2008) doi:10.1103/PhysRevD.78.083507 [arXiv:0807.1726 [astro-ph]].

[74] H. Baer, C. Balazs and A. Belyaev, JHEP **0203**, 042 (2002) doi:10.1088/1126-6708/2002/03/042 [hep-ph/0202076].

[75] F. E. Paige, S. D. Protopopescu, H. Baer and X. Tata, hep-ph/0312045.

[76] J. Pradler and F. D. Steffen, Phys. Lett. B **648**, 224 (2007) doi:10.1016/j.physletb.2007.02.072 [hep-ph/0612291].

[77] K. Kohri, T. Moroi and A. Yotsuyanagi, Phys. Rev. D **73**, 123511 (2006) doi:10.1103/PhysRevD.73.123511 [hep-ph/0507245].

[78] A. Lessa, Cosmology of the PQMSSM

[79] R. Easther, R. Galvez, O. Ozsoy and S. Watson, Phys. Rev. D **89**, no. 2, 023522 (2014) doi:10.1103/PhysRevD.89.023522 [arXiv:1307.2453 [hep-ph]].

[80] K. J. Bae, H. Baer and E. J. Chun, Phys. Rev. D **89**, no. 3, 031701 (2014) doi:10.1103/PhysRevD.89.031701 [arXiv:1309.0519 [hep-ph]].

[81] K. Y. Choi, J. E. Kim, H. M. Lee and O. Seto, Phys. Rev. D **77**, 123501 (2008) doi:10.1103/PhysRevD.77.123501 [arXiv:0801.0491 [hep-ph]].

[82] K. J. Bae, H. Baer, A. Lessa and H. Serce, Front. Phys. **3**, 49 (2015) doi:10.3389/fphy.2015.00049 [arXiv:1502.07198 [hep-ph]].

[83] The ATLAS collaboration, ATLAS-CONF-2015-067.

[84] V. Khachatryan *et al.* [CMS Collaboration], arXiv:1603.04053 [hep-ex].

[85] T. Banks and M. Dine, Nucl. Phys. B **505**, 445 (1997) doi:10.1016/S0550-3213(97)00413-6 [hep-th/9608197].

[86] H. Baer, V. Barger and A. Mustafayev, JHEP **1205**, 091 (2012) doi:10.1007/JHEP05(2012)091 [arXiv:1202.4038 [hep-ph]].

[87] F. Wang, J. M. Yang and Y. Zhang, JHEP **1604**, 177 (2016) doi:10.1007/JHEP04(2016)177 [arXiv:1602.01699 [hep-ph]].

[88] D. Francescone, S. Akula, B. Altunkaynak and P. Nath, JHEP **1501**, 158 (2015) doi:10.1007/JHEP01(2015)158 [arXiv:1410.4999 [hep-ph]].

[89] L. Roszkowski, E. M. Sessolo and A. J. Williams, JHEP **1408**, 067 (2014) doi:10.1007/JHEP08(2014)067 [arXiv:1405.4289 [hep-ph]].

[90] J. Ellis, J. L. Evans, F. Luo, N. Nagata, K. A. Olive and P. Sandick, Eur. Phys. J. C **76**, no. 1, 8 (2016) doi:10.1140/epjc/s10052-015-3842-6 [arXiv:1509.08838 [hep-ph]].

[91] M. Endo, T. Moroi and M. M. Nojiri, JHEP **1504**, 176 (2015) doi:10.1007/JHEP04(2015)176 [arXiv:1502.03959 [hep-ph]].

[92] CMS Collaboration [CMS Collaboration], CMS-PAS-SUS-16-007.

[93] D. S. Akerib *et al.* [LUX Collaboration], Phys. Rev. Lett. **116**, no. 16, 161301 (2016) doi:10.1103/PhysRevLett.116.161301 [arXiv:1512.03506 [astro-ph.CO]].

[94] E. Aprile *et al.* [XENON100 Collaboration], Phys. Rev. Lett. **109**, 181301 (2012) doi:10.1103/PhysRevLett.109.181301 [arXiv:1207.5988 [astro-ph.CO]].

[95] M. Schumann, L. Baudis, L. Btikofer, A. Kish and M. Selvi, JCAP **1510**, no. 10, 016 (2015) doi:10.1088/1475-7516/2015/10/016 [arXiv:1506.08309 [physics.ins-det]].

[96] D. S. Akerib *et al.* [LZ Collaboration], arXiv:1509.02910 [physics.ins-det].

[97] E. Aprile *et al.* [XENON Collaboration], JCAP **1604**, no. 04, 027 (2016) doi:10.1088/1475-7516/2016/04/027 [arXiv:1512.07501 [physics.ins-det]].

[98] A. Bottino, F. Donato, N. Fornengo and S. Scopel, Phys. Rev. D **63**, 125003 (2001) doi:10.1103/PhysRevD.63.125003 [hep-ph/0010203].

[99] K. J. Bae, H. Baer, V. Barger, M. R. Savoy and H. Serce, Symmetry **7**, no. 2, 788 (2015) doi:10.3390/sym7020788 [arXiv:1503.04137 [hep-ph]].

[100] J. Billard, L. Strigari and E. Figueroa-Feliciano, Phys. Rev. D **89**, no. 2, 023524 (2014) doi:10.1103/PhysRevD.89.023524 [arXiv:1307.5458 [hep-ph]].

[101] A. Kusenko and L. J. Rosenberg, arXiv:1310.8642 [hep-ph].

[102] L. J. Rosenberg, Proc. Nat. Acad. Sci. (2015). doi:10.1073/pnas.1308788112

[103] G. Rybka [ADMX Collaboration], Phys. Dark Univ. **4**, 14 (2014). doi:10.1016/j.dark.2014.05.003

[104] ADMX Collaboration, online; accessed May 5, 2016. Retrieved from http://depts.washington.edu/admx/future.shtml .

[105] J. Lykken and M. Spiropulu, Sci. Am. **310N5**, 36 (2014); A. Strumia, JHEP **1104**, 073 (2011) doi:10.1007/JHEP04(2011)073; M. Dine, Ann. Rev. Nucl. Part. Sci. **65**, 43 (2015) doi:10.1146/annurev-nucl-102014-022053 [arXiv:1501.01035 [hep-ph]].

[106] H. Baer, V. Barger and M. Savoy, Phys. Scripta **90**, 068003 (2015) doi:10.1088/0031-8949/90/6/068003 [arXiv:1502.04127 [hep-ph]].

[107] K. Kowalska, L. Roszkowski, E. M. Sessolo and S. Trojanowski, JHEP **1404**, 166 (2014) doi:10.1007/JHEP04(2014)166 [arXiv:1402.1328 [hep-ph]].

[108] H. Baer, V. Barger, M. Savoy and X. Tata, arXiv:1604.07438 [hep-ph].

# Appendix A: Les Houches Outputs

## A.1. NUHM2 (RNS)

```
#  ISAJET SUSY parameters in SUSY Les Houches Accord 2 format
  #  Created by ISALHA 2.0 Last revision: H Baer 27 May 2014
  Block SPINFO   # Program information
     1   ISASUGRA/ISASUSY from ISAJET   # Spectrum Calculator
     2   7.85   04-NOV-2015 13:42:47    # Version number
  Block MODSEL   # Model selection
     1    13   # Non-universal supergravity model
  Block SMINPUTS   # Standard Model inputs
     1     1.28000000E+02   # alpha_em^(-1)
     2     1.16570000E-05   # G_Fermi
     3     1.19999997E-01   # alpha_s(M_Z)
     4     9.11699982E+01   # m_{Z}(pole)
     5     4.19999981E+00   # m_{b}(m_{b})
     6     1.73199997E+02   # m_{top}(pole)
     7     1.77699995E+00   # m_{tau}(pole)
  Block MINPAR   # SUSY breaking input parameters
     1     5.00000000E+03   # m_0
     2     8.00000000E+02   # m_{1/2}
     3     1.00000000E+01   # tan(beta)
     4     1.00000000E+00   # sign(mu)
     5    -8.40000000E+03   # A_0
  Block EXTPAR   # Non-universal SUSY breaking parameters
     0     1.75096013E+16   # Input scale
```

```
   21     1.26287913E+06   # Down type Higgs mass squared
   22     4.11406480E+07   #  Up  type Higgs mass squared
Block MASS   # Scalar and gaugino mass spectrum
#  PDG code    mass                 particle
        6     1.73199997E+02   #  top
       24     8.04229965E+01   #  W^+
       25     1.25037491E+02   #  h^0
       35     1.00677808E+03   #  H^0
       36     1.00000000E+03   #  A^0
       37     1.00322870E+03   #  H^+
  1000001     5.16943701E+03   #  dnl
  1000002     5.16881738E+03   #  upl
  1000003     5.16943701E+03   #  stl
  1000004     5.16881738E+03   #  chl
  1000005     3.61930225E+03   #  b1
  1000006     1.18295630E+03   #  t1
  1000011     5.11724414E+03   #  el-
  1000012     5.12300732E+03   #  nuel
  1000013     5.11724414E+03   #  mul-
  1000014     5.12300732E+03   #  numl
  1000015     4.72320264E+03   #  tau1
  1000016     5.08841357E+03   #  nutl
  1000021     2.00563013E+03   #  glss
  1000022     1.17538933E+02   #  z1ss
  1000023    -1.32669678E+02   #  z2ss
  1000024     1.29119186E+02   #  w1ss
  1000025     3.62576447E+02   #  z3ss
```

1000035 7.02567749E+02 # z4ss

1000037 6.92897339E+02 # w2ss

1000039 1.00000002E+20 # gvss

2000001 5.13537939E+03 # dnr

2000002 5.32709521E+03 # upr

2000003 5.13537939E+03 # str

2000004 5.32709521E+03 # chr

2000005 5.04107275E+03 # b2

2000006 3.58459839E+03 # t2

2000011 4.80174756E+03 # er-

2000013 4.80174756E+03 # mur-

2000015 5.08037939E+03 # tau2

Block GAUGE Q= 2.07106885E+03 #

1 3.57524902E-01 # g′

2 6.52378678E-01 # g_2

3 1.21929109E+00 # g_3

Block HMIX Q= 2.07106885E+03 # Higgs mixing parameters

1 1.25000000E+02 # mu(Q)

2 9.56639290E+00 # tan(beta)(Q)

3 2.52247894E+02 # Higgs vev at Q

4 1.00000000E+06 # m_Aˆ2(Q)

Block MSOFT Q= 2.07106885E+03 # DRbar SUSY breaking parameters

1 3.54821228E+02 # M_1(Q)

2 6.51365051E+02 # M_2(Q)

3 1.74825476E+03 # M_3(Q)

21 9.13494625E+05 # MHdˆ2(Q)

```
    22    -8.06329219E+04   # MHu^2(Q)
```

## A.2. CMSSM

```
#  ISAJET SUSY parameters in SUSY Les Houches Accord 2 format
  #  Created by ISALHA 2.0 Last revision: H Baer 27 May 2014
  Block SPINFO   # Program information
     1   ISASUGRA/ISASUSY from ISAJET   # Spectrum Calculator
     2   7.85   04-NOV-2015 13:42:47    # Version number
  Block MODSEL   # Model selection
     1    1   # Minimal supergravity (mSUGRA) model
  Block SMINPUTS   # Standard Model inputs
     1     1.28000000E+02   # alpha_em^(-1)
     2     1.16570000E-05   # G_Fermi
     3     1.19999997E-01   # alpha_s(M_Z)
     4     9.11699982E+01   # m_{Z}(pole)
     5     4.19999981E+00   # m_{b}(m_{b})
     6     1.73199997E+02   # m_{top}(pole)
     7     1.77699995E+00   # m_{tau}(pole)
  Block MINPAR   # SUSY breaking input parameters
     1     4.20000000E+03   # m_0
     2     8.00000000E+02   # m_{1/2}
     3     1.00000000E+01   # tan(beta)
     4     1.00000000E+00   # sign(mu)
     5    -8.40000000E+03   # A_0
  Block EXTPAR   # Non-universal SUSY breaking parameters
```

```
     0     1.47096660E+16   # Input scale
Block MASS   # Scalar and gaugino mass spectrum
#  PDG code    mass                particle
         6     1.73199997E+02   #  top
        24     8.04229965E+01   #  W^+
        25     1.25479080E+02   #  h^0
        35     5.25730518E+03   #  H^0
        36     5.22302637E+03   #  A^0
        37     5.25797314E+03   #  H^+
   1000001     4.45199902E+03   #  dnl
   1000002     4.45127930E+03   #  upl
   1000003     4.45199902E+03   #  stl
   1000004     4.45127979E+03   #  chl
   1000005     3.23229053E+03   #  b1
   1000006     1.02115253E+03   #  t1
   1000011     4.22503613E+03   #  el-
   1000012     4.22982715E+03   #  nuel
   1000013     4.22503613E+03   #  mul-
   1000014     4.22982715E+03   #  numl
   1000015     4.11297510E+03   #  tau1
   1000016     4.18394775E+03   #  nutl
   1000021     1.97668176E+03   #  glss
   1000022     3.60620392E+02   #  z1ss
   1000023     6.96862915E+02   #  z2ss
   1000024     7.00478760E+02   #  w1ss
   1000025    -3.23233228E+03   #  z3ss
   1000035     3.23335132E+03   #  z4ss
```

```
   1000037     3.24238672E+03   #  w2ss
   1000039     1.00000002E+20   #  gvss
   2000001     4.44360547E+03   #  dnr
   2000002     4.44384717E+03   #  upr
   2000003     4.44360547E+03   #  str
   2000004     4.44384717E+03   #  chr
   2000005     4.34034424E+03   #  b2
   2000006     3.18477637E+03   #  t2
   2000011     4.20682959E+03   #  er-
   2000013     4.20682959E+03   #  mur-
   2000015     4.18170361E+03   #  tau2

Block GAUGE Q=  1.77268323E+03   #
     1     3.57525110E-01   # g'
     2     6.52386069E-01   # g_2
     3     1.21941805E+00   # g_3

Block HMIX Q=  1.77268323E+03   # Higgs mixing parameters
     1     3.23216602E+03   # mu(Q)
     2     9.58626366E+00   # tan(beta)(Q)
     3     2.52108093E+02   # Higgs vev at Q
     4     2.72800040E+07   # m_A^2(Q)
Block MSOFT Q=  1.77268323E+03   # DRbar SUSY breaking parameters
     1     3.57933197E+02   # M_1(Q)
     2     6.54939941E+02   # M_2(Q)
     3     1.74084045E+03   # M_3(Q)
    21     1.63078470E+07   # MHd^2(Q)
    22    -1.03182250E+07   # MHu^2(Q)
```